JCTC Journal of Chemical Theory and Computation

Article

pubs.acs.org/JCTC

Accuracy of Quantum Chemical Methods for Large Noncovalent Complexes

Robert Sedlak,*[,†,‡] Tomasz Janowski,*[,§] Michal Pitoňák,[∥,⊥] Jan Řezáč,[†] Peter Pulay,[§] and Pavel Hobza*[,†,#]

[†]Institute of Organic Chemistry and Biochemistry, Academy of Sciences of the Czech Republic, 166 10 Prague, Czech Republic

[‡]Department of Physical and Macromolecular Chemistry, Faculty of Science, Charles University in Prague, Albertov 6, 128 43 Prague, Czech Republic

[§]Department of Chemistry and Biochemistry, Fulbright College of Arts and Sciences, University of Arkansas, Fayetteville, Arkansas 72701, United States

[∥]Department of Physical and Theoretical Chemistry, Faculty of Natural Sciences, Comenius University, Mlynská Dolina, 842 15 Bratislava, Slovak Republic

[⊥]Computing Center of the Slovak Academy of Sciences, Dúbravská cesta č. 9, 845 35 Bratislava, Slovak Republic

[#]Regional Center of Advanced Technologies and Materials, Department of Physical Chemistry, Palacký University, 771 46 Olomouc, Czech Republic

Supporting Information

ABSTRACT: We evaluate the performance of the most widely used wave function, density functional theory, and semiempirical methods for the description of noncovalent interactions in a set of larger, mostly dispersion-stabilized noncovalent complexes (the L7 data set). The methods tested include MP2, MP3, SCS-MP2, SCS(MI)-MP2, MP2.5, MP2.X, MP2C, DFT-D, DFT-D3 (B3-LYP-D3, B-LYP-D3, TPSS-D3, PW6B95-D3, M06-2X-D3), and M06-2X, and semiempirical methods augmented with dispersion and hydrogen bonding corrections: SCC-DFTB-D, PM6-D, PM6-DH2, and PM6-D3H4. The test complexes are the octadecane dimer, the guanine trimer, the circumcoronene···adenine dimer, the coronene dimer, the guanine-cytosine dimer, the circumcoronene···guanine-cytosine dimer, and an amyloid fragment trimer containing phenylalanine residues. The best performing method is MP2.5 with relative root-mean-square deviation (rRMSD) of 4%. It can thus be recommended as an alternative to the CCSD(T)/CBS (alternatively QCISD(T)/CBS) benchmark for molecular systems which exceed current computational capacity. The second best non-DFT method is MP2C with rRMSD of 8%. A method with the most favorable "accuracy/cost" ratio belongs to the DFT family: BLYP-D3, with an rRMSD of 8%. Semiempirical methods deliver less accurate results (the rRMSD exceeds 25%). Nevertheless, their absolute errors are close to some much more expensive methods, such as M06-2X, MP2, or SCS(MI)-MP2, and thus their price/performance ratio is excellent.

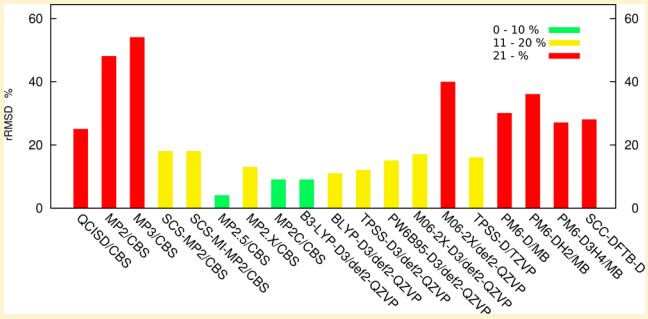

INTRODUCTION

Noncovalent interactions, such as hydrogen bond, halogen bond, $\pi\cdots\pi$ stacking, etc., play an important role in processes like the molecular recognition, crystal packing, protein folding, vapor−liquid condensation, stacking of nucleobases, etc. Although these interactions are at least by an order of magnitude weaker than covalent interactions, they accumulate for larger systems and their impact on structure and function of biomolecules is fundamental.[1−3]

Different binding motifs require different levels of theory to reach a given accuracy. Interactions driven mostly by electrostatics, such as the hydrogen bonding,[4,5] are (at least qualitatively) described properly already at the Hartree−Fock (HF) level. However, neither Hartree−Fock theory nor traditional local or semilocal density functional theories include dispersion,[6−8] and not even highly parametrized exchange-correlation functionals are able to describe dispersion in the asymptotic limit,[9] leading to an underestimation of the stability of dispersion dominated complexes at the density functional (DFT) and semiempirical levels of theory. The simplest method which accounts for dispersion *for the right reason*, second order Møller−Plesset perturbation theory (MP2), strongly overestimates dispersion for π systems.[10] In many cases, accurate results are obtained only at the computationally expensive coupled cluster level with the perturbative inclusion of triple excitations in extended basis sets. Two, unfortunately mutually contradictory goals govern the method development.

Received: January 15, 2013
Published: July 10, 2013

   dx.doi.org/10.1021/ct400036b | J. Chem. Theory Comput. 2013, 9, 3364−3374

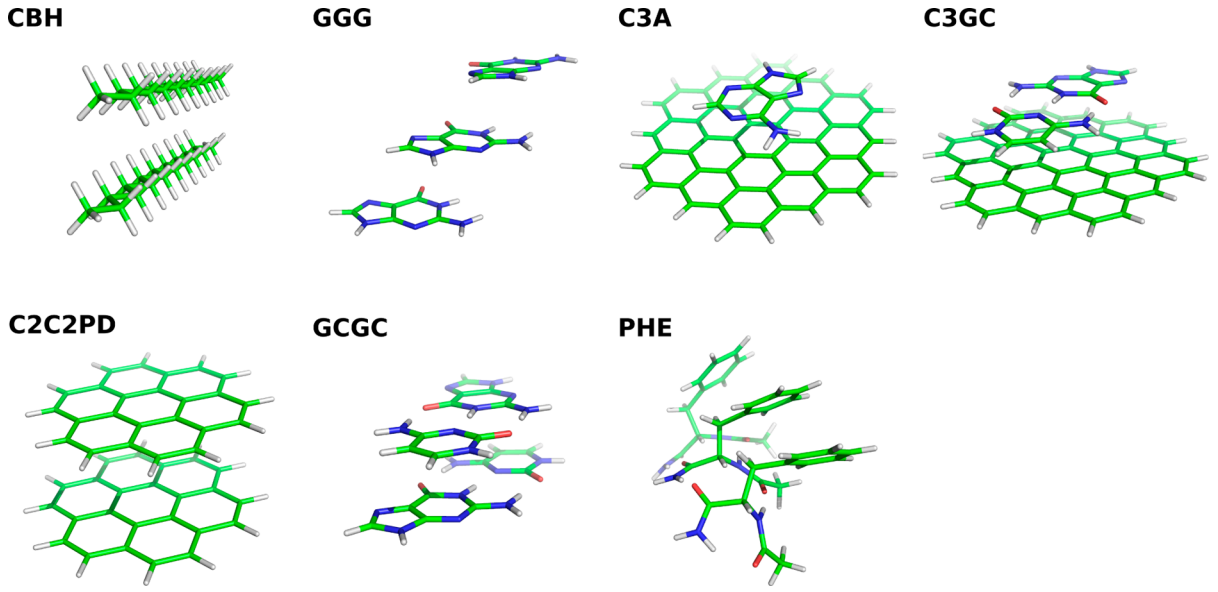

Figure 1. Structures of the investigated complexes.

The first one is to achieve maximum accuracy, while the second one is the ability to describe large molecular systems efficiently. Significant effort was spent in the past decade to develop methods that strike a reasonable compromise between accuracy and computational cost for dispersion-dominated interactions.[11] Some examples are empirical scaling of different contributions in wave function-based methods,[12−15] parametrizing exchange-correlation functionals to account for dispersion,[16] combining short-range DFT correlation with long-range MP2 (MP2C)[17] or RPA[18] and adding explicit dispersion terms to conventional DFT.[19] Other promising approaches are local electron correlation theories,[20] Symmetry-Adapted Perturbation Theory[21] based on DFT,[22,23] modification of the core potentials to mimic dispersion,[24,25] and methods aiming at incorporating the physics of dispersion in DFT.[26−28] Although many of these methods are very promising, we will focus on the following classes of methods: (a) post-HF wave function theory (WFT) methods containing empirical parameters, (b) DFT based methods with added dispersion terms, and (c) semiempirical quantum mechanical methods augmented with empirical corrections for noncovalent interactions.

The first group is represented by the SCS-MP2, SCS(MI)-MP2, MP2C, MP2.5, and MP2.X methods.[12,14,17,29,30] The formal scaling of these methods is $O(N^5)$, for the MP2-based, and $O(N^6)$ for MP3-based methods, where N is proportional to the size of the system (assuming constant basis set quality). Perturbational methods such as MP*n* are noniterative and are thus about an order of magnitude more efficient than iterative methods, and they are also more readily parallelized.

The most widely used family of quantum chemical methods, local or semilocal density functional theory (DFT) does not account for the dispersion interaction.[6−8] Dispersion can be included by empirical corrections[19,31,32] or by fitting the exchange-correlation functional to reproduce dispersion near the van der Waals minimum[33] (note, however, that these methods fail to represent the long-range behavior of dispersion). DFT-based methods have advantages over post-HF methods: smaller basis set superposition error (BSSE) and more favorable scaling. The DFT functionals investigated in this work scale one or two powers lower than post-Hartree−Fock methods, $O(N^3)$−$O(N^4)$ versus $O(N^5)$−$O(N^6)$.

The third group contains semiempirical methods[34] augmented with empirical corrections, such as the dispersion correction of Martin and Clark.[35] We focus on the PM6 method[36] enhanced with empirical corrections for dispersion and hydrogen bonding.[37,38] Empirical corrections used in this group are usually obtained from minimization of the root-mean-square deviation relative to high-quality benchmark data.

The design of reference data is of a crucial importance. They should be obtained by state-of-the-art methods, such as CCSD(T) in extended basis set or even extrapolated to the complete basis set (CBS) limit. They should also be available for a large, balanced set of molecules. Several such benchmark data sets for noncovalent complexes are available. The S22 set,[39] developed in Hobza's group, has become one of the most commonly used data sets for testing and parametrization of methods focused on the noncovalent interactions. This data set is now being replaced by larger and more balanced data sets, such as S22 × 5,[40] S22+,[41] and S66.[42] Super databases (databases containing several data sets) such as GMTKN[43,44] or NCIE[45−48] are also available.

All the data sets above share the same restriction: only medium-sized systems (less than ∼30 atoms) are included. The only exception is the recent study of Risthaus and Grimme,[49] where the performance of different dispersion-accounting DFT methods is tested with respect to experimental data on the S12L set (set of large molecular clusters). It is a tacit assumption that the accuracy of methods parametrized for small complexes/clusters is preserved for larger ones. This, however, may not be the case if a method works well near the van der Waals minimum but is deficient for distant interactions because larger molecules have more long-range dispersion terms. The potential accumulation of errors with increasing system size is not yet fully understood. Thus there is a need to test the accuracy of recent methods on larger systems. In the present paper, we provide benchmark data for noncovalent complexes considerably larger than those in S22 or S66 data sets: this data set is called L7. We test the performance of WFT, DFT, and semiempirical methods on a set of seven large

molecular complexes: "CBH", the octadecane dimer in stacked parallel conformation (representative of aliphatic dispersion-dominated interaction); "GGG", a stacked guanine trimer arranged as in DNA (representative of the aromatic stacking $\pi\cdots\pi$ dispersion interaction with implicit account for the three-body interaction, the binding energy of one of the outer guanine monomers is evaluated); "C3A", a stacked circumcoronene···adenine dimer (representative of strong aromatic dispersion interaction with implicit account for three-body interaction); "C3GC", a stacked circumcoronene and Watson−Crick hydrogen-bonded guanine-cytosine dimer (representative of a strong aromatic dispersion interaction with implicit account for H-bonding-stacking nonadditivity, the binding energy of circumcoronene and guanine−cytosine base pair is calculated); "C2C2PD", a parallel displaced stacked coronene dimer (representative of strong aromatic dispersion interaction); "GCGC", a stacked Watson−Crick H-bonded guanine-cytosine dimers arranged as in DNA (representative of strong aromatic dispersion interaction with implicit three- and four-body interactions, the binding energy of two guanine-cytosine base pairs is evaluated); and "PHE", an amyloid fragment, a trimer of phenylalanine residues in mixed H-bonded-stacked conformation (representative of "mixed-character" interaction with implicit account for many-body interactions. The binding of one of the "outer" residues is evaluated). Structures of all complexes are shown in Figure 1. The full geometry information of all seven complexes along with explicit specification of interacting subsystems is available in the Supporting Information. Their size ranges from 48 to 112 atoms and they are intentionally selected to be mostly dispersion dominated. The motivation is simple: it is to assemble a set of noncovalent complexes, the accurate description of which is a challenge for the contemporary computational chemistry. The data set includes a representative of aliphatic hydrocarbon dimers, which are, similarly to the $\pi\cdots\pi$ stacking complexes, dispersion dominated, but of a different flavor. Aliphatic dispersion interactions are important because their abundance in proteins[48] and membranes but their accurate description is problematic as well.[50,51] The dispersion originating from saturated hydrocarbons scales linearly with system size in the asymptotic limit, as opposed to interactions in aromatic systems, because of intrinsically local character of aliphatic hydrocarbons and a significant HOMO−LUMO gap. It still requires high-level ab initio methods to be described accurately. We believe that the complexes included in the data set are representative of the most important motifs dominated by dispersion in biological chemistry.

METHODS

Geometries. Geometries of the CBH, C3A, C3GC, and PHE systems were determined at the TPSS-D/TZVP level[32] with no constrains. The structures of GCGC and C2C2PD complexes were taken from Pitoňák et al.[52] and Janowski et al.,[53] respectively. The GCGC geometry was taken from crystal X-ray data,[52] and the C2C2PD structure was optimized at the QCISD(T) level of theory. The cc-pVDZ basis set for all atoms and the corresponding diffuse (aug-cc-pVDZ) basis set for every other, neighboring carbon atom were used. The GGG geometry was extracted from the 1ZF9 structure[54] with hydrogen atoms added using xleap,[55] one of the Amber software package tools. Subsequently, the coordinates of the hydrogen atoms only were optimized at the TPSS-D/TZVP level.[32] Cartesian coordinates of all the complexes studied in this work are included in the Supporting Information, as well as on the www.begdb.com[56] web page.

Interaction Energy Calculations. Interaction energies for all of the complexes investigated were calculated for geometries optimized at lower level (see above) without considering the deformation energy (so-called rigid monomer approximation was used). With the exception of semiempirical and DFT results, all calculation used the frozen core approximation and were corrected for BSSE by the counterpoise correction.[57]

QCISD(T)/CBS as the Reference. The QCISD(T)/CBS method was chosen as the reference method, because of an advantage in efficiency over CCSD(T) in the PQS program package[58] and the fact that the QCISD(T) results closely agree with "gold standard" CCSD(T) for the noncovalent interactions of closed-shell complexes.[59] The hybrid scheme of Sherrill et al.[10] and Jurečka and Hobza[60] was used to extrapolate the results to the Complete Basis Set limit

$$\Delta E(\mathrm{QCISD(T)/CBS}) = \Delta E(\mathrm{MP2/CBS})' + \Delta\mathrm{QCISD(T)|small\ basis} \quad (1)$$

where $\Delta E(\mathrm{MP2/CBS})'$ is a CBS limit estimate of the MP2 interaction energy, obtained as described further, and ΔQCISD(T)|small basis is a QCISD(T) correction term covering the higher-order correlation effects, determined in small sized basis set. The physical basis of this approximation is that the extra correlation energy provided by the large basis originates from highly oscillatory, high-energy basis functions which are well described by low-level perturbation theory. The most time-consuming part of the total interaction energy assembly is clearly the calculation of the ΔQCISD(T) correction term. The small basis set is defined as a 6-31G*(0.25) basis set.

$$\Delta\mathrm{QCISD(T)}|_{\mathrm{small\ basis}} = [\Delta E(\mathrm{QCISD(T)}) - \Delta E(\mathrm{MP2})]|_{6-31G*(0.25)} \quad (2)$$

The exponents of the diffuse d functions, used in this modified 6-31G* basis set, were changed from their original value of 0.8 to 0.25.[61] This basis set and the 6-31G**-(0.25,0.15) basis[61] were designed for the treatment of noncovalent interactions. They have been extensively validated for hydrogen bonded and stacked DNA base pairs in Hobza's group,[62] and surprisingly, good performance was demonstrated also for more diverse data sets[63,64] containing noncovalent interactions. The QCISD(T)/CBS method constructed as described above was used for all complexes with exception of GCGC and C2C2PD ones where slightly different methodology was applied (see later).

The $\Delta E(\mathrm{MP2/CBS})'$ term was calculated slightly differently from the routinely used cubic extrapolation of Halkier et al.[65,66] Typically, a different two-point extrapolation is performed for the HF and post-HF terms, usually using Dunning's[67,68] aug-cc-pVXZ (aXZ) basis sets with X = 2 (D) and 3(T)

$$E(\mathrm{HF}/X) = E(\mathrm{HF/CBS}) + A\exp(-\alpha X),\ \alpha = 1.43 \quad (3)$$

and

$$E(\mathrm{corr}/X) = E(\mathrm{corr/CBS}) + BX^{-3} \quad (4)$$

The use of augmented basis set for extended cluster fragments (or monomers) is problematic, if not impossible. The reason is not so much excessive computational time and storage requirements but numerical instabilities caused by

overcompleteness of the atomic basis set. The overcompleteness problem can be overcome in the most straightforward way by excluding the linear dependent basis functions from the basis set. Doing so, the numerical problems usually disappear, but the error with respect to the complete basis set is unpredictable and discontinuities may occur on the potential energy surface. One of the methods of eliminating this problem, as used in this work, is to scale the ΔE(MP2/CBS) term obtained from extrapolation using nonaugmented Dunning's[67−69] cc-pVXZ (XZ) basis sets, so that the value is close to that obtained from the augmented basis set series. The scaling factors were determined for four model complexes which are simplified representatives of a particular complex category, and for which the ΔE(MP2/CBS) term could be rigorously calculated in both nonaugmented and augmented basis sets. The four model complexes were created in accordance with the character of interaction of complexes in the data set: coronene···adenine (C2A) as a representative of C3A, C3CG, GCGC, and C2C2PD; guanine···guanine (GG) as a representative of GGG; and PHE and octane dimers (C8 dimer) as representatives of PHE trimer and CBH, respectively. The structures of the model complexes are shown in Figure 2 and

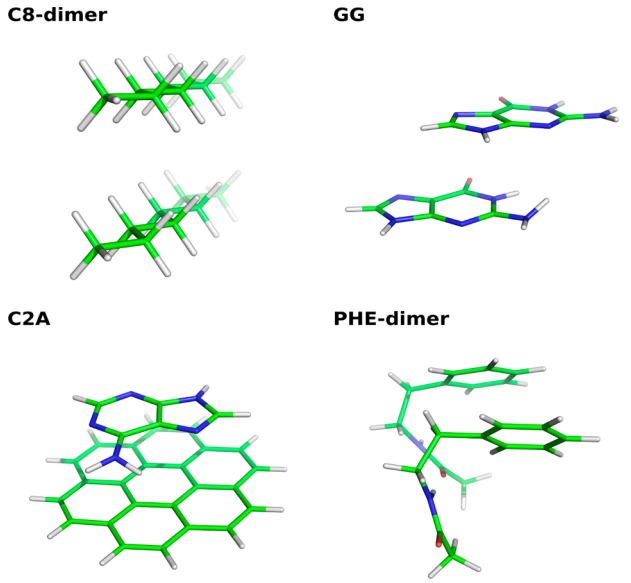

Figure 2. Structures of the four simplified (model) complexes.

the complete geometry is available in the Supporting Information. Two ΔE(MP2/CBS) values were calculated for each complex, obtained from two-point aDZ → aTZ and DZ → TZ extrapolation. To our surprise the scaling factors obtained vary only a little, from 1.01 for C8(CBH) to 1.05 for GG(GGG), thus an average value for the scaling coefficient could have been used as well. The values of other two scaling coefficients are 1.02 for C2A model complex and 1.03 for the PHE dimer. The ΔE(MP2/CBS) values are summarized in Table 1.

Higher-order correlation correction for the GCGC and C2C2PD complexes were calculated slightly differently than for the other systems, these numbers were taken from our previous publications (ref 52 and 53). The GCGC was calculated at the CCSD(T)/6-31G**(0.25,0.15) level.[52] The C2C2PD complex at QCISD(T) level with basis set augmented with diffuse functions (aug-cc-pVDZ) on every second carbon atom only,

Table 1. MP2/CBS Interaction Energies (in kcal/mol) of the Simplified (Model) Complexes (See Figure 2) Calculated Using Nonaugmented and Augmented Dunning's (aug-)cc-pVXZ, X = D, T, Basis Sets

complex/method	MP2[CBS] (DZ → TZ)[a]	MP2[CBS] (aDZ → aTZ)[a]	MP2[CBS] (aDZ → aTZ)/ MP2[CBS] (DZ → TZ)δ[b]
C2A	−20.51	−20.82	1.02
GG	−5.56	−5.86	1.05
PHE-dimer	−13.26	−13.67	1.03
C8-dimer	−4.73	−4.80	1.01

[a]Two-point cubic extrapolation according to eqs 3 and 4. [b]The average value of the scaling factor is 1.03.

the rest of carbon atoms together with hydrogen atoms were described with nonaugmented basis set (cc-VDZ).[53] These two levels provide results similar to QCISD(T)/6-31G*(0.25), which was used for the rest of the complexes. This statement is supported by an observation that QCISD(T) and CCSD(T) methods deliver practically identical results for the interaction energies for similar systems,[59] as well as by extensive benchmarking of the 6-31G**(0.25,0.15) and 6-31G*(0.25) basis sets.[62,64] It is less obvious that the aDZ basis performs similarly to the 6-31G*(0.25) basis. Nevertheless, for larger complexes the results match surprisingly well.[63] We did not recalculate these two complexes at QCISD(T) level used for remaining complexes, because of high similarity between QCISD(T) and CCSD(T) techniques.

The presented strategy of obtaining reference binding energy has some limitations that should be mentioned. First, it is the accuracy of the MP2/CBS energies. For such large molecular systems there is not much evidence how effective is the counterpoise correction and whether it should be used or not. Our tests suggest that the CP correction should be applied, for more details see Tables S5 and S6 in the Supporting Information material and the discussion therein. Second, the scaling of the resulting MP2/CBS values also brings some degree of uncertainty. Nevertheless, we are convinced that the scaling improves the result, and that it is a legitimate approach since (a) the scaling is based on similar model systems that differ only in size (typically one-half or two-thirds of the size of the original molecule from the L7 set, octane is used as a model for octadecane, guanine dimer for guanine trimer, coronene for circumcoronene, amyloid chain dimer for amyloid chain trimer) and (b) the procedure is done separately for each specific molecule from the set. Finally, the calculation of the correction term, where the relatively small 6-31G*(0.25) basis set is used, is another potential source of uncertainty, but we should bear in mind that use of bigger basis set would not be feasible for cluster of presented size and that this basis set has been proven to work well in smaller systems. We may speculate that the same basis set should, in principle, provide better description of larger systems. This opinion is based on the observation that large basis sets, which provide satisfactory description in small systems tend to become overcomplete and numerically unstable in larger systems. The same effect should diminish under-completeness of small basis sets, when applied to large molecules.

Explicitly Correlated MP2-F12 Methods. The explictly correlated RI-MP2-F12 calculations with cc-pVDZ and cc-pVTZ basis set were utilized to estimate error in scaled MP2/CBS values (see above). Because of computational complexity

of these calculations along with extended size of the studied complexes explicitly correlated calculations were carried out only for GGG and GCGC complexes. The RI-MP2-F12/CBS values were obtained utilizing the Schwenke general type of extrapolation.[70]

MP2 and Scaled-MP2 Methods. MP2 along with its spin component scaled variants SCS-MP2 and SCS(MI)-MP2 were tested. The procedure for obtaining the MP2/CBS values is described in the previous paragraph. For calculation of the CBS value of the spin-component scaled MP2 methods, we refer to DiStasio et al.[14] The following scaling coefficients were used for the opposite-spin (os, "singlet") and same-spin (ss, "triplet") terms: SCS-MP2 $c_{os} = 1.20$, $c_{ss} = 0.33$; SCS(MI)-MP2 $c_{os} = 0.29$, $c_{ss} = 1.46$, regardless of the basis set.

Higher-Order Correlation Methods. The performance of several methods, which go beyond the MP2 level (marked as post-MP2): MP3, MP2.5, MP2.X, MP2C (not exactly a WFT method), and QCISD were investigated. The extrapolation procedure followed for these methods toward the CBS limit was the same as for the QCISD(T) benchmark, eq 1

$$\Delta E(\text{post-MP2/CBS}) = \Delta E(\text{MP2/CBS})' + \Delta(\text{post-MP2} - \text{MP2})|_{\text{small basis}} \quad (5)$$

To facilitate the discussion, we group the WFT methods into two categories: "non-empirical", QCISD, MP3, MP2C, and "empirical", MP2.5 and MP2.X.

Both QCISD and MP3 are traditional methods based on approximating the molecular wave function, while the MP2C method of Hesselmann[17,71] is slightly different. It combines time-dependent DFT with supramolecular MP2 energy, and therefore it cannot be correctly categorized as a nonempirical WFT method. However, it improves the MP2 results significantly with only a minor computational overhead, thus represents a promising strategy for noncovalent interaction calculations.[42,50]

The group of empirical methods includes methods with the inclusion of the third-order correlation contribution, MP2.X and MP2.5. The MP2.5 method, proposed by Pitoňák et al.,[72] takes advantage of the error cancellation between the MP2 (overestimation) and the MP3 (underestimation) binding energies.[11] The MP2.5 binding energy is obtained according eq 6 (the "small size basis set" used in the correction term is consistent with reference QCISD(T) calculation for each complex):

$$\Delta E(\text{MP2.5/CBS}) = \Delta E(\text{MP2/CBS})' + c[\Delta E(\text{MP3}) - \Delta E(\text{MP2})]|_{\text{small basis}} \quad (6)$$

with $c = 0.5$. Riley et al.[30] optimized the parameter c for the S66 data set and different basis set. For large basis sets c converges to 0.5 and for extended basis it is almost exactly 0.5. The MP2.X method is analogous to MP2.5, however, the coefficient c is optimized for a specific basis set. Excellent stabilization energies were obtained already for 6-31G*(0.25) basis set with $c = 0.62$.[30]

DFT Methods. In this group, the following approaches have been investigated: (a) Grimme's[71] DFT-D3 using the BLYP/def2-QZVP, B3-LYP/def2-QZVP, TPSS/def2-QZVP, PW6B95/def2-QZVP, and M06-2X/def2-QZVP combinations of the functional and the basis set.[15] These methods were tested with both the "zero" and the Becke−Johnson damping.[73−76] According to previous studies, these methods provide reasonably accurate description of dispersion interaction.[77] (b) Jurecka's DFT-D method with the TPSS/TZVP combination of the functional/basis set,[32] and (c) Truhlar's M06-2X functional with the def2-QZVP basis set.[33]

Semiempirical Quantum Chemical Methods. The PM6[36] based methods augmented with the empirical correction for the dispersion and the H-bonding interactions (PM6-D,[37] PM6-DH2,[78] and PM6-D3H4[38]) as well as the SCC-DFTB-D[79,80] method were investigated.

Computational Details. The DFT calculations (with the exception of M06-2X), and MP2 calculations were carried out using TURBOMOLE program package, versions 6.0, 6.1, and 6.4.[81] The single point calculations and gradient optimizations were done with a convergence threshold imposed on the change in energy between consecutive SCF iterations, and was set to 10^{-7} E_h; the geometry convergence criteria were unchanged from default values: energy change of 10^{-5} E_h and maximum gradient norm of 10^{-3} E_h/a_0. The integral neglect threshold was set by the program automatically: between 10^{-11} and 10^{-13} E_h and Turbomole grid m3 was used for all the calculations.

QCISD(T) calculations were done using the PQS program.[58] The integral neglect threshold was set to 10^{-15} E_h. The reason for such a tight threshold was to prevent any numerical problems resulting from possible linear dependencies in the basis set. The QCISD convergence criteria were set to 10^{-6} E_h for the maximum change in energy and the same threshold was imposed on the largest QCISD residuum element.

MP2C and RI-MP2-F12 calculations were performed using MOLPRO version 2009.[82] The integral neglect threshold was set to 10^{-12} E_h and 10^{-11} E_h for one-electron and two-electron integrals, respectively. The energy threshold and orbital threshold for the SCF procedure was set to 10^{-8} E_h. The maximum allowed eigenvalue of the overlap matrix was set to 10^{-8} E_h. The grid accuracy (per atom) in TDDFT part of MP2C calculation was set to 10^{-8} E_h. Density fitting approximation in MP2-F12 calculations (RI-MP2-F12) was done with cc-pVD(T)Z/JKFIT and cc-pVD(T)Z/MP2FIT basis sets and the following thresholds: neglect of contracted 3-index integrals in AO basis (10^{-10} E_h), neglect of half-transformed 3-index integrals (10^{-9} E_h), Schwarz screening threshold (10^{-5} E_h), neglect of 2-index integrals in AO basis (10^{-12} E_h), product screening threshold for first half transformation (10^{-9} E_h) and screening threshold for F12 integrals (10^{-8} E_h). Further, the 3C(FIX) *Ansatz* with geminal Slater exponent set to 1.0 were used.

MP3 calculations were performed using MOLCAS program package.[83] The Cholesky decomposition of two-electron integrals[84] was applied, with the integral threshold set to 10^{-5} E_h. The thresholds for the energy change, RMSD of the density matrix and RMSD of the Fock matrix were set to 10^{-5} E_h, 10^{-4} E_h, and 10^{-4} E_h, respectively.

The M06-2X calculations were carried out using Gaussian09[85] program package with the thresholds for the energy change and RMSD of the density matrix set to 10^{-5} and 10^{-7} E_h, respectively. The default grid with 75 radial shells and 302 angular points per shell was used in all the calculations.

PM6 calculations were carried out with MOPAC2009[86] program, the SCF convergence was set to 1.6×10^{-7} E_h. SCC-DFTB-D calculations were done via DFTB+[79,80] program, here

Table 2. Interaction Energies in kcal/mol of the Investigated Complexes at Different Levels of Theory[a]

method/basis set//complex	CBH	C2C2PD	C3A	C3GC	GCGC	GGG	PHE
QCISD(T)/CBS	−11.06	−24.36[b]	−18.19	−31.25	−14.37[c]	−2.40	−25.76
QCISD/CBS	−9.53	–	−14.52	−24.79	–	−1.30	−24.23
MP2.X/CBS	−10.63	−22.15	−15.52	−26.65	−12.26	−1.85	−25.24
MP2.5/CBS	−10.88	−22.80	−17.85	−30.40	−13.41	−2.34	−25.46
MP2C/CBS	−11.29	−20.88	−16.89	−28.71	−12.89	−2.22	−24.82
MP3/CBS	−9.84	−6.61	−8.15	−14.77	−8.61	−0.32	−24.56
MP2/CBS	−11.92	−38.98	−27.54	−46.02	−18.21	−4.36	−26.36
SCS(MI)-MP2/CBS[d]	−9.64	−31.71	−22.92	−37.92	−14.08	−2.23	−26.16
SCS-MP2/CBS[d]	−7.87	−27.53	−19.61	−32.07	−11.70	−1.79	−22.77
B3-LYP-D3/def2-QZVP[e]	−12.96	−23.22	−17.99	−31.29	−15.48	−2.10	−25.99
BLYP-D3/def2-QZVP[e]	−14.34	−22.82	−18.12	−31.79	−16.44	−2.48	−25.56
TPSS-D3/def2-QZVP[e]	−12.35	−21.19	−16.71	−28.58	−13.38	−1.87	−24.23
PW6D95-D3/def2-QZVP[e]	−10.01	−19.93	−16.63	−29.71	−12.48	−1.70	−24.07
M06−2X-D3/def2-QZVP[f]	−8.23	−20.55	−15.96	−29.00	−14.28	−1.71	−25.63
M06−2X/def2-QZVP	−4.71	−16.85	−12.88	−23.68	−11.59	−0.65	−23.38
TPSS-D/TZVP	−14.49	−18.69	−16.53	−27.78	−13.69	−2.19	−24.46
PM6-D3H4/SMB[g]	−9.64	−17.53	−16.01	−26.47	−19.87	−3.50	−25.43
PM6-DH2/SMB[g]	−9.96	−21.99	−18.04	−30.25	−22.55	−4.18	−24.91
PM6-D/SMB[g]	−9.96	−21.99	−18.04	−30.03	−20.99	−3.85	−22.80
SCC-DFTB-D/SMB[g]	−13.26	−18.7	−14.52	−24.41	−15.57	−1.08	−20.17

[a]The CBS limit is obtained according to eqs 1−6. [b]Correction term (cf., eq 2) was determined at QCISD(T) level using cc-pVDZ basis set for all atoms and the corresponding aug-cc-pVDZ basis set for every other, neighboring carbone atom. [c]Correction term (cf., eq 2) was determined at CCSD(T)/6-31G**(0.25,0.15) level of theory. [d]CBS limit calculated using cc-pVDZ and the cc-pVTZ basis sets. [e]Becke Johnson damping of the dispersion correction used. [f]Zero damping of the dispersion correction used. [g]SMB stands for "subminimal" basis set.

Table 3. Signed Errors (in kcal/mol) and the Respective Relative Values (in %) for the Investigated Complexes at Different Level of Theory[a]

method/bases//complex	CBH	C2C2PD	C3A	C3GC	GCGC	GGG	PHE
QCISD/CBS	1.53/13.8	–	3.67/20.2	6.46/20.7	–	1.10/45.9	1.53/5.9
MP2.X/CBS	0.43/3.9	2.20/9.1	2.67/14.7	4.61/14.7	2.11/14.7	0.54/22.7	0.52/2.0
MP2.5/CBS	0.18/1.6	1.56/6.4	0.34/1.9	0.86/2.7	0.96/6.7	0.06/2.5	0.30/1.2
MP2C/CBS	−0.24/−2.1	3.48/14.3	1.30/7.2	2.54/8.1	1.48/10.3	0.17/7.2	0.94/3.7
MP3/CBS	1.22/11.0	17.74/72.9	10.04/55.2	16.48/52.7	5.75/40.0	2.08/86.8	1.20/4.7
MP2/CBS	−0.86/−7.8	−14.63/−60.1	−9.35/−51.4	−14.77/−47.3	−3.84/−26.7	−1.96/−81.8	−0.60/−2.3
SCS(MI)-MP2/CBS[b]	1.41/12.8	−7.35/−30.2	−4.73/−26.0	−6.67/−21.4	0.29/2.0	0.16/6.8	−0.40/−1.6
SCS-MP2/CBS[b]	3.18/28.8	−3.17/−13.0	−1.42/−7.8	−0.82/−2.6	2.67/18.6	0.60/25.2	2.99/11.6
MP2/CBS[b]	−0.74/−6.7	−13.86/−56.9	−8.81/−48.4	−13.87/−44.4	−3.48/−24.2	−1.75/−73.1	0.17/0.7
B3-LYP-D3/def2-QZVP[c]	−1.90/−17.2	1.1/4.7	0.20/1.1	−0.03/−0.1	−1.1/−7.8	0.30/12.4	−0.23/−0.91
BLYP-D3/def2-QZVP[c]	−2.35/−21.3	−1.05/−4.3	−0.61/−3.3	−1.91/−6.1	−2.14/−14.9	−0.16/−6.8	0.80/3.1
TPSS-D3/def2-QZVP[c]	−1.29/−11.7	3.16/13.0	1.48/8.1	2.67/8.5	−0.99/−6.9	−0.53/−22.0	1.52/5.9
PW6D95-D3/def2-QZVP[c]	1.04/9.5	4.42/18.2	1.56/8.6	1.55/5.0	1.89/13.2	−0.70/−29.1	−1.68/−6.5
M06−2X-D3/def2-QZVP[d]	2.83/25.6	3.81/15.6	2.23/12.2	2.25/7.2	0.09/0.6	0.69/28.7	0.13/0.5
M06−2X/def2-QZVP	6.35/57.4	7.51/30.8	5.31/29.2	7.57/24.2	2.80/19.5	1.75/72.9	2.38/9.2
TPSS-D/TZVP	−3.43/−31.0	5.67/23.3	1.66/9.1	3.47/11.1	0.68/4.7	0.21/8.7	1.30/5.0
PM6-D3H4/SMB[e]	1.42/12.8	6.83/28.0	2.18/12.0	4.78/15.3	−5.50/−38.3	−1.10/−46.0	0.33/1.3
PM6-DH2/SMB[e]	1.10/9.9	2.37/9.7	0.15/0.8	1.00/3.2	−8.18/−57.0	−1.78/−74.4	0.85/3.3
PM6-D/SMB[e]	1.10/9.9	2.37/9.7	0.15/0.8	1.22/3.9	−6.62/−46.1	−1.45/−60.6	2.96/11.5
SCC-DFTB-D/SMB[e]	−2.20/−19.9	5.66/23.2	3.67/20.2	6.84/21.9	−1.20/−8.4	1.32/55.0	5.59/21.7

[a]Negative sign (−) indicates overestimation of the interaction energy. The CBS limit is obtained according to eqs 5−6. [b]CBS limit constructed using cc-pVDZ and cc-pVTZ basis sets. [c]Becke Johnson damping of the dispersion correction used. [d]Zero damping of the dispersion correction used. [e]SMB stands for "subminimal" basis set.

the threshold for self-consistent charge (SCC) procedure was set to 10^{-5} *e*.

All the calculations presented in this study, except for the semiempirical ones, were done using spherical basis functions, if not explicitly stated otherwise.

Error Analysis. The performance of the studied methods with respect to the benchmark results is measured by the following statistical indicators: root mean square deviation (RMSD), mean unsigned error (MUE), mean signed error (MSE), and maximum unsigned error (MAX). RMSD and MUE characterize the overall accuracy of a method. MSE provides information about systematic errors. MAX identifies the worst described entity and thus it measures the robustness of the method. The total binding energies for the noncovalent complexes investigated vary significantly, from 2 to 32 kcal/mol. Hence, the relative (percentage) values marked with prefix

"r", defined as $100 \times (\Delta E_{method} - \Delta E_{reference})/\Delta E_{reference}$ are more appropriate for the comparison across the whole data set.

RESULTS AND DISCUSSION

Table 1 summarizes the MP2/CBS interaction energies for four model complexes, obtained from extrapolating the augmented and nonaugmented cc-pVXZ, X = D, T basis sets to the basis set limit. The extrapolated values of stabilization energies follow the expectations that the former are larger than the later ones, thus leading to the scaling coefficients above one. The variation of the scaling coefficients, as already noted, is surprisingly small, in orders of only few percent (1−5%). This is most likely the consequence of the basis set saturation already at the nonaugmented level due to the extended size of the investigated complexes.

Interaction energies obtained at various levels of theory for all seven complexes are listed in Table 2. Signed errors and the corresponding relative values are shown separately in Table 3. Statistical quantities, that is, RMSD, MSE, MUE, and MAX for the tested methods are summarized in Table 4. In Figure 3, the relative signed errors for the best performing method within the specific subgroup (for more details see Error Analysis section) are visualized, while Figure 4 depicts the relative RMSD for all methods.

Only the results obtained using the largest basis set for a particular complex and theoretical method are discussed below, separately for each group of methods. To emphasize the effect of large cluster size, presented data are compared to results obtained for the S66 data set which contains smaller systems.

Table 4. Set of Statistical Measures (in kcal/mol) Calculated with Respect to the Reference (QCISD(T)/CBS) Data for the Investigated Complexes[a]

method/basis set//statis. measure	RMSD	MUE	MSE	MAX
QCISD/CBS[b]	3.50	2.86	2.86	6.46
MP2.X/CBS	2.34	1.87	1.87	4.61
MP2.5/CBS	0.79	0.61	0.61	1.56
MP2C/CBS	1.83	1.45	1.38	3.48
MP3/CBS	10.19	7.79	7.79	17.74
MP2/CBS	8.78	6.57	−6.57	14.77
SCS-MP2/CBS[c]	2.37	2.12	0.58	3.18
SCS(MI)-MP2/CBS[c]	4.20	3.00	−2.47	7.35
B3-LYP-D3/def2-QZVP[d]	0.95	0.70	−0.24	1.90
BLYP-D3/def2-QZVP[d]	1.60	1.39	−1.16	2.36
TPSS-D3/def2-QZVP[d]	1.87	1.66	−1.29	3.16
PW6D95-D3/def2-QZVP[d]	2.15	1.83	−1.83	4.42
M06−2X-D3/def2-QZVP[e]	2.17	1.72	1.72	3.81
M06−2X/def2-QZVP	5.33	4.81	4.81	7.57
TPSS-D/TZVP[f]	2.95	2.34	1.36	5.67
PM6-D3H4/SMB[g]	3.92	3.16	1.28	6.83
PM6-DH2/SMB[g]	3.35	2.20	−0.64	8.18
PM6-D/SMB[g]	3.00	2.27	0.04	6.62
SCC-DFTB-D/SMB[g]	4.33	3.78	2.81	6.84

[a]The CBS limit is obtained according to eqs 5 and 6. [b]Statistical measures are calculated only for five out of seven complexes (C2C2PD and GCGC complexes omitted). [c]CBS limit constructed using cc-pVDZ and cc-pVTZ basis sets. [d]Becke Johnson damping of the dispersion correction used. [e]Zero damping of the dispersion correction used. [f]Jurecka's dispersion correction. [g]SMB stands for "subminimal" basis set.

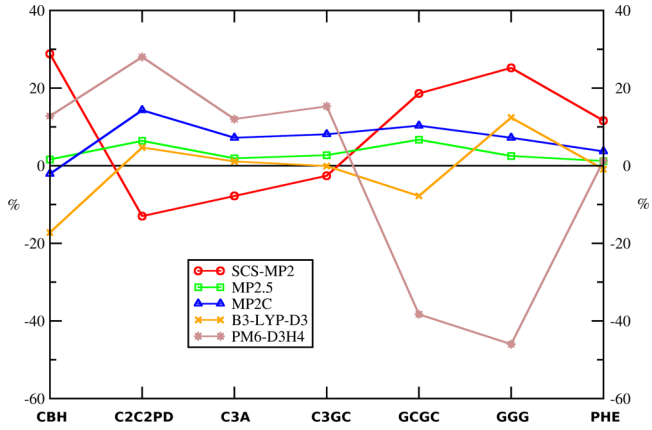

Figure 3. Relative signed errors (in %) of SCS-MP2, MP2.5, MP2C, BLYP-D3 (Becke−Johnson damping), and PM6-D3H4 methods for the investigated complexes. Negative sign (−) indicates overestimation of the interaction energy. Methods listed are the best performing methods within each category of methods: (a) post-HF wave function theory (WFT) methods containing empirical parameters (SCS-MP2, MP2.5, MP2C), (b) DFT based methods with added dispersion terms (BLYP-D3 (Becke-Johnson damping)), and (c) semiempirical quantum mechanical methods augmented with empirical corrections for noncovalent interactions (PM6-D3H4).

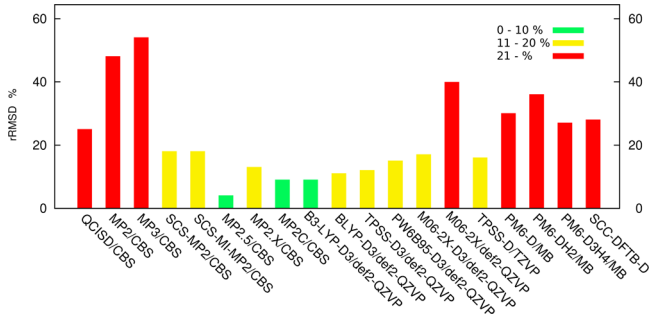

Figure 4. Relative RMSD (rRMSD in %) with respect to the reference (QCISD(T)/CBS) for the investigated methods.

QCISD. Comparison of the QCISD values (Table 2) with the reference QCISD(T) data (provided only for 5 complexes, see QCISD(T)/CBS as the Reference section) confirms the well-known fact that the contribution of the triples is substantial. The RMSD and rRMSD values are rather large, 3.5 kcal/mol and 25%, respectively (cf., Table 4 and Figure 4). For the C3GC complex, the error even exceeded 6 kcal/mol (20%) (cf., Table 3).

MP2. The accuracy of the MP2 method, documented by RMSD value of 8.8 kcal/mol, is poor (cf., Table 4). This is a consequence of the data set being dominated by $\pi\cdots\pi$ stacked interactions. The span of relative errors for $\pi\cdots\pi$ dispersion dominated complexes is large 27−82% (see Table 3). However, signed errors of −0.9 kcal/mol (8%) for the CBH complex and −0.6 kcal/mol (2%) for the PHE trimer (cf., Table 3) confirms that MP2 properly describes the aliphatic dispersion and hydrogen bonding.[7,32]

The explicitly correlated RI-MP2-F12 calculations with cc-pVDZ and cc-pVTZ basis set were utilized in order to estimate error in scaled MP2/CBS values (cf. Methods; for more information see Table S6 in the Supporting Information material). The absolute (relative) underestimation of scaled MP2/CBS stabilization energy with respect to RI-MP2-F12/

dx.doi.org/10.1021/ct400036b | J. Chem. Theory Comput. 2013, 9, 3364−3374

CBS values is 0.39 (9%) and 1.57 (9%) kcal/mol for GGG and GCGC complexes, respectively. On the basis of these values, we can estimate the relative error in scaled MP2/CBS values.

Scaled MP2. Empirically scaling the spin components in MP2 improves the description of noncovalent interactions,[12] particularly for π stacking. Our RMSD and relative RMSD values for MP2, SCS-MP2, and SCS(MI)-MP2[52] are 8.8 (48%), 2.4 (18%), and 4.2 (18%), respectively (cf., Table 4 and Figure 4). However, the performance for some dispersion dominated complexes is still inadequate, for example, the signed error for C2C2PD at the SCS(MI)-MP2 level is −7.4 kcal/mol (−30%) (cf. Table 3). According to the results in Table 4, SCS(MI)-MP2 performs worse than the original SCS-MP2. This is surprising, considering that SCS(MI)-MP2 was, unlike SCS-MP2, parametrized toward the best performance on interaction energies. Comparing the performance of both methods for dispersion dominated complexes in the S66 set, the opposite conclusion in obtained. The relative RMSD of SCS(MI)-MP2 and SCS-MP2 are 18% and 26%, respectively,[42] which indicates that the size of the investigated molecular cluster has a significant effect. SCS-MP2 underestimates the bonding between aliphatic species.[87,51] The relative error, roughly 30% for the aliphatic CBH complex, is among the largest from all the methods within the group (cf., Table 3 and Figure 3) confirms this observation.

MP3, MP2.5, MP2.X, and MP2C. The performance of the plain MP3 method is poor, perhaps comparable with MP2 in the RMSD, MUE, and MAX values (cf. Table 4). Typical feature of the MP3 method is underestimation of the aromatic dispersion interaction (MSE about 7.8 kcal/mol, cf. Table 4), contrary to MP2 (MSE about −6.6 kcal/mol, cf. Table 4). However, both MP2 and MP3 describe hydrogen bonded complexes very well. The error cancellation between MP2 and MP3 is responsible for substantially higher accuracy of MP2.5, with RMSD of only about 0.8 kcal/mol (4%, cf. Table 4 and Figure 4). A statistical evaluation of the MP2.X performance gives 2.3, 1.9, and 4.6 kcal/mol and 13% for RMSD, MUE, MAX, and rRMSD, respectively (cf. Table 4), which is quite good. MP2.X outperforms both scaled-MP2 variants. However, its performance is worse than MP2.5, in spite of the optimization of the mixing parameter (cf. Table 3 and 4). This is most likely a consequence of parametrization toward substantially smaller molecular clusters in the S66 data set.

The MP2C method shows a real improvement over MP2. In terms of the relative errors, it is the second best performer among the WFT methods evaluated in this work with an rRMSD of about 8% (1.8 kcal/mol, cf. Table 4 and Figure 4) and an rMAX of 14% (3.5 kcal/mol) (for the coronene dimer, cf. Table 3 and 4).

DFT Methods. The performance of the group of functionals augmented with the Grimme's D3 correction utilizing the Becke-Johnson (B-J) damping is better in comparison with the Zero damping (cf., Table S1−S4 in Supporting Information). These results are consistent with findings of Grimme, where the use of the DFT-D3 methods with B−J damping yield better results for most of the functionals.[77] Hence, in this paper, we will discuss almost exclusively DFT-D3 methods using B-J damping procedure. The M06-2X-D3 method will be discussed in combination with Zero damping, because there are no B−J damping parameters for the D3 correction. The best performing functional is the B3-LYP followed by the BLYP, TPSS, PW6B95, and M06-2X. Corresponding RMSD in kcal/mol (rRMSD in %) are 1.0 (9), 1.6 (11), 1.9 (12), 2.2 (15), and 2.2 (17), cf. Table 4 and Figure 4. The performance of the PW6B95 and the M06−2X are almost equivalent (cf. Table 4). In Grimme's study, where different DFT functional were tested against the S66 data set, the best performing functional for the dispersion bounded subset was B3-LYP.[77] This is consistent with our findings. The relative ordering of other functionals in this paper is different compared to Grimme's study.[77] However, the absolute differences in performance of functionals are, in both studies, of order of tenths of kcal/mol. Hence, any definitive conclusions about the general performance based on these results would be questionable.

The M06-2X method in combination with zero damping form of the D3 correction leads to the RMSD value of 2.2 kcal/mol (17%) as already mentioned. The plain M06-2X functional provides substantially larger value of the RMSD 5.3 kcal/mol or 40% (cf. Table 4). All the statistical indicators are reduced, two to three times, after applying D3 correction (cf. Table 4). This result serves as the proof that functionals which were fitted to reproduce dispersion near van der Waals minimum (for example M06-2X) are not able to cover long-range dispersion interaction. This feature was already demonstrated by Grimme.[77]

On the basis of the findings from Grimme's study, the double-hybrid functionals should provide even better performance than the B3-LYP.[88] Moreover, it was shown that double-hybrids as DSD-BLYP-D3 or PWPB95-D3 outperform scaled variants of MP2 such as SCS-MP2, S2-MP2, and SOS-MP2 methods.[88] However, we should bear in mind that the computational complexity of the double-hybrids is higher when compared with other groups of functionals. Methods involving double-hybrid functionals include nonlocal perturbation correction for the correlation part; hence their scaling is equivalent to the regular MP2 method.

The magnitude of the many-body nonadditivity term is by an order of magnitude smaller than the interaction energies.[52,89] It is believed that the three-body (Axilrod−Teller−Mutto) correction term is non-negligible for extended molecular systems.[19,49] When it is implemented as described in ref 19 and is added to the Becke−Johnson and zero-damped dispersion, it weakens the interaction. Because it is not known much about the 3-body correction and its impact on the accuracy of a method, the results are only listed in Supporting Information (cf., Table S1−S4), without any further discussion. In general the accuracy of the DFT-D3 methods after applying the 3-body correction deteriorates. The only exception is the BLYP functional in combination with B-J damping. The RMSD is reduced from 1.6 kcal/mol (11%) to 1.1 kcal/mol (9%), cf., Table S4 in Supporting Information. The same correction, when added to the zero-damped results, raises the overall error to 2.0 kcal/mol (12%), cf., Table S4 in Supporting Information. . In Grimme's study,[49] it was shown that the three-body correction is not negligible, and it correlates positively with the size of a molecule. In the S12L set, this effect varies between 2% and 15% of the total stabilization energy. Moreover, the inclusion of three-body correction in the DFT values of binding energies at quadruple-ζ level improves the overall performance of the investigated methods even in smaller systems (for more details see ref 49.).

The TPSS-D/TZVP method of Jurečka et al.[32] performs slightly worse than tested density functionals with D3 correction but clearly better than the M06−2X/def2-QZVP method of Zhao and Truhlar, with RMSD of 3.0 kcal/mol (16%) and 5.3 kcal/mol (40%) (cf. Table 4 and Figure 4),

respectively. The direct comparison of the TPSS-D/TZVP with the TPSS-D3/def2-QZVP reveals that the latter method is slightly more accurate. However, this comparison is not completely fair because of the unequal quality of the used basis sets. The def2-QZVP basis set is of better quality than TZVP which could be the reason for the higher accuracy. The TPSS-D/TZVP combination of the functional and the basis set was chosen as the best feasible. The use of the TPSS-D/6-311++G(3df,3pd) method, which should provide best results for dispersion bounded complexes,[32] was not possible, due to problems with linear dependences in the basis set in the case of the coronene dimer and circumcoronene. This issue is discussed in the Interaction Energy Calculation subsection.

DFT methods describe H-bonding (or electrostatic dominated interactions in general) fairly well (see Table 3 and Figure 3), and empirically corrected DFT-D and DFT-D3 methods share a similar feature. Signed errors for the H-bonded PHE complex (ranging from 0.2 to 2.4 kcal/mol, that is, 1−9%, cf., Table 3) are significantly lower than for other complexes. Dispersion dominated interactions are described less accurately. The largest signed errors of Grimme's (DFT-D3) methods are: 4.4 kcal/mol (18%) in the case of C2C2PD complex for PW6D95 functional and −2.1 kcal/mol (8%) in the case of GCGC complex for BLYP functional (see Table 3). The latter one is the largest negative error for all DFT methods considered here. Aliphatic dispersion, for instance in the CBH complex, is even worse: the signed errors range from −1.3 kcal/mol up to 6.4 kcal/mol (see Table 3).

Semiempirical Methods. The PM6 method,[36] corrected for dispersion[37] (PM6-D) gives an RMSD of 3.0 kcal/mol, see Table 4. Correction for hydrogen bonding[38,78] (PM6-DH2, PM6-D3H4) does not, however, increase of accuracy further (RMSD of 3.4 and 3.9 kcal/mol, respectively) (cf., Table 4). The correction for hydrogen bonding is most likely the source of undesirable errors, and it is responsible for slightly worse correlation with the benchmark data for complexes stabilized by dispersion interaction. On the other hand, errors decrease significantly for the PHE complex upon inclusion of the hydrogen bonding correction: the signed error drops from 3.0 (PM6-D) to 0.9 (PM6-DH2) and 0.3 (PM6-D3H4) kcal/mol, respectively (cf., Table 3). The SCC-DFTB-D method[79,80] is comparable with that of PM6-D3H4 (cf., Table 4). In terms of relative RMSD, the ordering of the semiempirical methods we tested is the following: SCC-DFTB-D and PM6-D3H4, roughly equal, are the most accurate, followed by PM6-D and PM6-DH2 (cf., Figure 4). The rRMSD and rMAX values vary between 26−36% and 46−74%, respectively (cf., Table 4). Nevertheless, the absolute errors of the semiempirical methods are comparable with some of more sophisticated methods such as M06-2X/def2-QZVP, MP2/CBS, MP3/CBS, or SCS(MI)-MP2 (see Table 4).

CONCLUSIONS

Seven extended molecular complexes, stabilized mostly by dispersion interaction, were investigated with a number of modern quantum chemical methods. This set of molecules, called the L7 set, includes the octadecane dimer, the circumcoronene···adenine dimer, the circumcoronene···guanine−cytosine dimer, the coronene dimer, the guanine−cytosine dimer, the guanine trimer, and a trimer of amyloid residues containing phenylalanine. These complexes are representative of dispersion-dominated supramolecular associations in biological systems, although a few systems have also significant hydrogen bonding. The methods include wave function-based, density functional based and semiempirical methods, spanning a wide range of accuracy and computational cost. We have included both fully nonempirical wave function methods, such as MP2, MP3, and QCISD, and methods which contain adjustable parameters. The parametrized methods perform in general better, justifying their use for larger molecular clusters. The performance of the methods was evaluated by comparing them to high-level QCISD(T) (and CCSD(T)) results. These benchmark results, along with the geometries of the L7 complexes, are available online in the BEGDB database (www.begdb.com).

The results of this large-molecule test set differ from earlier results for smaller complexes, most likely because the large molecule test set emphasizes longer-range interactions. The best method in this study in absolute performance is MP2.5, delivering binding energies with an average error of 4% relative to QCISD(T). The performance of the MP2.X method, parametrized toward noncovalent interactions, is surprisingly slightly worse. MP2C provides fairly accurate results, with an average relative error of 8%. It has a clear computational advantage over the MP2.5 by being an order of magnitude faster. The SCS-MP2 and SCS-(MI)-MP2 methods are rather disappointing, although they perform better for this test set than for the S66 data set of medium-sized noncovalent complexes. SCS-MP2 does not resolve fully the overbinding of MP2 for π stacking, while it underestimates dispersion between σ systems.

Among density functional based methods, DFT-D3 is clearly superior to other approaches tested in this work. It represents the best trade-off between the accuracy and computational cost and, at an average relative error of only 11%, it outperforms some more sophisticated methods, such as SCS(MI)-MP2 or M06-2X.

The accuracy of the semiempirical quantum mechanical methods, with empirical corrections for dispersion or hydrogen bonding is less satisfactory. The best are SCC-DFTB-D and PM6-D3H4, and their relative standard deviation exceeds 25%. Nevertheless, the performance of these methods is not much worse than that of dramatically more expensive ones, such as M06-2X, MP2, or SCS(MI)-MP2, and thus their price/performance ratio is excellent.

ASSOCIATED CONTENT

Supporting Information

Detailed DFT-D3 results for presented complexes together with their full geometry information are provided. This material is available free of charge via Internet at http://pubs.acs.org/.

AUTHOR INFORMATION

Corresponding Author

*E-mail: robert.sedlak@uochb.cas.cz (R.S.); janowski@uark.edu (T.J.); pavel.hobza@uochb.cas.cz (P.H.).

Notes

The authors declare no competing financial interest.

ACKNOWLEDGMENTS

This work was a part of RVO No. 61388963 of the Institute of Organic Chemistry and Biochemistry, Academy of Sciences of the Czech Republic, and was supported by Czech Science Foundation, Project No. P208/12/G016 and the operational program Research and Development for Innovations of

European Social Fund (CZ1.05/2.1.00/03/0058). This work was also supported by the Slovak Research and Development Agency, Contract No. APVV-0059-10. Support by the U.S. National Science Foundation (CHE-0911541 and CHE-1213870), by the National Institute of General Medical Sciences of the National Institutes of Health under a COBRE phase III pilot project (P30 GM103450-03), the Arkansas Biosciences Institute, and by the Mildred B. Cooper Chair at the University of Arkansas are gratefully acknowledged. We thank Prof. Jon Baker for implementing DFT-D3 in PQS.

REFERENCES

(1) Riley, K. E.; Hobza, P. *Acc. Chem. Res.* **2013**, *46*, 927−936.
(2) Hohenstein, E. G.; Sherrill, C. D. *Wiley Interdiscip. Rev.: Comput. Mol. Sci.* **2012**, *2*, 304−326.
(3) Vondrášek, J.; Kubař, T.; Jenney, F. E.; Adams, M. W. W.; Kožíšek, M.; Černý, J.; Sklenář, V.; Hobza, P. *Chem.—Eur. J.* **2007**, *13*, 9022−9027.
(4) Šponer, J.; Leszczynski, J.; Hobza, P. *Biopolymers* **2001**, *61*, 3−36.
(5) Šponer, J.; Leszczynski, J.; Hobza, P. *J. Mol. Struct (THEOCHEM)* **2001**, *573*, 43−53.
(6) Kristyán, S.; Pulay, P. *Chem. Phys. Lett.* **1994**, *229*, 175−180.
(7) Perez-Jorda, J. M.; Becke, A. D. *Chem. Phys. Lett.* **1995**, *233*, 134−137.
(8) Hobza, P.; Šponer, J.; Reschel, T. *J. Comput. Chem.* **1995**, *16*, 1315−1325.
(9) Janowski, T.; Pulay, P. *Chem. Phys. Lett.* **2007**, *447*, 27−32.
(10) Sinnocrot, M. O.; Valeev, E. F.; Sherrill, C. D. *J. Am. Chem. Soc.* **2002**, *124*, 10887−10893.
(11) Riley, K. E.; Pitoňák, M.; Jurečka, P.; Hobza, P. *Chem. Rev.* **2010**, *110*, 5023−5063.
(12) Grimme, S. *J. Chem. Phys.* **2003**, *118*, 9095−9102.
(13) Marchelli, O.; Werner, H.-J. *J. Phys. Chem. A* **2009**, *113*, 11580−11585.
(14) Distasio, A. R., Jr.; Head-Gordon, M. *Mol. Phys.* **2007**, *105*, 1073−1083.
(15) Takatani, T.; Hohenstein, E. G.; Sherrill, C. D. *J. Chem. Phys.* **2008**, *128*, 124111/1−7.
(16) Zhao, Y.; Truhlar, D. G. *Acc. Chem. Res.* **2008**, *41*, 157−167.
(17) Hesselmann, A. *J. Chem. Phys.* **2008**, *128*, 144112.
(18) Chermak, E.; Mussard, B.; Angyan, Jj. G.; Reinhardt, P. *Chem. Phys. Lett.* **2012**, *550*, 162−169.
(19) Grimme, S.; Antony, J.; Ehrlich, S.; Krieg, H. *J. Chem. Phys.* **2010**, *132*, 154104/1−17.
(20) Schütz, M.; Werner, H.-J. *Chem. Phys. Lett.* **2000**, *318*, 370−378.
(21) Jeziorski, B.; Moszynski, R.; Szalewicz, K. *Chem. Rev.* **1994**, *94*, 1887−1930.
(22) Misquitta, A. J.; Szalewicz, K. *Chem. Phys. Lett.* **2002**, *357*, 301−306.
(23) Hesselmann, A.; Jansen, G. *Chem. Phys. Lett.* **2002**, *357*, 464−470.
(24) von Lilienfeld, O. A.; Tavernelli, I.; Rothlisberger, U.; Sebastiani, D. *Phys. Rev. Lett.* **2004**, *93*, 153004/1−4.
(25) DiLabio, G. A. *Chem. Phys. Lett.* **2008**, *455*, 348−353.
(26) Dion, M.; Rydberg, H.; Schröder, E.; Langreth, D. C.; Lundqvist, B. I. *Phys. Rev. Lett.* **2004**, *92*, 246401/1−4.
(27) Dion, M.; Rydberg, H.; Schröder, E.; Langreth, D. C.; Lundqvist, B. I. *Phys. Rev. Lett.* **2005**, *95*, 109902/1.
(28) Becke, A. D.; Johnson, E. R. *J. Chem. Phys.* **2007**, *127*, 154108/1−6.
(29) Pitoňák, M.; Neogrády, P.; Černý, J.; Grimme, S.; Hobza, P. *Phys. Chem. Chem. Phys.* **2009**, *10*, 282−289.
(30) Riley, E. K.; Řezáč, J.; Hobza, P. *Phys. Chem. Chem. Phys.* **2011**, *13*, 21121−21125.
(31) Grimme, S. *J. Comput. Chem.* **2006**, *27*, 1787−1799.
(32) Jurečka, P.; Černý, J.; Hobza, P.; Salahub, D. R. *J. Comput. Chem.* **2007**, *28*, 555−569.
(33) Zhao, Y.; Truhlar, D. G. *Theor. Chem. Acc.* **2008**, *120*, 215−241.
(34) Dewar, J. S. M.; Thiel, W. *J. Am. Chem. Soc.* **1977**, *99*, 4899−4907.
(35) Martin, B.; Clark, T. *Int. J. Quantum Chem.* **2006**, *106*, 1208−1216.
(36) Stewart, J. J. P. *J. Mol. Model.* **2007**, *13*, 1173−1213.
(37) Řezáč, J.; Fanfrlik, J.; Salahub, D.; Hobza, P. *J. Chem. Theory Comput.* **2009**, *5*, 1749−1760.
(38) Řezáč, J.; Hobza, P. *J. Chem. Theory Comput.* **2012**, *8*, 141−151.
(39) Jurečka, P.; Šponer, J.; Černý, J.; Hobza, P. *Phys. Chem. Chem. Phys.* **2006**, *8*, 1985−1993.
(40) Gráfová, L.; Pitoňák, M.; Řezáč, J.; Hobza, P. *J. Chem. Theory Comput.* **2010**, *6*, 2365−2376.
(41) Molnar, L.; He, X.; Wang, B.; Merz, K. *J. Chem. Phys.* **2009**, *131*, 065102/1−16.
(42) Řezáč, J.; Riley, K. E.; Hobza, P. *J. Chem. Theory Comput.* **2011**, *7*, 2427−2438, 3466−3470.
(43) Goerigk, L.; Grimme, S. *J. Chem. Theory Comput.* **2010**, *6*, 107−126.
(44) Goerigk, L.; Grimme, S. *J. Chem. Theory Comput.* **2011**, *7*, 291−309.
(45) Zhao, Y.; Truhlar, D. G. *J. Chem. Theory Comput.* **2005**, *1*, 415−432.
(46) Zhao, Y.; Truhlar, D. G. *J. Phys. Chem. A* **2005**, *109*, 5656−5667.
(47) Zhao, Y.; Truhlar, D. G. *J. Chem. Theory Comput.* **2007**, *3*, 289−300.
(48) Berka, K.; Laskowski, R.; Hobza, P.; Vondrášek, J. *J. Chem. Theory Comput.* **2010**, *6*, 2191−2203.
(49) Risthaus, T.; Grimme, S. *J. Chem. Theory Comput.* **2013**, *9*, 1580−1591.
(50) Granatier, J.; Pitoňák, M.; Hobza, P. *J. Chem. Theory Comput.* **2012**, *7*, 2282−2292.
(51) Janowski, T.; Pulay, P. *J. Am. Chem. Soc.* **2012**, *134*, 17520−17525.
(52) Pitoňák, M.; Neogrády, P.; Hobza, P. *Phys. Chem. Chem. Phys.* **2010**, *12*, 1369−1378.
(53) Janowski, T.; Ford, A. R.; Pulay, P. *Mol. Phys.* **2010**, *108*, 249−257.
(54) Hays, F. A.; Teegarden, A.; Jones, Z. J.; Harms, M.; Raup, D.; Watson, J.; Cavaliere, E.; Ho, P. S. *Proc. Natl. Acad. Sci. U.S.A.* **2005**, *102*, 7157−7162.
(55) Case, A. D.; Darden, A. T.; Cheatham, E. T., III; Simmerling, L. C.; Wang, J.; Duke, E. R.; Luo, R.; Merz, M. K.; Pearlman, A. D.; Crowley, M.; Walker, C. R.; Zhang, W.; Wang, B.; Hayik, S.; Roitberg, A.; Seabra, G.; Wong, F. K.; Paesani, F.; Wu, X.; Brozell, S.; Tsui, V.; Gohlke, H.; Yang, L.; Tan, C.; Mongan, J.; Hornak, V.; Cui, G.; Beroza, P.; Mathews, H. D.; Schafmeister, C.; Ross, S. W.; Kollman, A. P. *AMBER 9*; University of California: San Francisco, CA, 2006.
(56) Řezáč, J.; Jurečka, P.; Riley, K. E.; Černý, J.; Valdes, H.; Pluháčková, K.; Berka, K.; Řezáč, T.; Pitoňák, M.; Vondrášek, J.; Hobza, P. *Collect. Czech. Chem. Commun.* **2008**, *73*, 1261−1270.
(57) Boys, S. F.; Bernardi, F. *Mol. Phys.* **1970**, *19*, 553−566.
(58) Baker, J.; Wolinski, K.; Janowski, T.; Saebo, S.; Pulay, P. *PQS*, version 4.0; Parallel Quantum Solutions: Fayetteville, Arkansas, USA, 2012; www.pqs-chem.com.
(59) Janowski, T.; Pulay, P. *Chem. Phys. Lett.* **2007**, *447*, 27−32.
(60) Jurečka, P.; Hobza, P. *Chem. Phys. Lett.* **2002**, *365*, 89−94.
(61) van Lenthe, J. H.; van Duijneveldt-van de Rijdt, J. G. C. M.; van Duijneveldt, F. B. *Adv. Chem. Phys.* **1987**, *69*, 521−544.
(62) Hobza, P.; Šponer. *J. Chem. Rev.* **1999**, *99*, 3247−3276.
(63) Svozil, D.; Hobza, P.; Šponer, J. *J. Phys. Chem. B* **2010**, *114*, 1191−1203.
(64) Riley, E. K.; Řezáč, J.; Hobza, P. *Phys. Chem. Chem. Phys.* **2011**, *13*, 21121−21125.
(65) Halkier, A.; Helgaker, T.; Jorgensen, P.; Klopper, W.; Koch, H. J.; Wilson, K. A. *Chem. Phys. Lett.* **1998**, *286*, 243−252.
(66) Halkier, A.; Helgaker, T.; Jorgensen, P.; Klopper, W.; Olsen, J. *Chem. Phys. Lett.* **1999**, *302*, 437−446.
(67) Kendall, R. A.; Dunning, T. H., Jr.; Harrison, R. J. *J. Chem. Phys.* **1992**, *96*, 6796−806.

(68) Woon, D. E.; Dunning, T. H., Jr. *J. Chem. Phys.* **1993**, *98*, 1358−1371.
(69) Dunning, T. H., Jr. *J. Chem. Phys.* **1989**, *90*, 1007−1023.
(70) Schwenke, D. W. *J. Chem. Phys.* **2007**, *122*, 014107/1−7.
(71) Pitoňák, M.; Hesselmann, A. *J. Chem. Theory Comput.* **2010**, *6*, 168−178.
(72) Pitoňák, M.; Neogrády, P.; Černý, J.; Grimme, S.; Hobza, P. *Chem. Phys. Chem.* **2009**, *10*, 282−289.
(73) Grimme, S.; Ehrlich, S.; Goerigk, L. *J. Comput. Chem.* **2011**, *32*, 1456−1465.
(74) Johnson, E. R.; Becke, A. D. *J. Chem. Phys.* **2005**, *123*, 024101/1−7.
(75) Becke, A. D.; Johnson, E. R. *J. Chem. Phys.* **2005**, *123*, 154101/1−9.
(76) Johnson, E. R.; Becke, A. D. *J. Chem. Phys.* **2006**, *124*, 174104/1−9.
(77) Goerigk, L.; Kruse, H.; Grimme, S. *Chem Phys Chem* **2011**, *12*, 3421−3433.
(78) Korth, M.; Pitoňák, M.; Řezáč, J.; Hobza, P. *J. Chem. Theory Comput.* **2010**, *6*, 168−178.
(79) Elstner, M.; Porezag, D.; Jungnickel, G.; Elsner, J.; Haugk, M.; Frauenheim, T.; Suhai, S.; Seifert, G. *Phys. Rev. B* **1998**, *58*, 7260−7268.
(80) Elstner, M.; Hobza, P.; Frauenheim, T.; Suhai, S.; Kaxiras, E. *J. Chem. Phys.* **2001**, *114*, 5149−5155.
(81) Ahlrichs, R.; Bär, M.; Häser, M.; Horn, H.; Kölmel, C. *Chem. Phys. Lett.* **1989**, *162*, 165−169.
(82) Werner, H.-J; Knowles, P. J.; Lindh, R.; Manby, F. R.; Schütz, M.; Celani, P.; Korona, T.; Mitrushenkov, A.; Rauhut, G.; Adler, T. B.; Amos, R. D.; Bernhardsson, A.; Berning, A.; Cooper, D. L.; Deegan, M. J. O.; Dobbyn, A. J.; Eckert, F.; Goll, E.; Hampel, C.; Hetzer, G.; Hrenar, T.; Knizia, G.; Köppl, C.; Liu, Y.; Lloyd, A. W.; Mata, R. A.; May, A. J.; McNicholas, S. J.; Meyer, W.; Mura, M. E.; Nicklass, A.; Palmieri, P.; Pflüger, K.; Pitzer, R.; Reiher, M.; Schumann, U.; Stoll, H.; Stone, A. J.; Tarroni, R.; Thorsteinsson, T.; Wang, M.; Wolf, A. MOLPRO, A package of ab initio programs, version 2009.1. http://www.molpro.net.
(83) (a) Karlstrom, G.; Lindh, R.; Malmqvist, P. A.; Roos, B. O.; Ryde, U.; Veryazov, V.; Widmark, P. O.; Cossi, M.; Schimmelpfennig, B.; Neogrady, P.; Seijo, L. *Comput. Mater. Sci.* **2003**, *28*, 222−239. (b) Malmqvist, P. A.; Rendell, A.; Roos, B. O. *J. Phys. Chem.* **1990**, *94*, 5477−5482. (c) Roos, B. O.; Taylor, P. R. *Chem. Phys.* **1980**, *48*, 157−173.
(84) Beebe, N. H. F.; Linderberg, J. *Int. J. Quantum Chem.* **1977**, *12*, 683−705.
(85) Frisch, M. J.; Trucks, G. W.; Schlegel, H. B.; Scuseria, G. E.; Robb, M. A.; Cheeseman, J. R.; Scalmani, G.; Barone, V.; Mennucci, B.; Petersson, G. A.; Nakatsuji, H.; Caricato, M.; Li, X.; Hratchian, H. P.; Izmaylov, A. F.; Bloino, J.; Zheng, G.; Sonnenberg, J. L.; Hada, M.; Ehara, M.; Toyota, K.; Fukuda, R.; Hasegawa, J.; Ishida, M.; Nakajima, T.; Honda, Y.; Kitao, O.; Nakai, H.; Vreven, T.; Montgomery, J. A., Jr.; Peralta, J. E.; Ogliaro, F.; Bearpark, M.; Heyd, J. J.; Brothers, E.; Kudin, K. N.; Staroverov, V. N.; Kobayashi, R.; Normand, J.; Raghavachari, K.; Rendell, A.; Burant, J. C.; Iyengar, S. S.; Tomasi, J.; Cossi, M.; Rega, N.; Millam, J. M.; Klene, M.; Knox, J. E.; Cross, J. B.; Bakken, V.; Adamo, C.; Jaramillo, J.; Gomperts, R.; Stratmann, R. E.; Yazyev, O.; Austin, A. J.; Cammi, R.; Pomelli, C.; Ochterski, J. W.; Martin, R. L.; Morokuma, K.; Zakrzewski, V. G.; Voth, G. A.; Salvador, P.; Dannenberg, J. J.; Dapprich, S.; Daniels, A. D.; Farkas, O.; Foresman, J. B.; Ortiz, J. V.; Cioslowski, J.; Fox, D. J. *Gaussian 09*, revision A.1; Gaussian, Inc.: Wallingford, CT, 2009.
(86) Stewart, J. J. P. *MOPAC2009*; Stewart Computational Chemistry: Colorado Springs, CO, U.S.A., 2008; http://OpenMOPAC.net.
(87) Antony, J.; Grimme, S. *J. Phys. Chem, A* **2007**, *111*, 4862−4868.
(88) Goerigk, L.; Grimme, S. *Phys. Chem. Chem. Phys.* **2011**, *13*, 6670−6688.
(89) Antony, J.; Brüske, B.; Grimme, S. *Phys. Chem. Chem. Phys.* **2009**, *11*, 8440−8447.

THE JOURNAL OF PHYSICAL CHEMISTRY A

ARTICLE

pubs.acs.org/JPCA

on the Nature of Stabilization in Weak, Medium, and Strong Charge-Transfer Complexes: CCSD(T)/CBS and SAPT Calculations

S. Karthikeyan,[†] Robert Sedlak,[†,‡] and Pavel Hobza*[,†,‡]

[†]Department of Chemistry, Pohang University of Science and Technology, San 31, Hyojadong, Namgu, Pohang 790-784, Korea

[‡]Institute of Organic Chemistry and Biochemistry, Academy of Sciences of the Czech Republic and Center for Biomolecules and Complex Molecular Systems, Prague 6, 166 10, Czech Republic

ABSTRACT: Weak, medium, and strong charge-transfer (CT) complexes containing various electron donors (C_2H_4, C_2H_2, NH_3, NMe_3, HCN, H_2O) and acceptors (F_2, Cl_2, BH_3, SO_2) were investigated at the CCSD(T)/complete basis set (CBS) limit. The nature of the stabilization for these CT complexes was evaluated on the basis of perturbative NBO calculations and DFT-SAPT/CBS calculations. The structure of all of the complexes was determined by the counterpoise-corrected gradient optimization performed at the MP2/cc-pVTZ level, and most of complexes possess a linear-like contact structure. The total stabilization energies lie between 1 and 55 kcal/mol and the strongest complexes contain BH_3 as an electron acceptor. When ordering the electron donors and electron acceptors on the basis of these energies, we obtain the same order as that based on the perturbative E2 charge-transfer energies, which provides evidence that the charge-transfer term is the dominant energy contribution. The CCSD(T) correction term, defined as the difference between the CCSD(T) and MP2 interaction energies, is mostly small, which allows the investigation of the CT complexes of this type at the "cheap" MP2/CBS level. In the case of weak and medium CT complexes (with stabilization energy smaller than about 15 kcal/mol), the dominant stabilization originates in the electrostatic term; the dispersion as well as induction and δ(HF) terms covering the CT energy contribution are, however, important as well. For strong CT complexes, induction energy is the second (after electrostatic) most important energy term. The role of the induction and δ(HF) terms is unique and characteristic for CT complexes. For all CT complexes, the CCSD(T)/CBS and DFT-SAPT/CBS stabilization energies are comparable, and surprisingly, it is true even for very strong CT complexes with stabilization energy close to 50 kcal/mol characteristic by substantial charge transfer (more than 0.3 e). It is thus possible to conclude that perturbative DFT-SAPT analysis is robust enough to be applied even for dative-like complexes with substantial charge transfer.

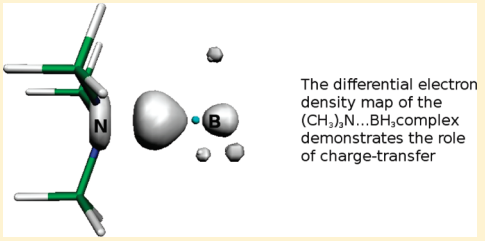

The differential electron density map of the $(CH_3)_3N...BH_3$ complex demonstrates the role of charge-transfer

INTRODUCTION

A charge-transfer (CT) complex, sometimes also labeled as an electron-donor−acceptor complex, is a complex of two (or more) systems where one is an electron donor (high ionization potential) and the other an electron acceptor (low electron affinity). CT complexes are frequent, there are organic as well as inorganic donors and acceptors, and CT complexes play a role also in the biological[1−4] and material[5−8] sciences. Where does the stabilization of these complexes come from? Quantum mechanically, this is described as a resonance between the nonbonded state |D, A> and the dative state |D+...A->. The isolated electron donor as well as the electron acceptor are mostly electro-neutral, but after electron transfer the donor possesses a partial positive charge while the electron acceptor possesses a partial negative charge. These charges attract each other and the resulting electrostatic attraction represents an important energy contribution. Besides this term, all of the other standard energy contributions like induction, dispersion, and exchange-repulsion take place. Charge-transfer complexes should be, however, also stabilized by the charge-transfer energy contribution (E^{CT}), which within the NBO theory[9] is approximated by the second-order E2 energies defined as follows:

$$E^{CT} \sim \mathrm{E2} = -2F_{\sigma\sigma^*}/\varepsilon_{\sigma^*} - \varepsilon_{\sigma} \qquad (1)$$

where F is the Fock matrix element between the σ and σ^* NBO orbitals, and ε_{σ^*} and ε_{σ} are the energies of the σ^* and σ orbitals. Large stabilization is expected when the energy difference between the σ orbital of the donor and the σ^* orbital of the acceptor is small and simultaneously when the Fock matrix element (including the overlap of the σ and σ^* orbitals) is large. The perturbation E2 charge-transfer energies are overestimated and cannot be compared with the other energy terms taken e.g. from perturbation theory. The E2 energies can be compared within different CT complexes and provide information on the relative importance of the CT energy term. Consequently, it is not clear which energy component is dominant for weak, medium

Special Issue: David W. Pratt Festschrift

Received: November 25, 2010
Revised: January 25, 2011
Published: March 04, 2011

and strong CT complexes formed by organic subsystems, and any systematic study using the advanced technique of computational chemistry is lacking. Here, the CT7/04 database of Truhlar should be mentioned.[10] Seven small CT complexes covering weak and medium CT complexes (with a stabilization energy between 1 and 11 kcal/mol) were investigated at the W1 level (CCSD(T)/CBS level), but no energy decomposition was performed.

The total stabilization energy of the CT complexes (as well as of any other noncovalent complexes) can be determined at the CCSD(T)/complete basis set (CBS) level. The CCSD(T)/CBS is considered to be the "golden-standard" method because of its outstanding accuracy for covalent as well as noncovalent systems (see ref 11 and the references therein). The method yields accurate stabilization energies and the properties of different noncovalent complexes but does not provide any information on the nature of the stabilization. This very useful information is yielded by perturbation SAPT calculations,[12] which compose the total interaction energy as the sum of the first- and second-order contributions energy components (electrostatic, exchange-repulsion, induction, exchange-induction, dispersion, and exchange-dispersion). The SAPT analysis is for larger complexes time-consuming and this problem was solved by introduction of DFT approximations. The resulting DFT-SAPT (or SAPT-(DFT))[13,14] method allows to investigate much larger complexes. The total interaction energy is constructed from the same first- and second-order energy terms and, additionally, the δ(HF) term covering all of the induction and charge-transfer energies of higher than second order at the Hartree−Fock level is added. This term is determined as the difference between the supermolecular HF interaction energy and the sum of electrostatic, exchange and induction energies determined at the HF level. Due to this construction, the δ(HF) term is the only term in the SAPT expansion which covers also energy contributions connected with the electron transfer between subsystems. Despite approximations included in the DFT-SAPT technique, the total interaction energies developed at the CCSD(T)/CBS and DFT-SAPT/CBS levels agree very well.[15] The rmsd between the DFT-SAPT/CBS and CCSD(T)/CBS interaction energies for 22 H-bonded, stacked, and mixed complexes of the S22 data set[16] are smaller than 0.5 kcal/mol.[15] The SAPT analysis performed for the S22 data set clearly identified the dominant energy contribution for the different types of noncovalent complexes: electrostatic for H-bonded and dispersion for stacked complexes. The use of this analysis for CT complexes is surprisingly not straightforward, mainly because the perturbation SAPT theory is not well-defined for CT complexes. It is believed that the SAPT theory can be applied for systems without any electron transfer or with only "small" electron transfer. It must be kept in mind that the CT term is not explicitly defined within the perturbative SAPT theory and this energy is covered partially in the induction and mainly in the "variational" δ(HF) term (see above).

An important characteristic of CT complexes is the amount of the electron transferred between the donor and acceptor. The electron transfer from the donor to the acceptor is usually small but may become important when the donor's and/or acceptor's abilities improve. The total electron transfer is deduced from the total charge of each subsystem and depends strongly on the type of atomic charges used. The most frequently used Mulliken charges are known to be extremely basis-set dependent, and therefore the use of other charges, like the NBO ones, is recommended.

Contradictory to other types of noncovalent complexes (like H-bonded or stacked complexes) little is known about the nature of their stabilization. The question arises whether these complexes are mainly stabilized by charge-transfer energy or by combination of different energy terms like electrostatic, dispersion, and charge-transfer. To shed light on this problem, we investigated in the present paper the structure and stabilization of small CT complexes of various strengths (from weak through medium to strong) formed by various small electron donors (C_2H_4, C_2H_2, NH_3, NMe_3, HCN, H_2O) and small acceptors (F_2, Cl_2, BH_3, SO_2). The aim of the study is 3-fold: (i) to elucidate the nature of stabilization in CT complexes, that is, to find the dominant energy term, (ii) to test the performance of the MP2 method, and (iii) to investigate the applicability of the SAPT treatment. The nature and stabilization of the present CT complexes will be compared with the same (benchmark) values determined for H-bonded, stacked and mixed complexes of the S22 data set.[16] Further insight into the nature of the stabilization of CT complexes can be gained by passing from the correlated calculations (MP2 and CCSD(T)) to the Hartree−Fock (HF) ones. It must be kept in mind that charge-transfer energy (contrary to dispersion energy) is at least partially covered already at the HF level. In the present study, we have investigated small, mostly pseudolinear (contact) CT complexes while in the future we will perform the same study for stacked CT complexes, where the electron donor and electron acceptor are localized in parallel, stacked planes.

METHODS

Geometry. The structure of all of the complexes investigated was determined by the counterpoise-corrected gradient optimization performed at the MP2/cc-pVTZ level. It was shown that these geometries are close to those obtained at the CCSD(T)/CBS level.[17] The isolated subsystems were optimized at the MP2/cc-pVTZ level. All of the complexes studied (and their subsystems) were also optimized at the HF/cc-pVTZ level.

Stabilization Energy. The CCSD(T)/CBS stabilization energy was constructed as the sum of the MP2/CBS stabilization energy and the CCSD(T) correction term. The former energy was extrapolated (Helgaker extrapolation)[18] from the MP2 energies evaluated at the MP2/aug-cc-pVDZ, MP2/aug-cc-pVTZ and MP2/aug-cc-pVQZ levels. The CCSD(T) correction term (the difference between the CCSD(T) and MP2 interaction energies) was determined with the aug-cc-pVDZ basis set. In the case of the $NH_3\cdots F_2$ complex, the CCSD(T)/CBS interaction energy was also evaluated by a direct extrapolation of the CCSD(T) energies calculated with the aug-cc-pVDZ and aug-cc-pVTZ and aug-cc-pVTZ and aug-cc-pVQZ basis sets. The deformation energies were systematically not considered. More details about determination of CCSD(T)/CBS stabilization energy can be found in our recent review.[15]

The DFT-SAPT calculations were performed with the PBE0 functional and aug-cc-pVTZ basis sets. For the NH_3...F_2 complex, the DFT-SAPT calculations were also performed with the smaller aug-cc-pVDZ basis set, and for the same complex the MP2-SAPT calculations with the aug-cc-pVDZ and aug-cc-pVTZ basis sets were also performed.

Atomic Charges. The atomic charges were approximated by the Mulliken and NBO charges and in both cases they were developed at the HF/6-31G*, HF/cc-pVDZ, and HF/cc-pVTZ levels, respectively.

Frontier Orbitals. The HOMO and LUMO energies of all of the subsystems were calculated at the HF/cc-pVTZ level of theory.

Table 1. HOMO and LUMO Energies (in au) of the Donors and Acceptors at the Hartree-Fock/cc-pVTZ Level of Theory

HF/cc-pVTZ	HOMO	LUMO
C_2H_4	−0.376	0.152
C_2H_2	−0.408	0.151
F_2	−0.662	0.105
ClF	−0.493	0.063
NH_3	−0.429	0.137
Cl_2	−0.444	0.039
BH_3	−0.499	0.060
SO_2	−0.493	0.006
HCN	−0.492	0.141
H_2O	−0.505	0.142
NMe_3	−0.357	0.139

All of the calculations were carried out using the Gaussian 09[19] and Molpro06[20] codes.

RESULTS AND DISCUSSION

Frontier Orbitals of the Donors and Acceptors. Table 1 collects the HOMO and LUMO energies of all of the donors and acceptors. Electron donors can be ordered as follows: H_2O < HCN < NH_3 < C_2H_2 < C_2H_4 < NMe_3; while the acceptor ability increases in the following order: F_2 < ClF < BH_3 < Cl_2 < SO_2. It should be kept in mind that the frontier orbitals were taken from Hatree-Fock and not from correlated calculations.

Structure and Geometry. The structures of all complexes studied are depicted in Figure 1, where selected intermolecular coordinates are also shown. The full geometrical information on these complexes is available in Table 1. Investigating these results, we found that in the case of BH_3-containing complexes the intermolecular distance becomes very small, almost at the range of covalent bonding. The theoretical estimates of the B···N distance in BH_3···NH_3 and BH_3···NMe_3 complexes (1.658 and 1.643 Å) agree well with the gas-phase experiments (1.627 and 1.65 Å).[21,22]

Charge-Transfer. Table 2 shows the amount of the electron transferred from the donor to acceptor. In all of the cases, the HF was combined with the 6-31G*, cc-pVDZ, and cc-pVTZ basis sets. Surprisingly, the Mulliken and NBO charges are similar and the extension of the basis set is again connected with rather small differences. As the most reliable, we have selected the NBO charges determined at the HF/cc-pVTZ level, and these charges will be used in the further discussion. A substantial CT (more than 0.3 e) was observed in complexes 10 and 11 with a BH_3 acceptor, and a very large CT (more than 0.1 e) was also detected in the NH_3···ClF and NMe_3···SO_2 complexes. A moderately large CT exists in the NH_3···Cl_2 and H_2O···ClF complexes, whereas in all of the remaining complexes it is below 0.05 e. The complexes with CT higher than 0.3e are characterized by very small intersystem distance and exhibit a dative bond.

Stabilization Energy. The CCSD(T), MP2, and HF stabilization energies as well as their components are presented in Table 3, whereas the DFT-SAPT energies and the corresponding energy contributions are collected in Table 4. Investigating the CCSD(T)/CBS stabilization energies, we found that the weakest complexes are those with F_2 as an electron acceptor (the stabilization energies were below 2 kcal/mol), which agrees with the ranking of fluorine as the worst electron acceptor. Moderately strong CT complexes with a stabilization energy between 3 and 11 kcal/mol have ClF, Cl_2, and SO_2 (complex with NH_3) as an acceptor. Finally, the complexes with the BH_3 acceptor and also the NMe_3···SO_2 complex are strong CT complexes with a stabilization energy exceeding 14 kcal/mol. The stabilization energy of the complexes with the BH_3 acceptor is extremely high, more than 43 kcal/mol. The latter complexes are in fact systems with a dative bond. All of the complexes investigated are mostly stronger than similar complexes without a CT energy component.[15] Allow us to mention as an example CT complexes with NH_3 as a donor. Of the five CT complexes studied, only NH_3···F_2 can be labeled as weak, all the others as moderately strong or strong. The CCSD(T)/CBS stabilization energy of the ammonia dimer with a N—H···N H-bond, which is determined at the same theoretical level,[16] is 3.17 kcal/mol, which is less than that of the four strongest CT complexes with a NH_3 donor. Similarly, the CCSD(T)/CBS stabilization energy for ethane···ethane is 1.53 kcal/mol,[16] which is less than one-half of stabilization energy of the present acetylene···ClF complex (3.82 kcal/mol).

On the basis of calculated stabilization energies, we can state that NH_3 is a stronger donor than both hydrocarbons as well as HCN and water. Following expectations, NMe_3 is a stronger donor than NH_3. Consequently, the donors can be ordered in the following sequence: NMe_3 > NH_3 > H_2O > HCN > C_2H_2 > C_2H_4. When comparing the stabilization energies of various acceptors, we found the following sequence: F_2 < Cl_2 < SO_2 < ClF < BH_3. Comparing these orders with those based on HOMO/LUMO values, we have found important differences. This arises from the fact that the present ordering is based on the total stabilization energies and not only on the HOMO/LUMO energies.

For 9 of the 11 complexes investigated, we have determined the E2 charge-transfer energies (cf. Table 2). The E2 energies could not be evaluated for the complexes with BH_3, as the NBO analysis identify the respective complexes as one unit. The E2 energies are very large, between 1.8 and 59 kcal/mol (cc-pVTZ basis set), and they are larger than the interaction energies. When we order the electron donors and electron acceptors, we obtain identical orders to those above. This provides rather strong evidence that the charge-transfer term by itself is a dominant or very important stabilizing term.

Investigating the single energy terms in the variation interaction energy, we found that the MP2/CBS term forms the dominant energy contribution, with the CCSD(T) correction term being much smaller (forming on average about 8% of the MP2/CBS value). The only exception represent the "stacked" complexes ethylene···fluorine and acetylene···ClF, where the CCSD(T) correction term is larger. A similar situation occurred with the H-bonded complexes, where the CCSD(T) correction terms were also rather small.[15] The MP2/CBS and CCSD(T)/CBS interaction energies for all complexes investigated are visualized in Figure 2. This figure clearly shows that for CT complexes of this type ("contact" structure) the time-consuming and thus expensive CCSD(T) correction term can be omitted and reliable stabilization energies are safely obtained already at the MP2/CBS level. The resulting error should be less than 10%.

Table 3 further shows that all of the complexes are stable even at the HF level. Investigating these values, we found that the HF/MP2 ratio (calculated at the cc-pVTZ level) is largest for the strong CT complexes, where it reaches more than 50%. On the other hand, this ratio considerably decreases (to less than 20%) when passing to weak CT complexes. Nevertheless, the HF

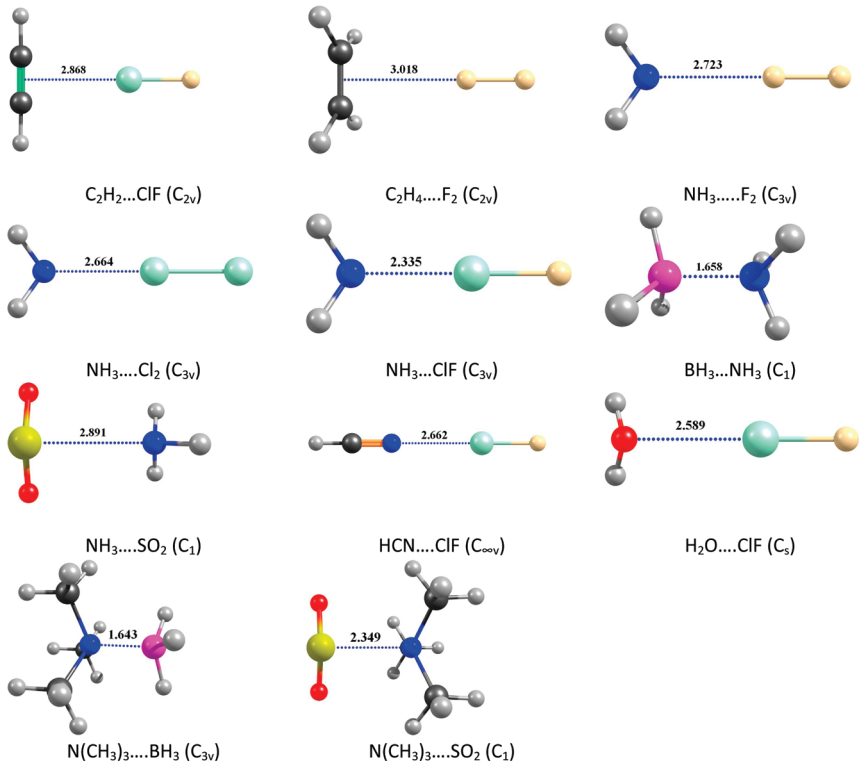

Figure 1. MP2/cc-pVTZ optimized structures of all of the CT complexes; the main intermolecular distance (in Å) is also presented. The symmetry group is given in the parentheses.

Table 2. Mulliken and NBO Charge-Transfer (in e) and E2 (kcal/mol) for all of the CT Complexes Evaluated at the HF/(6-31G*/cc-pVTZ/cc-pVTZ) Level of Theory; the Electrons are Systematically Transferred from the Electron Donor to Electron Acceptor

		HF/6-31G*			HF/cc-pVDZ			HF/cc-pVTZ		
		NBO	Mulliken	E2	NBO	Mulliken	E2	NBO	Mulliken	E2
1	$C_2H_4\cdots F_2$	0.011	0.008	1.62	0.009	0.004	1.70	0.007	0.002	1.80
2	$NH_3\cdots F_2$	0.021	0.019	2.53	0.020	0.021	2.64	0.014	0.008	2.88
3	$C_2H_2\cdots ClF$	0.022	0.036	9.06	0.020	0.024	8.72	0.031	0.028	8.24
4	$NH_3\cdots Cl_2$	0.093	0.095	14.66	0.078	0.093	14.37	0.063	0.071	14.04
5	$HCN\cdots ClF$	0.020	0.029	1.31	0.024	0.030	1.31	0.025	0.028	2.34
6	$H_2O\cdots ClF$	0.042	0.056	10.59	0.046	0.062	11.11	0.037	0.050	9.55
7	$NH_3\cdots SO_2$	0.035	0.047	8.36	0.029	0.043	9.09	0.030	0.047	7.43
8	$NH_3\cdots ClF$	0.117	0.107	40.82	0.125	0.128	42.95	0.149	0.142	39.84
9	$NMe_3\cdots SO_2$	0.157	0.153	42.96	0.135	0.133	51.21	0.185	0.212	58.71
10	$NH_3\cdots BH_3$	0.353	0.308		0.327	0.445		0.378	0.459	
11	$NMe_3\cdots BH_3$	0.337	0.312		0.321	0.428		0.357	0.510	

results clearly demonstrate that the CT term is covered already at the HF level. Let us remind the reader here that dispersion energy is not covered at this level.

The CCSD(T)/CBS interaction energies for seven complexes can be compared with the Truhlar W1 results.[10] The latter stabilization energies are systematically slightly larger, which arises from the fact that their MP2/CBS energies as well as the CCSD(T) correction terms were determined with larger basis sets. We have intentionally used relatively small basis sets because in the near future we are going to expand our study to extended stacked CT complexes, where calculations even at the present level will be tedious.

The CCSD(T)/CBS interaction energy roughly correlates with the amount of CT, but a detailed examination shows some discrepancies. For example, the $NMe_3\cdots BH_3$ complex is considerably stronger than the $NH_3\cdots BH_3$ complex, but the CT is reversed, and the same is true for the pair $NH_3\cdots SO_2$ and $H_2O\cdots ClF$ as well as for others.

Investigating the DFT-SAPT energies, we can conclude the following: (1) The first-order polarization (electrostatic) energy is systematically the largest (attractive) term, and this term is always larger than the SAPT stabilization energy. The same is true for H-bonded complexes of the S22 set; for stacked and mixed complexes, the dispersion energy is dominant and the electrostatic

Table 3. Interaction Energies (in kcal/mol) of All of the CT Complexes

		HF/cc-pVTZ	MP2/cc-pVTZ	MP2/aVDZ	MP2/aVTZ	MP2	CCSD(T)/ aVDZ	CCSD(T)
		ΔE_{bsse}	ΔE_{bsse}	ΔE_{bsse}	ΔE_{bsse}	ΔE_{bsse}/CBS	ΔE_{bsse}	ΔE_{bsse}/CBS
1	$C_2H_4\cdots F_2$	−0.06	−0.83	−1.14	−1.24	−1.29	−0.80	−0.95
2	$NH_3\cdots F_2$	−0.33	−1.47	−1.70	−1.73	−1.74	−1.53	−1.57
3	$C_2H_2\cdots ClF$	−1.16	−3.26	−3.32	−4.32	−4.74	−2.40	−3.82
4	$NH_3\cdots Cl_2$	−2.23	−4.90	−4.67	−5.07	−5.24	−3.91	−4.48
5	$HCN\cdots ClF$	−2.71	−4.43	−4.65	−5.17	−5.39	−3.84	−4.58
6	$H_2O\cdots ClF$	−3.40	−4.88	−4.66	−5.12	−5.31	−4.21	−4.86
7	$NH_3\cdots SO_2$	−4.70	−4.74	−4.56	−5.15	−5.40	−4.68	−5.52
8	$NH_3\cdots ClF$	−5.29	−10.63	−9.82	−11.61	−12.37	−8.14	−10.69
9	$NMe_3\cdots SO_2$	−5.08	−11.65	−11.36	−14.44	−15.74	−10.03	−14.41
10	$NH_3\cdots BH_3$	−35.21	−44.00	−40.67	−43.89	−45.24	−39.34	−43.91
11	$NMe_3\cdots BH_3$	−41.82	−54.91	−52.06	−55.66	−57.17	−49.78	−54.89

Table 4. DFT-SAPT Interaction Energy Components (in kcal/mol) of All of the CT Complexes (at the PBE0 Level with the aug-cc-pVTZ Basis Set)

	DFT-SAPT (PBE0)/aVTZ)	E_{elec}	E_{ind}	E_{disp}	E_{exch}	δ_{HF}	E_{int}	DFT-SAPT/CBS
1	$C_2H_4\cdots F_2$	−1.40	0.04	−1.39	2.54	−0.74	−0.96	−1.04
2	$NH_3\cdots F_2$	−2.86	−0.17	−1.53	4.33	−0.93	−1.17	−1.27
3	$C_2H_2\cdots ClF$	−6.67	−1.10	−4.03	10.85	−2.81	−3.77	−4.09
4	$NH_3\cdots Cl_2$	−11.49	−2.15	−4.34	16.81	−3.04	−4.20	−4.55
5	$HCN\cdots ClF$	−7.21	−1.35	−3.35	9.53	−1.67	−4.05	−4.30
6	$H_2O\cdots ClF$	−8.76	−1.47	−3.32	11.08	−1.91	−4.39	−4.66
7	$NH_3\cdots SO_2$	−10.22	−1.78	−3.61	11.79	−1.92	−5.75	−5.99
8	$NH_3\cdots ClF$	−28.81	−8.06	−7.53	43.88	−8.94	−9.46	−10.15
9	$NMe_3\cdots SO_2$	−40.31	−13.84	−14.58	66.66	−12.80	−14.86	−15.75
10	$NH_3\cdots BH_3$	−77.22	−48.82	−17.83	111.16	−10.27	−42.98	−44.20
11	$NMe_3\cdots BH_3$	−89.51	−54.22	−23.64	126.53	−10.37	−51.21	−52.63

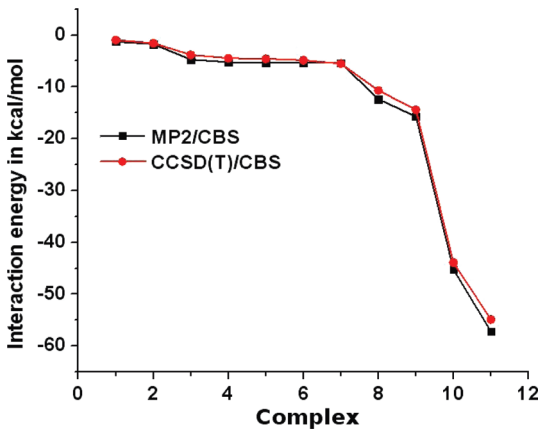

Figure 2. MP2/CBS and CCSD(T)/CBS interaction energies for all complexes investigated. For labeling of *x*-axis, see Table 2.

term is mostly smaller than the SAPT stabilization energy. (2) The dispersion energy and the δ(HF) term are comparable. In most cases, the dispersion energy is slightly more attractive and only in the case of the $NH_3\cdots ClF$ complex is the δ(HF) larger. The complexes containing the BH_3 as an acceptor are different and here the induction energy is much larger than the dispersion and δ(HF) terms. The induction energy is larger than (or comparable to) the dispersion energy also for the $NH_3\cdots ClF$ and $NMe_3\cdots SO_2$ complexes. In the S22 set, the δ(HF) term is always smaller (or even much smaller) than the dispersion energy, and the induction energy is systematically the smallest term. The rather large δ(HF) and induction terms are thus characteristic features of CT complexes and reflect the importance of the charge-transfer energy term. The above-mentioned comparison confirms the different character of the complexes investigated and also a different nature of the stabilization when compared with H-bonded or stacked complexes. (3) Four complexes (8, 9, 10, and 11) are characteristic with a large CT (more than 0.1 e). This CT correlates well with induction energy and the δ(HF) term. Only in the case of the largest CT (more than 0.3 e) the induction energy is larger than the δ(HF) term (complexes 10 and 11), for complexes 8 and 9 both terms are comparable. In seven remaining complexes, the δ(HF) term is larger than the induction energy and CT roughly correlates with induction energy and δ(HF) term. (4) Stabilization energies for complexes 2 and 8, having NH_3 as an electron donor, differ substantially. While the former complex represents a typical vdW complex the later one can be characterized as a complex with strong halogen bond. The very positive σ-hole of ClF molecule is responsible for large electrostatic energy term. Further the charge-transfer energy in this complex is also very large. (5) Comparing the DFT-SAPT interaction energies with the CCSD(T)/CBS ones, we found that in most cases they are roughly comparable, with the average

error of 7%. Only in case $NH_3\cdots F_2$ the error is significantly larger, about 20%. Not considering this complex, the average error of DFT-SAPT is only about 5%. In the S22 set, the CCSD(T)/CBS stabilization energies were mostly larger than the DFT-SAPT/CBS ones; only in eight (out of 22) complexes was the opposite true, but the difference was systematically very small (mostly lower than 3%). Evidently, an average error is with present CT complexes comparable to that found for H-bonded and stacked complexes. This finding is surprising because we expected that in case of strong CT complexes and especially with very strong CT complexes with very large CT, the DFT-SAPT interaction energy will differ from the benchmark CCSD(T)/CBS values. Evidently this is not the case and perturbative DFT-SAPT analysis can be applied even for complexes having a nearly dative bond. This is evidently due to inclusion of "variational" δ(HF) term which is, for strong CT complexes, exceptionally large. An agreement of stabilization energies determined by both techniques is, for these complexes (10 and 11), surprisingly good. Only in one case was the CCSD(T)/CBS stabilization energy considerably larger, namely, with the $NH_3\cdots F_2$ complex. Here the DFT-SAPT is underestimated by about 20%, and we have not been able to find the reason for such a failure. We performed several additional calculations to validate the existing results: (i) The CCSD(T)/CBS interaction energy was determined by the direct extrapolation of CCSD(T) energies calculated with the aug-cc-pVDZ and aug-cc-pVTZ basis sets and also with aug-cc-pVTZ and aug-cc-pVQZ basis sets. The resulting values (−1.60 and −1.71 kcal/mol) are slightly larger than the original one, that is, the difference is even larger. (ii) The MP2/CBS was extrapolated from aug-cc-pVTZ and aug-cc-pVQZ basis sets. The final CCSD(T)/CBS stabilization energy when CCSD(T) correction term was taken from aug-cc-pVQZ calculation (−1.70 kcal/mol) is well comparable with the CCSD(T) interaction energy determined from direct extrapolation from aug-cc-pVTZ and aug-cc-pVQZ basis sets (−1.71 kcal/mol). (iii) The effect of quadrupole excitations was included but the resulting difference was negligible (the respective calculations were done with QCISD(T) and QCISD(TQ) method using the aug-cc-pVDZ and aug-cc-pVTZ basis sets). (iv) The DFT-SAPT/CBS energy was extrapolated from aug-cc-pVDZ and aug-cc-pVTZ basis sets as well as from aug-cc-pVTZ and aug-cc-pVQZ basis sets, but resulting values (−1.27 and −1.30 kcal/mol) differ from the original values only negligible. (v) Instead of the DFT-SAPT, we used the MP2-SAPT method based on the aug-cc-pVDZ basis set. The resulting total interaction energy (−1.29 kcal/mol) differs only slightly from the original DFT-SAPT value. Summarizing all these calculations, we must conclude that there exists a rather large relative difference between both interaction energies, but the absolute error of 0.3 kcal/mol is certainly not critical.

In addition, when considering other similar complexes, we do not see any reason for this difference. The CT in this complex is very small (0.014 e), neither the induction energy nor the δ(HF) term is exceptionally large, the other four CT complexes with NH_3 as the electron donor behave quite normally (i.e., the SAPT stabilization energy is systematically larger than the CCSD(T) one), and also the other complex with F_2 as the acceptor is not exceptional.

CONCLUSION

(i) The CT energy contribution is covered already at the HF level and the HF/MP2 ratio increases for strong CT complexes.

(ii) The CCSD(T)/CBS stabilization energy for all of the CT complexes studied is close to the DFT-SAPT/CBS values and only exception represents the $NH_3\cdots F_2$ complex. The difference between both interaction energies is rather large (about 20%) and can only be explained by the fact that some higher-order interaction energy terms are missing either in the supermolecular CCSD(T) or perturbation DFT-SAPT calculations. Agreement between DFT-SAPT and CCSD(T) stabilization energies even for complexes with substantial charge transfer is surprisingly good and gives evidence that the former method can be safely used even for complexes with dative bond.

(iii) The perturbation E2 energies yield the same order of electron donors and acceptors as the CCSD(T)/CBS calculations, which supports the idea that the complexes studied are stabilized by the charge-transfer term.

(iv) The DFT-SAPT analysis has shown the dominant position of the first-order polarization (electrostatic) term, which is systematically the most important one. Dispersion energy is in most cases the second most important term; it is the induction energy only for BH_3-containing complexes while for the $NH_3\cdots ClF$ it is the δ(HF) term. The induction and δ(HF) terms covering the charge-transfer energy are smaller for these complexes; they are, however, systematically larger than in the H-bonded and stacked complexes of the S22 set. We can thus conclude that the dominant stabilization of the CT complexes (characterized by a moderate CT, that is, less than 0.1 e) comes from the electrostatic energy term; the induction and δ(HF) terms are, however, important as well (unlike the H-bonded complexes, where these terms are less important).

(v) The amount of the CT and E2 perturbative energy roughly correlate with the stabilization energy.

(vi) The MP2/CBS stabilization energy is mostly larger than the CCSD(T)/CBS one, but the difference is rather small (less than 10%). This means that the CPU-favorable MP2/CBS calculations can be safely used for this type of CT complexes (those with a contact structure).

ACKNOWLEDGMENT

This work was a part of Research Project No. Z40550506 of the Institute of Organic Chemistry and Biochemistry, Academy of Sciences of the Czech Republic and was supported by Grant Nos. LC512 and MSM6198959216 from the Ministry of Education, Youth and Sports of the Czech Republic. The support of Praemium Academiae, Academy of Sciences of the Czech Republic, awarded to P.H. in 2007 is also acknowledged. This work was also supported by the Korea Science and Engineering Foundation (World Class Univ. Program: *R*32-2008-000-10180-0) through the Korea Science and Engineering Foundation funded by the Ministry of Education, Science and Technology.

REFERENCES

(1) Krapf, S.; Koslowski, T.; Steinbrecher, T. *Phys. Chem. Chem. Phys.* **2010**, *12*, 9516.

(2) Warshel, A *Acc. Chem. Res.* **2002**, *35*, 385.

(3) Hervas, M.; Navarro, J.; Rosa, M. D. L. *Acc. Chem. Res.* **2003**, *36*, 798.

(4) Mallajosyula, S.; Gupta, A.; Pati, S. *J. Phys. Chem. A* **2009**, *113*, 3955.

(5) Halls, J. J. M.; Walsh, C. A.; Greenham, N. C.; Marseglia, E. A.; Friend, r. H; Moratti, S. C.; Holmes, A. B. *Nature* **1995**, *376*, 498.
(6) Yu, G.; Gao, J.; Hummelen, J. C.; Wudi, f.; Heeger, A. J. *Science* **1995**, *270*, 1789.
(7) Schmidt-Mende, L.; Fechtenkotter, A.; Mullen, K.; Moons, E.; Friend, R. H.; Mackenzie, J. D. *Science* **2001**, *293*, 1119.
(8) Hoppe, H.; Sariciftci, N. S. *J. Mater. Res.* **2004**, *19*, 1924.
(9) Reed, A. E.; Curtiss, L. A.; Weinhold, F. *Chem. Rev.* **1988**, *88*, 899.
(10) Zhao, Y.; Truhlar, D. G. *J. Chem. Theory Comput.* **2005**, *1*, 415.
(11) Helgaker, T.; Jorgensen, P.; Olson, J. *Molecular Electronic-Structure Theory*; Wiley: New York, 2000.
(12) Jeziorski, B.; Moszynski, R.; Szalewicz, K. *Chem. Rev.* **1994**, *94*, 1887.
(13) Misquita, A. J.; Jeziorski, B.; Szalewicz, K. *Phys. Rev. Lett.* **2003**, *91*, 033201.
(14) Hesselmann, A.; Jansen, G. *Chem. Phys. Lett.* **2002**, *357*, 464.
(15) Riley, K. E.; Pitonak, M.; Jurecka, P.; Hobza, P. *Chem. Rev.* **2010**, *110*, 5023.
(16) Jurecka, P.; Sponer, J.; Cerny, J.; Hobza, P. *Phys. Chem. Chem. Phys.* **2006**, *8*, 1985.
(17) Dabkowska, I.; Jurecka, P.; Hobza, P. *J. Chem. Phys.* **2005**, *122*, 204322.
(18) Halkier, A.; Helgaker, T.; Jorgensen, P.; Klopper, W.; Koch, H.; Olsen, J.; Wilson, A. K. *Chem. Phys. Lett.* **1998**, *286*, 243.
(19) Frisch, M. J.; Trucks, G. W.; Schlegel, H. B.; Scuseria, G. E.; Robb, M. A.; Cheeseman, J. R.; Scalmani, G.; Barone, V.; Mennucci, B.; Petersson, G. A.; Nakatsuji, H.; Caricato, M.; Li, X.; Hratchian, H. P.; Izmaylov, A. F.; Bloino, J.; Zheng, G.; Sonnenberg, J. L.; Hada, M.; Ehara, M.; Toyota, K.; Fukuda, R.; Hasegawa, J.; Ishida, M.; Nakajima, T.; Honda, Y.; Kitao, O.; Nakai, H.; Vreven, T.; Montgomery Jr, J. A.; Peralta, J. E.; Ogliaro, F.; Bearpark, M.; Heyd, J. J.; Brothers, E.; Kudin, K. N.; Staroverov, V. N.; Kobayashi, R.; Normand, J.; Raghavachari, K.; Rendell, A.; Burant, J. C.; Iyengar, S. S.; Tomasi, J.; Cossi, M.; Rega, N.; Millm, J. M.; Klene, M.; Knox, J. E.; Cross, J. B.; Bakken, V.; Adamo, C.; Jaramillo, J.; Gomperts, R.; Stratmann, R. E.; Yazyev, O.; Austin, A. J.; Cammi, R.; Pomelli, C.; Ochterski, J. W.; Martin, R. L.; Morokuma, K.; Zakrzewski, V. G.; Voth, G. A.; Salvador, P.; Dannenberg, J. J.; Dapprich, S.; Daniels, A. D.; Farkas, O.; Foresman, J. B.; Ortiz, J. V.; Cioslowski, J.; Fox, D. J. *Gaussian 09*, Revision A.1; Gaussian, Inc.: Wallingford, CT, 2009.
(20) Werner, H. −J.; Knowles, P. J.; Lindh, R.; Manby, F. R.; Schutz, M.; Celani, P.; Korona, T.; Rauhut, G.; Amos, R. D.; Bernhardsson, A.; Berning, A.; Cooper, D. L.; Deegan, M. J. O.; Dobbyn, A. J.; Eckert, F.; Hampel, C.; Hetzer, G.; Lloyd, A. W.; McNicholas, S. J.; Meyer, W.; Mura, M. E.; Nicklass, A.; Palmieri, P.; Pitzer, R.; Schumann, U.; Stoll, H.; Stone, A. J.; Tarroni, R.; Thorsteinsson, T. *MOLPRO*, version 2006.1, a package of ab initio programs; see http://www.molpro.net.
(21) Jackel, F.; Perera, U. G. E.; Iancu, V.; Braun, K.-F.; Koch, N.; Rabe, J. P.; Hla, S.-W. *Phys. Rev. Lett.* **2008**, *100*, 126102.
(22) Chesnut, D. B. In *Annual report on NMR spectroscopy*; Webb, G. A., Ed.; Academic Press: London, 1994; Vol. 29, p 89.

DOI: 10.1002/cphc.201100455

On the Nature of the Stabilization of Benzene···Dihalogen and Benzene···Dinitrogen Complexes: CCSD(T)/CBS and DFT-SAPT Calculations

Elango Munusamy,[a] Robert Sedlak,[a, b] and Pavel Hobza*[a, b, c]

The structure and stabilization energies of benzene (and methylated benzenes)···X_2 (X = F, Cl, Br, N) complexes were investigated by performing CCSD(T)/complete basis set limit and density functional theory/symmetry-adapted perturbation theory (DFT-SAPT) calculations. The global minimum of the benzene···dihalogen complexes corresponds to the T-shaped structure, whereas that of benzene···dinitrogen corresponds to the sandwich one. The different binding motifs of these complexes arise from the different quadrupole moments of dihalogens and dinitrogen. The different sign of the quadrupole moments of these diatomics is explained based on the electrostatic potential (ESP). Whereas all dihalogens, including difluorine, possess a positive σ hole, such a positive area of the ESP is completely missing in the case of dinitrogen. Moreover, benzene···X_2 (X = Br, Cl) complexes are stronger than benzene···X_2 (X = F, N) complexes. When analyzing DFT-SAPT electrostatic, dispersion, induction, and δ(Hartree–Fock) energies, we recapitulate that the former complexes are stabilized mainly by dispersion energy, followed by electrostatic energy, whereas the latter complexes are stabilized mostly by the dispersion interaction. The charge-transfer energy of benzene···dibromine complexes, and surprisingly, also of methylated benzenes···dibromine complexes is only moderate, and thus, not responsible for their stabilization. Benzene···dichlorine and benzene···dibromine complexes can thus be characterized merely as complexes with a halogen bond rather than as charge-transfer complexes.

1. Introduction

Benzene is a prototypical aromatic electron donor, whereas dihalogens (F_2, Cl_2, and Br_2) are known to be good electron acceptors. The electron-donating orbitals in the former are π molecular bonding orbitals, whereas the electron-accepting orbitals in the latter are σ* antibonding molecular orbitals. When moving from fluorine to bromine (or iodine), the electron-acceptor ability increases. An increase in the donor ability of benzene can be obtained, for example, from a substitution of hydrogen with an electron-donating group, such as a methyl group. It is thus expected that the dominant stabilization energy in complexes of benzene with dihalogens should be the charge-transfer (CT) energy term. Moving, however, from fluorine to bromine yields not only the mentioned increase in acceptor ability, but also an increase in the quadrupole moment and polarizability. Consequently, the electrostatic quadrupole–quadrupole and dispersion energies are expected to increase as well. A discussion of the dominant stabilization term in the complexes mentioned becomes even more complicated by the finding that dihalogens, including fluorine, exhibit a σ hole, which is a prerequisite for the existence of a halogen bond.[1–4] In the particular case of the C–X···π interaction (X = F, Cl, and Br), the halogen bond is of a strength comparable to that of a hydrogen bond and its existence can at least partially explain the stabilization of benzene···dihalogen complexes. The existence of a σ hole in dihalogens and especially in fluorine is surprising because it is known that fluorine, as the only halogen, does not exhibit a σ hole in fluoro derivatives of organic molecules.

The total stabilization energy of the complexes investigated (and also of any other noncovalent complexes) can be successfully determined by performing CCSD(T)/complete basis set (CBS) calculations. CCSD(T)/CBS is the "gold-standard" method owing to its outstanding accuracy for covalent and noncovalent systems (see reference [5] and references therein). The method provides accurate stabilization energies and properties of different noncovalent complexes, but does not offer any information on the nature of the stabilization. This very useful information is generally provided by symmetry-adapted perturbation theory (SAPT) calculations,[6] or in the case of larger complexes, by its DFT variant (DFT-SAPT),[7,8] which assumes

[a] *Dr. E. Munusamy,[+] R. Sedlak,[+] Prof. P. Hobza*
Department of Chemistry
Pohang University of Science and Technology
San 31, Hyojadong, Namgu, Pohang 790-784 (Korea)
E-mail: hobza@uochb.cas.cz

[b] *R. Sedlak,[+] Prof. P. Hobza*
Institute of Organic Chemistry and Biochemistry
Academy of Sciences of the Czech Republic
and Center for Biomolecules and Complex Molecular Systems
Prague 6, 166 10 (Czech Republic)

[c] *Prof. P. Hobza*
Regional Centre of Advanced Technologies and Materials
Department of Physical Chemistry, Faculty of Science
Palacky University, 771 46 Olomouc (Czech Republic)

[+] *These authors contributed equally to this work.*

Supporting information for this article is available on the WWW under http://dx.doi.org/10.1002/cphc.201100455.

that the total interaction energy is a sum of the energy components of the first- and second-order contributions (electrostatic, exchange repulsion, induction, exchange induction, dispersion and exchange dispersion, and the δ(HF) term). From the list of different energy terms, however, it is evident that a genuine CT energy term is missing. Therefore, the question arises as to the existence of this term and also where it is covered in the SAPT decomposition.

The CT energy can be approximated by the *E*2 perturbation second-order energy evaluated within the nonbonding orbital (NBO) analysis[9] by using Equation (1):

$$E^{CT} \sim E2 = -2F_{\sigma\sigma*}/\varepsilon_{\sigma*}-\varepsilon_{\sigma} \quad (1)$$

in which *F* is the Fock matrix element between the σ and σ* NBO orbitals, and ε_{σ^*} and ε_{σ} are the energies of the σ* and σ orbitals, respectively. A high degree of stabilization is expected when the energy difference between the σ orbital of the donor and the σ* orbital of the acceptor is small and simultaneously when the Fock matrix element (including the overlap of the σ and σ* orbitals) is large. The different character of the perturbation *E*2 CT energy and SAPT perturbation energies should be mentioned. Whereas the former is based on the concept of electron transfer between the donor and acceptor, the latter is derived with the assumption that there is no electron transfer between subsystems. From this point of view, it is impossible to compare these energies directly with one another. On the other hand, the *E*2 energies can be compared within different CT complexes, allowing us to estimate the relative importance of the CT energy term.

The above-mentioned question of the relationship between CT and the perturbative SAPT expansion is surprisingly complicated. All of the first- and second-order terms are derived on the assumption that there is no electron transfer between subsystems, as a result of which the only term to "allow" for this electron transfer is the δ(HF) term, which is determined as the difference between the supermolecular Hartree–Fock (HF) interaction energy and the sum of the electrostatic, exchange, and induction energies determined at the HF level. Because of this construction, the nonperturbation δ(HF) term also covers those energy contributions connected with electron transfer between subsystems. Genuine perturbation DFT-SAPT terms do not include CT energy because the subsystem energy within DFT-SAPT is determined with monomer basis sets. When, however, the dimer basis set is used (which is the default in MOLPRO calculations),[10] the induction energy covers not only the classical multipole-induced multipole energy, but also the CT energy. This arises from the fact that the sums, in this case, cover not only the occupied and unoccupied orbitals of one subsystem, but also the occupied orbitals of the first subsystem and the unoccupied orbitals of the second subsystem. We can thus conclude that the CT term (when the dimer basis set is used for the monomers) is partially covered in the second-order induction and mainly in the nonperturbative δ(HF) term.[11] An important question concerns the relationship between the *E*2 CT energy from NBO analysis [Eq. (1)] and the CT contribution from the above-mentioned SAPT treatment. *E*2 is overestimated; this was confirmed by results from our previous report where we investigated medium and strong CT complexes.[24] For four NH_3···X complexes (X = F_2, Cl_2, SO_2, ClF), we found that the *E*2 NBO CT energy was 2.4 times larger than the sum of the induction and δ(HF) terms.

Herein, we have investigated the structure and stabilization of benzene, mesitylene, and hexamethylbenzene complexes with dihalogens (F_2, Cl_2, Br_2) and, for the sake of comparison, also with dinitrogen (N_2). The aim of the study was to elucidate the nature of stabilization in the complexes investigated, specifically to find the role of CT, electrostatic interactions, and halogen bonding. To do so, we performed benchmark calculations at the variational CCSD(T)/CBS limit and at the perturbation DFT-SAPT levels.

Computational Methods

Structure and Geometry

The structures of all of the complexes were determined by counterpoise-corrected gradient optimization using the MP2/cc-pVTZ method. It was shown that these geometries were close to those obtained at the CCSD(T)/CBS level.[12] The geometries of the isolated systems were determined at the MP2/cc-pVTZ level. All of the complexes and the isolated systems were also optimized at the HF/6-311 + G* level.

Stabilization Energies

The CCSD(T)/CBS stabilization energy was constructed as the sum of the MP2/CBS stabilization energy and a CCSD(T) correction term (ΔCCSD(T)). The former energy was extrapolated (Helgaker extrapolation)[13] from the MP2 energies evaluated at the MP2/aug-cc-pVDZ and MP2/aug-cc-pVTZ levels. The CCSD(T) correction term (the difference between the CCSD(T) and MP2 interaction energies) was determined with the aug-cc-pVDZ basis set. The total stabilization energy exhibited at least chemical accuracy, that is, it was accurate within +/−1 kcal mol^{-1}. More details about the procedure can be found in our recent review.[14]

DFT-SAPT calculations were performed with the PBE0 functional and aug-cc-pVTZ basis sets.[8] In the DFT-SAPT method,[8] the interaction energy was given as the sum of first- and second-order energies E_1, E_2, and also the δ(HF) term. E_1 contains electrostatic, E_1^{Pol}, and exchange repulsion, E_1^{Ex}, contributions and E_2 contained induction, E_2^{Ind}, exchange induction, $E_2^{Ex\text{-}Ind}$, dispersion, E_2^{D}, and exchange dispersion, $E_2^{Ex\text{-}D}$, contributions. Accordingly, second-order exchange components were included in the induction E_2^{Ind} and dispersion E_2^{D} terms. The CT energy was considered to be part of the induction energy and δ(HF) terms, which estimated higher-order HF contributions. The DFT-SAPT/CBS value was based on calculations with the aug-cc-pVTZ basis set. Only the dispersion contribution was constructed differently. The E_2^{D} term was replaced by the $E_2^{D/CBS}$ value, which was constructed from E_2^{D}/aug-cc-pVDZ and E_2^{D}/aug-cc-pVTZ terms utilizing the Helgaker extrapolation scheme.[13]

The charge transferred between the electron donor and acceptor was deduced from the atomic charges of both subsystems. The atomic charges were approximated by NBO[9] charges calculated with the HF/6-311 + G* levels method.

Frontier Orbitals, Electric Quadrupole Moments, and Polarizabilities

The HOMO and LUMO energies, electric quadrupole moments, and polarizabilities of all of the subsystems were calculated at the HF/6-311 + G* level of theory.

The electrostatic multipole–multipole interaction energy (abbreviated as Q–Q, because the quadrupole–quadrupole contribution was the most important one) was determined with the Orient program package,[15] which utilized distributed multipole moments. These multipole moments were derived by the GDMA[16] program by using the distributed multipole analysis (DMA) method.[17–19] The GDMA code utilized the formatted checkpoint file produced by the Gaussian package.[20] The distributed multipole moments for all of the molecules were calculated up to rank four (up to hexadecapole) based on the PBE0/aug-cc-pVDZ calculation.

All of the calculations were carried out by using the Gaussian 09,[20] Molpro06,[10] Orient4.6.16,[15] and GDMA2.2.04[16] codes.

2. Results and Discussion

2.1 Isolated Subsystems

2.1.1. Frontier Orbitals of Donors and Acceptors

The HOMO and LUMO energies of all of the donors and acceptors are provided in Table 1. According to our expectations, the electron donors can be ordered as follows: benzene < mesitylene < hexamethylbenzene, while the electron-acceptor ability increases in the following order: $N_2 < F_2 < Cl_2 < Br_2$.

2.1.2. Multipole Moments, Polarizabilities, and ESP

The first nonzero multipole moment for all of the (symmetrical) subsystems corresponds to the quadrupole moment and their values are collected in Table 1. Benzene belongs to the group of aromatic compounds with a negative Q_{zz} component of the quadrupole moment (the *z* axis coincides with the main rotational axis of the symmetry of the molecule). Benzene has a quadrupole moment that can be schematically written as + − − +; the plus signs stand for regions of hydrogen atoms, whereas the minus signs represent π-electron density over and below the carbon ring. This "linear" representation of the benzene quadrupole moment does not coincide with the C_6 axis of the benzene molecule. The quadrupole moment of dinitrogen is represented in our study as − + + −. In the case of a linear molecule, all four signs are projected into the main rotational axis of the symmetry of the molecule (C_∞), which is contrary to the benzene representation. The absolute value of the Q_{zz} component of nitrogen is considerably smaller than that of benzene. The signs of the dinitrogen schematic quadrupole moment are not surprising because the molecule possesses a triple bond and has a lone electron pair at each nitrogen (|N≡N|). When moving to dihalogens, the orientation of the quadrupole is changed.[21] Dihalogen possesses a single bond and each halogen has three lone electron pairs, (|F̄–F̄|); we expected that their quadrupole moments could be schematically written (as in the case of dinitrogen) as (− + + −).

It should be mentioned here that quantum mechanical calculations predicted quadrupole moments of all systems in agreement with experiment results. But these "black-box" calculations do not offer an interpretation of the different signs of the dihalogen and dinitrogen quadrupole moments (see above). This uncertainty could be solved by performing NBO analyses. Figure 1 shows the ESP near all of the dihalogens and, for comparison, also for dinitrogen. A substantial difference is evident at first glance. Whereas the ESP at the top (cusp point) of the dihalogen molecules is positive (i.e., each molecule exhibits a σ hole), it is negative in the case of dinitrogen. Correspondingly, the Q_{zz} component of the quadrupole moments in these systems should be opposite, that is, positive

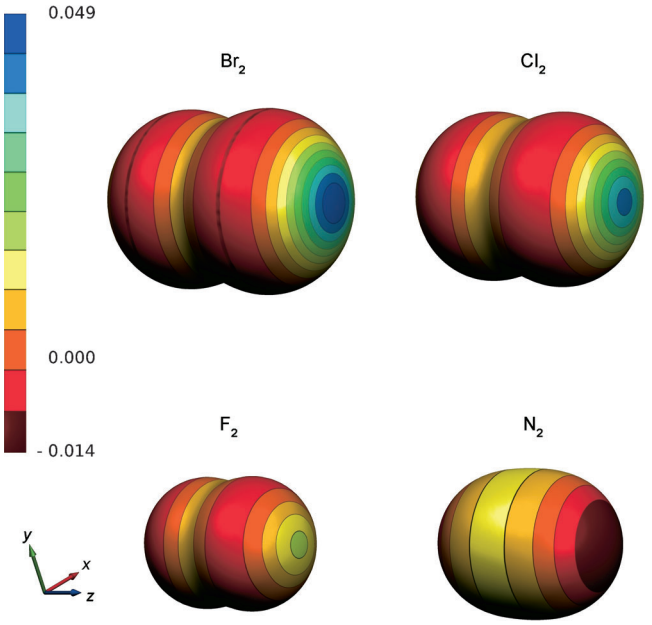

Figure 1. ESP [au] at the 0.001 e Bohr^{-3} isodensity surface for all four X_2 diatomics based on the HF/6-311 + G* calculations. The orientation of axes and a color scale are also depicted.

Table 1. The HOMO/LUMO, quadrupole moments (*Q*, the *z* axis coincides with the main rotational axis of the symmetry of the molecule), and polarizabilities (α) for all of the isolated subsystems. ESP of the X_2 molecule is also given; all of the values were calculated at the HF/6-311 + G*level of theory.

Subsystem	HOMO [eV]	LUMO [eV]	Q_{zz} [D.A.]	α [Bohr^3]	ESP[a]
F_2	–	1.986	0.33	6.3	0.017/−0.002
Cl_2	–	0.569	1.90	20.8	0.041/−0.003
Br_2	–	−0.231	3.24	33.1	0.049/−0.007
N_2	–	3.344	−1.00	10.0	−0.014/0.010
C_6H_6	−9.162	–	−6.44	63.7	–
$C_6H_3(CH_3)_3$	−8.572	–	−5.47	98.9	–
$C_6(CH_3)_6$	−8.033	–	−4.33	132.1	–

[a] Given in au at 0.001 e Bohr^3 isodensity surface for the cusp-respective belt point

(+ − − +) for dihalogens and negative (− + + −) for dinitrogen. These values are confirmed by the NBO populations (Table 2), for which differences in the *z* axis (which coincides with the covalent bond) are clearly apparent. In the case of dihalogens, the population in the *z* axis is smaller than that in the *x* and *y* axes, whereas the opposite is true for dinitrogen. Dihalogens thus lack electrons in the *z* axis, whereas dinitrogen has a surplus of electrons in this axis. Figure 2 shows the ESP along the C_∞ axis for all of the diatomics; it is evident that dinitrogen has a negative ESP between 2.25 and 5 Bohr, whereas all of the dihalogens have positive ESP values in this range. It should be mentioned here that the ESP values of all three dihalogens are similar, that is, they all exhibit a positive σ hole, which yields a positive Q_{zz} component for all of these dihalogens.

Table 2. The natural atomic orbital (AO) population of the valence p orbital for the X atom in X_2 molecules based on HF/6-311 + G* calculations. The orientation of the p_z orbital coincides with the X–X bond in the X_2 molecule.

X	Orbital		
	p_x	p_y	p_z
F	2.00	2.00	1.05
Cl	2.00	2.00	1.05
Br	2.00	2.00	1.04
N	0.99	0.99	1.36

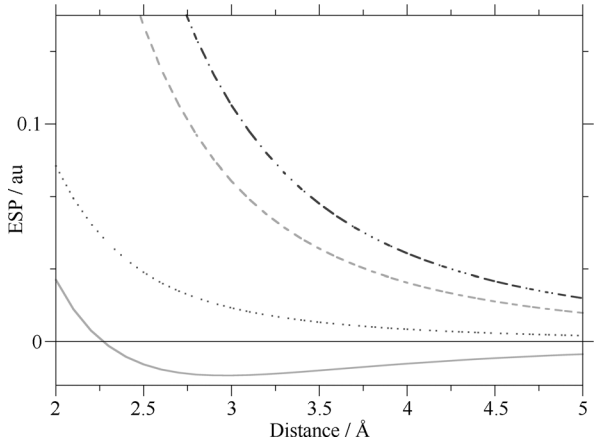

Figure 2. ESP [au] along the *z* axis (which is identical to the X–X bond in the X_2 molecule) in the range between 2 and 5 Bohr in the outermost region of the X_2 diatomic molecules [N_2 (——), F_2 (•••••), Cl_2 (-----), Br_2 (–•–•)].

Investigating the subsystem polarizabilities (Table 1), we recognize a substantial increase upon the methylation of benzene and hexamethylbenzene possesses twice the polarizability of benzene. Similarly, there is a polarizability increase when moving from F_2 to Br_2: the polarizability of dibromine is more than five times greater than that of difluorine. The polarizability of difluorine and dinitrogen are similar. These values indicate that the dispersion energy in benzene···dihalogen complexes significantly increases upon moving from F to Br and is comparable for complexes of benzene with difluorine and benzene with dinitrogen.

2.2. Complexes

2.2.1. Structure and Stabilization Energies

The structures of all of the complexes investigated are depicted in Figure 3, where selected intermolecular coordinates are also shown. Full geometry information on all of the complexes studied is available in Table S1 in the Supporting Information. The HF, MP2, and CCSD(T) interaction energies are shown in Table 3, whereas Table 4 (shown below) contains the DFT-SAPT energies. From Table 3, it is apparent that the T-shaped structures Ta and Tb are more stable than the symmetrical Tc structure. The energy difference between these structures is largest for dibromine (about 0.5 kcal mol^{-1}) and smallest for difluorine (less than 0.1 kcal mol^{-1}). The total stabilization energies of the complexes investigated are rather large, which is especially true for the dibromine-containing complexes. The stabilization energies of benzene···Br_2, mesitylene···Br_2, and hexamethylbenzene···Br_2 (for the substituted benzenes, only the Tc structure was considered) amount to 3.2, 4.2, and 5.7 kcal mol^{-1}, respectively. It should be mentioned here that the stabilization energy of the water dimer with a strong O–H···O hydrogen bond is about 5 kcal mol^{-1}.[22] By investigating the components of the CCSD(T)/CBS stabilization energy, we found that the CCSD(T) correction term was systematically repulsive and surprisingly large. For the Ta structure, it reduced the MP2/CBS stabilization energy of benzene···dihalogen complexes by 1.77, 1.32, and 0.46 kcal mol^{-1} (33, 32, and 28%), respectively, which meant that, when calculating the interaction energies of these complexes at the MP2/CBS level, a substantial (about one-third) error was made and the resulting stabilization energies were strongly overestimated.

The situation with benzene···dinitrogen was different because here the sandwich structures was more stable than the T-shaped one. The role of the CCSD(T) correction term was similar here and the MP2/CBS stabilization energies were again strongly overestimated (by more than 30%).

The interpretation of the different structural preferences of the benzene···dihalogen and benzene···dinitrogen complexes in terms of the monomer quadrupole moments is straightforward. The signs and orientations of the quadrupole moments of benzene and dihalogens lead to a preference for T-shaped structures, whereas in the case of the benzene···dinitrogen complex stacked structures are preferred. The electrostatic quadrupole–quadrupole interaction thus explains the structure of the complexes investigated. A comparison of the DFT-SAPT electrostatic energy (E_1^{pol}) with the multipole–multipole (Q–Q) electrostatic energy in the region with a negligible overlap of the subsystem electron spheres provides a picture of the accuracy of the multipole electrostatic energy. Such a comparison for the C_6H_6···Br_2-Tc complex is depicted in Figure 4, from which very good agreement between both energies arises. Very similar agreement was also achieved for the C_6H_6···Cl_2 and

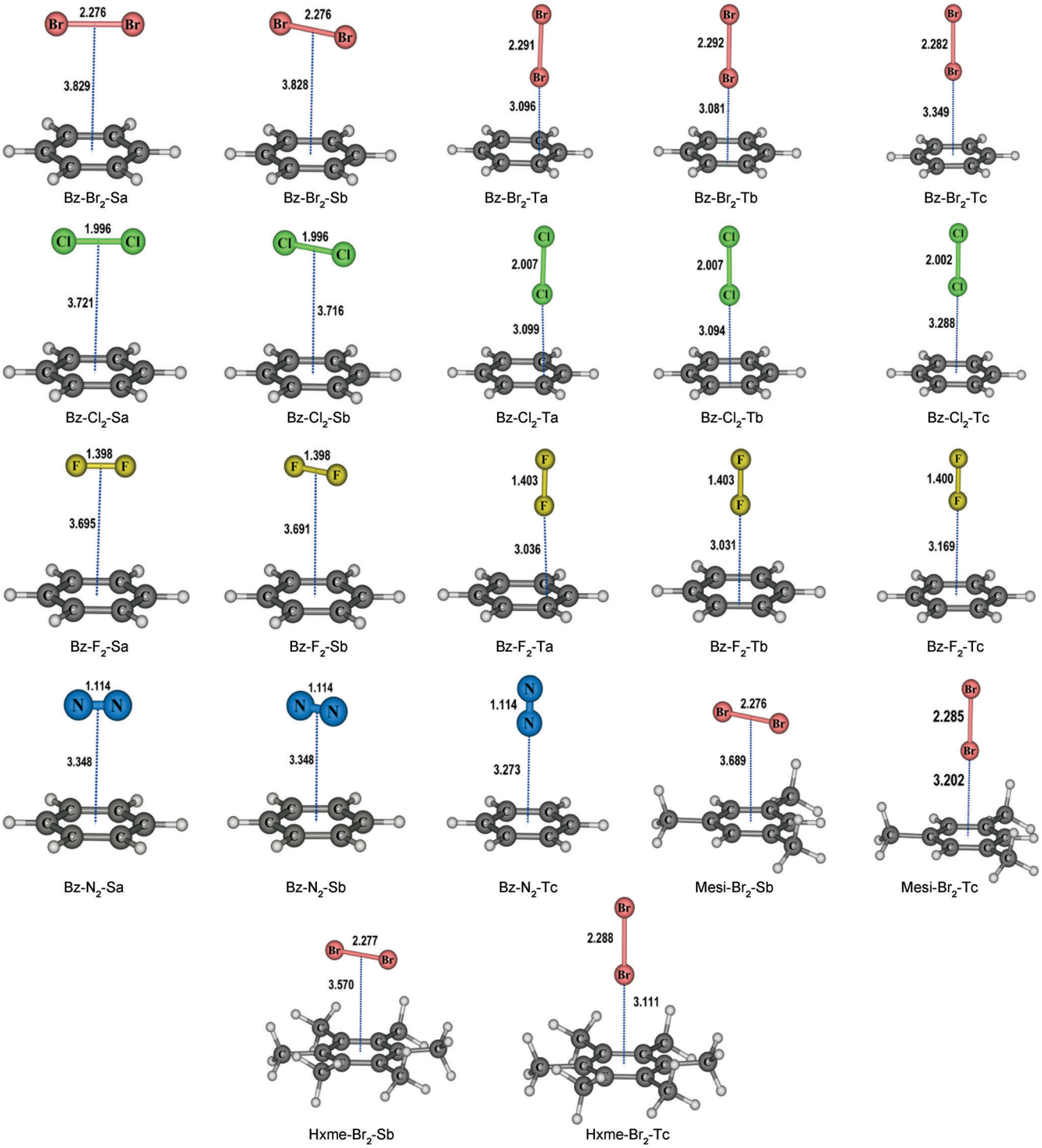

Figure 3. Optimized structures of all complexes investigated. The main intramolecular and intermolecular coordinates (in Å) are also depicted. Bz = benzene; Mesi = mesitylene; Hxme = hexamethylbenzene; Ta, Tb, and Tc are three different T-shaped structures, Sa and Sb are sandwich structures.

$C_6H_6\cdots F_2$ complexes. Figure 5 shows the different character of the Q–Q interaction energy when moving to a benzene···dinitrogen complex. The Q–Q interaction for the Sa structure is attractive, whereas in the case of the Tc structure it is repulsive. This is in full accordance with our previous conclusion based only on the signs and orientations of the quadrupole moments of benzene and dinitrogen. The Q–Q interaction energies for the Tc structures of the $C_6H_6\cdots Br_2$, $C_6H_6\cdots Cl_2$, and $C_6H_6\cdots F_2$ complexes for distances from 5.5 to 12 Å are depicted in Figure 6. The largest stabilization energies belong to the complexes of benzene with dibromine, followed by dichlorine, and difluorine. This order correlates with the magnitude of the σ hole and naturally also with the ESP values along the main rotational axis of the dihalogens (Figure 2).

Table 3. Interaction energies [kcal mol^{-1}] and charges transferred between the electron donor and acceptor (in e$^-$) for the complexes depicted in Figure 3.

Complex	HF	MP2		CCSD(T)		CT[a]
	cc-pVTZ	aug-cc-pVDZ	aug-cc-pVTZ	CBS	CBS	
Bz-Br2-Sa	0.06	−2.02	−2.63	−2.89	−1.98	0.0028
Bz-Br2-Sb	0.07	−2.02	−2.63	−2.89	−1.98	0.0029
Bz-Br2-Ta	−0.59	−4.42	−5.13	−5.43	−3.66	−0.0167
Bz-Br2-Tb	−0.59	−4.43	−5.15	−5.45	−3.66	−0.0169
Bz-Br2-Tc	−0.59	−3.71	−4.19	−4.39	−3.17	−0.0024
Bz-Cl2-Sa	0.06	−1.82	−2.28	−2.47	−1.70	0.0035
Bz-Cl2-Sb	0.08	−1.83	−2.28	−2.47	−1.70	0.0035
Bz-Cl2-Ta	−0.43	−3.44	−3.95	−4.16	−2.84	−0.0078
Bz-Cl2-Tb	−0.43	−3.45	−3.97	−4.19	−2.86	−0.0077
Bz-Cl2-Tc	−0.43	−3.01	−3.37	−3.52	−2.53	−0.0001
Bz-F2-Sa	0.08	−0.66	−0.81	−0.87	−0.73	0.0016
Bz-F2-Sb	0.08	−0.66	−0.81	−0.87	−0.73	0.0016
Bz-F2-Ta	−0.04	−1.45	−1.59	−1.65	−1.19	−0.0006
Bz-F2-Tb	−0.06	−1.44	−1.57	−1.62	−1.17	−0.0005
Bz-F2-Tc	−0.05	−1.27	−1.39	−1.44	−1.10	0.0008
Bz-N2-Sa	−0.07	−1.94	−2.18	−2.28	−1.50	−0.0018
Bz-N2-Sb	−0.07	−1.94	−2.18	−2.28	−1.50	−0.0018
Bz-N2-Tc	0.05	−1.05	−1.20	−1.26	−0.81	−0.0028
Mesi-Br2-Sb	0.05	−3.31	−4.10	−4.43	−3.13	0.0051
Mesi-Br2-Tc	−0.73	−5.10	−5.66	−5.90	−4.23	−0.0023
Hxme-Br2-Sb	0.09	−4.60	−5.55	−5.95	−4.12	0.0007
Hxme-Br2-Tc	−0.85	−6.94	−7.67	−7.98	−5.66	−0.0033

[a] Based on the HF/6-311 + G* NBO charges. Negative values indicate CT from benzene (substituted benzene) to the diatomic molecule.

(halogen bond) was based on the existence of a σ hole. There are many known molecules with σ holes that satisfy the above-mentioned description.[23] The σ hole is also present in dihalogens, even in difluorine, and surprisingly, it is very positive. The σ hole in dihalogens (cf. Table 1) is as positive as the highly positive σ hole at bromine in trifluorobromomethane (0.050 au). Consequently, a halogen bond should also be formed between dihalogens and electron donors such as benzene or substituted benzenes. Figure 7 shows the ESP of isolated benzene and it is apparent that the most negative ESP is located above (and below) the skeleton of carbon atoms, whereas it becomes more positive when moving to the center of the aromatic ring. Consequently, the halogen bond

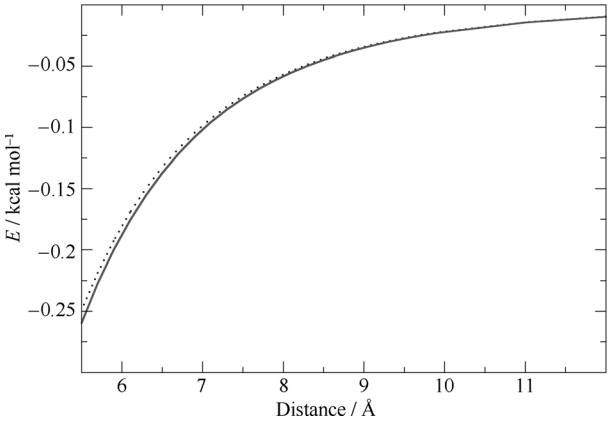

Figure 4. A comparison of the Q–Q interaction (••••) and E_1^{pol} (——) for the C_6H_6···Br_2-Tc complex between 5.5 and 12 Å. The distributed multipole moments are based on the PBE1PBE/aug-cc-pVDZ calculation.

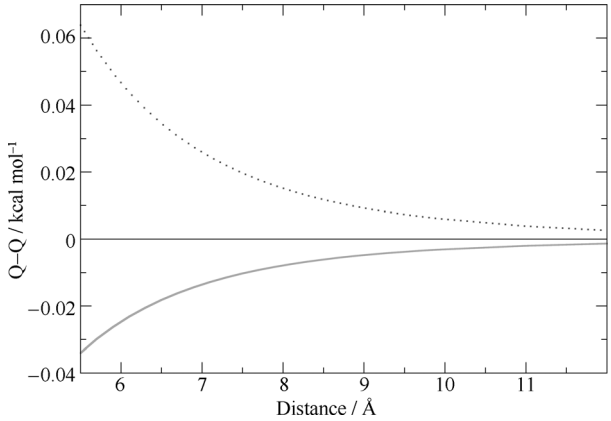

Figure 5. The Q–Q interaction for the C_6H_6···N_2-Sa (——) and -Tc (••••) complexes between 5.5 and 12 Å. The distributed multipole moments are based on PBE1PBE/aug-cc-pVDZ calculations.

Deeper insight into the nature of the stabilization of the complexes investigated was acquired by analyzing the DFT-SAPT energy terms. Table 4 shows that the dominant attractive energy contribution for all of the structures of all complexes originates in the dispersion energy. Only in the case of the T-shaped structures of benzene (and substituted-benzene)···dibromine is the first-order electrostatic E_1^{Pol} energy comparable to the dispersion energy; in all of the other complexes, the electrostatic energy is systematically smaller.

The explanation for the attractive interaction between halogens (with the exception of fluorine) covalently bonded to carbon and an electron donor such as the carbonyl oxygen between benzene and the dihalogens will be preferentially formed above the carbon skeleton and not above the center of the aromatic ring. DFT-SAPT electrostatic energies fully confirm this assumption and the electrostatic energy for Ta and Tb structures of all of the benzene···dihalogen complexes is considerably more attractive than that for the symmetrical Tc structure. We can thus conclude that the rather large stabilization energies of benzene···dihalogen complexes, as well as the fact that the Ta and Tb structures are more favorable than Tc, can be explained by the existence of a halogen bond between the dihalogens and benzene.

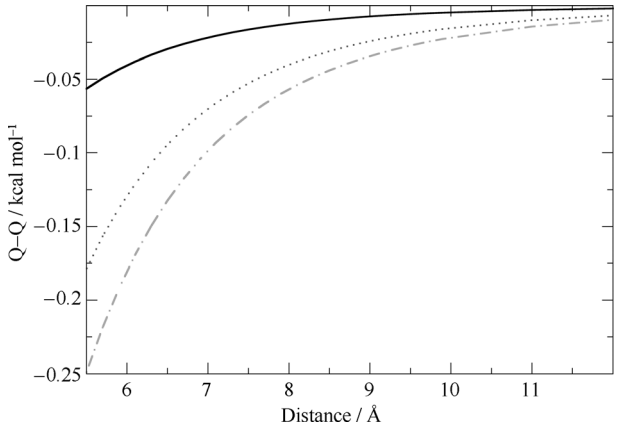

Figure 6. The Q–Q interaction for the $C_6H_6\cdots X_2$-Tc series between 5.5 and 12 Å for X = Br (–•–•), Cl (••••), and F (——). The distributed multipole moments are based on PBE1PBE/aug-cc-pVDZ calculations.

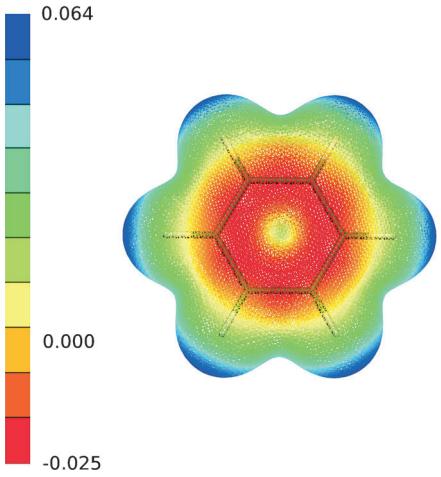

Figure 7. The illustrative ESP [au] at the 0.006 e Bohr^{-3} isodensity surface of the benzene molecule based on HF/6-311 + G* calculations.

Table 4. DFT-SAPT (PBE0/aug-cc-pVTZ level) interaction energies (in kcal mol^{-1}) of the complexes depicted in Figure 3.[a]

Complex	E_1^{Pol}	E_1^{Ex}	$E_2^{Ind}+E_2^{Ex\text{-}Ind}$	$E_2^{D}+E_2^{Ex\text{-}D}$	δ(HF)	$\Delta E_{int/CBS}$	$E2$[b]
Bz-Br2-Sa	−0.89	3.29	−0.10	−4.00	−0.14	−2.07	–
Bz-Br2-Sb	−0.89	3.30	−0.10	−4.01	−0.14	−2.07	–
Bz-Br2-Ta	−4.88	9.60	−0.91	−5.81	−1.87	−4.22	−4.52
Bz-Br2-Tb	−5.01	9.83	−0.94	−5.85	−1.93	−4.23	−5.53
Bz-Br2-Tc	−2.60	4.82	−0.38	−4.48	−0.56	−3.44	−1.44
Bz-Cl2-Sa	−0.69	2.71	−0.07	−3.44	−0.13	−1.79	–
Bz-Cl2-Sb	−0.71	2.75	−0.07	−3.47	−0.13	−1.80	–
Bz-Cl2-Ta	−3.19	6.55	−0.43	−4.52	−1.31	−3.13	−2.61
Bz-Cl2-Tb	−3.17	6.52	−0.43	−4.53	−1.30	−3.14	−3.06
Bz-Cl2-Tc	−1.87	3.69	−0.23	−3.69	−0.42	−2.70	−0.90
Bz-F2-Sa	−0.08	0.55	−0.01	−1.11	−0.03	−0.76	–
Bz-F2-Sb	−0.08	0.55	−0.01	−1.12	−0.03	−0.76	–
Bz-F2-Ta	−0.97	2.14	0.00	−1.81	−0.51	−1.23	−0.59
Bz-F2-Tb	−0.96	2.08	0.00	−1.77	−0.49	−1.22	−0.75
Bz-F2-Tc	−0.55	1.20	−0.03	−1.52	−0.14	−1.11	–
Bz-N2-Sa	−1.09	2.78	−0.06	−2.79	−0.31	−1.59	−0.40
Bz-N2-Sb	−1.09	2.77	−0.06	−2.79	−0.31	−1.59	−0.40
Bz-N2-Tc	−0.28	1.88	−0.05	−2.12	−0.21	−0.84	−0.30
Mesi-Br2-Sb	−1.63	5.22	−0.16	−6.07	−0.27	−3.22	–
Mesi-Br2-Tc	−4.04	7.31	−0.57	−6.34	−0.93	−4.89	−2.19
Hxme-Br2-Sb	−2.52	7.25	−0.21	−7.96	−0.41	−4.23	–
Hxme-Br2-Tc	−5.43	9.60	−0.77	−7.79	−1.30	−6.06	–

[a] E_1^{Pol} is the first-order electrostatic energy, E_1^{Ex} is the first-order exchange energy, $E_2^{Ind}+E_2^{Ex\text{-}Ind}$ is the sum of the second-order induction and exchange induction energies, $E_2^{D}+E_2^{Ex\text{-}D}$ is the sum of the second-order dispersion and exchange dispersion energies, δ(HF) is the higher-order HF terms, and $\Delta E_{int/CBS}$ is the total interaction energy with the dispersion term extrapolated to the CBS limit. [b] $E2$ energy connected with BD→BD* interaction only for complexes with negative value of the CT (cf. Table 3).

The stabilization energy of the benzene···dinitrogen complex is considerably smaller than that of the benzene···X_2 (X = Br, Cl) complexes and is roughly comparable to that of benzene···difluorine. Investigating the energy terms, we found that the larger stabilization of dibromine and dichlorine complexes arose from the larger dispersion, induction, and mainly electrostatic terms. This is in accordance with previous conclusions, showing that the greater stabilization of benzene···X_2 (X = Br, Cl) complexes arises from the existence of a halogen bond.

Some insight into the nature of the stabilization of complexes investigated could be also found from a comparison of the HF and correlated interaction energies. By comparing the HF and MP2 stabilization energies (Table 3), we see that most of the complexes are stable even at the HF level, but that the respective stabilization energy represents only a fraction of that of the MP2 one. This shows that the correlation (dispersion) energy is responsible for the rather large stabilization energies of the complexes studied.

2.2.2. Charge Transfer (CT)

Table 3 shows the amount of electrons transferred between the subsystems. According to expectations, CT is negligible for benzene···dinitrogen. Of the benzene···dihalogen complexes, the greatest electron transfer is found for the dibromine complex, followed by those of the dichlorine and difluorine complexes. An overlap between the benzene HOMO and dihalogen LUMO is significant only for the T-shaped structures. Consequently, structures Ta and Tb exhibited much greater electron transfer than the sandwich structure. In all cases, electron transfer is, however, rather small and does not exceed 0.02 e. From these values, we can deduce that electron-transfer energy will be also moderate. CT energy contributions can be deduced from DFT-SAPT analysis, for which CT energy is covered in the induction energy and δ(HF)

terms. Table 4 shows that for all of the complexes and all of the structures, the induction energy represents the smallest energy term. It is non-negligible only for the Ta and Tb structures of the benzene···dichlorine and benzene (and substituted-benzene)···dibromine complexes. In both cases, it reaches less than 25% of the electrostatic energy. The δ(HF) term is about 50% larger, but still forms less than 50% of the electrostatic term. Even if we add the induction and δ(HF) terms together, the respective sum is still smaller than the electrostatic energy. This is true even for the hexamethylbenzene···Br_2 complex, for which we expected the CT energy to be much more important if not dominant. In the case of strong CT complexes with substantial CT, the induction and δ(HF) terms are comparable and much larger than these terms in the complexes dealt with herein.[24] We can thus conclude that in the present complexes the CT energy contribution does not represent the dominant stabilization energy term. An alternative way to determine the CT energy term is to use NBO analysis. The *E*2 perturbation energy given by Equation (1) is collected for the complexes with CT from benzene to diatomic (cf. Table 3) in Table 4. It should be mentioned that the *E*2 CT values are overestimated (see above) and that, owing to their different origin, they cannot be compared with the DFT-SAPT energy terms. The *E*2 energies can be compared for different structures of the complex or for different complexes. When analyzing these energies, we found that they reached the highest values for the Tb structures; for the Ta and Tc structures, they are significantly smaller. According to our expectations, *E*2 was largest for benzene···Br_2 (-5.44 kcal mol^{-1}), followed by the benzene···Cl_2, and benzene···F_2. For the sake of comparison, here are some of the *E*2 values from our previous paper for some typical CT complexes: NH_3···Cl_2 (-14.0 kcal mol^{-1}), NH_3···SO_2 (-7.4 kcal mol^{-1}) and NMe_3···SO_2 (-58.7 kcal mol^{-1}).[24] It is thus clear that the CT *E*2 energy within the benzene···dibromine complex is not exceptional, but is in fact moderate.

3. Conclusions

On the basis of our investigations, we can draw the following conclusions:

1) The quadrupole moments of dihalogens and dinitrogen have the opposite sign, which can be easily understood on the basis of the ESP of these systems. All of the dihalogens, including difluorine, possess a strong positive σ hole.

2) Benzene···X_2 (X = Br, Cl) complexes are stronger than benzene···X_2 (X = F, N) complexes. Analyzing the DFT-SAPT electrostatic, dispersion, induction, and δ(HF) energies, we conclude that the former complexes are stabilized mainly by dispersion energy, followed by the electrostatic term, whereas the latter are stabilized by the dispersion interaction.

3) The CT energy of the benzene···dihalogen complexes was only moderate and was considerably smaller than that in the contact CT complexes investigated in the previous study.[24] This was true even for methylated benzene···dihalogen complexes, for which a considerably larger role of the CT energy was expected.

4) Benzene···dichlorine and especially benzene (and methylated benzene)···dibromine were stabilized mainly by dispersion and electrostatic energies; the role of CT energy was smaller. These complexes could thus be characterized as halogen-bonded ones rather than CT complexes.

5) On the basis of results from our previous[24] and present paper we believe that an important CT energy contribution exists only in complexes with strong electron donors (NH_3, NMe_3) and acceptors (SO_2, BH_3). In all other "CT" complexes the dominant stabilization originates from the electrostatic and dispersion terms.

Acknowledgement

This work was a part of research project no. Z40550506 of the Institute of Organic Chemistry and Biochemistry, Academy of Sciences of the Czech Republic, and was supported by grants no. LC512 and MSM6198959216 from the Ministry of Education, Youth and Sports of the Czech Republic. This work was also supported by the Operational Program Research and Development for Innovations—European Social Fund (CZ.1.05/2.1.00/03.0058) of the Ministry of Education, Youth and Sports of the Czech Republic. The support of Praemium Academiae, Academy of Sciences of the Czech Republic, awarded to P.H. in 2007 is also acknowledged. This work was also supported by the Korea Science and Engineering Foundation (World Class Univ. program: R32-2008-000-10180-0).

Keywords: charge transfer · computational chemistry · density functional theory · halogen bonds · noncovalent interactions

[1] P. Metrangolo, G. Resnati, *Halogen Bonding: Fundamentals and Applications*, Springer, Berlin, **2008**.
[2] P. Metrangolo, H. Neukirch, T. Pilati, G. Resnati, *Acc. Chem. Res.* **2005**, *38*, 386.
[3] P. Politzer, J. S. Murray, T. Clark, *Phys. Chem. Chem. Phys.* **2010**, *12*, 7748.
[4] P. Politzer, P. Lane, M. C. Concha, Y. Ma, J. S. Murray, *J. Mol. Model.* **2007**, *13*, 305.
[5] T. Helgaker, P. Jorgensen, J. Olson, *Molecular Electronic-Structure Theory*, Wiley, New York, **2000**.
[6] B. Jeziorski, R. Moszynski, K. Szalewicz, *Chem. Rev.* **1994**, *94*, 1887.
[7] A. J. Misquitta, B. Jeziorski, K. Szalewicz, *Phys. Rev. Lett.* **2003**, *91*, 033 201.
[8] A. Heßelmann, G. Jansen, *Chem. Phys. Lett.* **2002**, *357*, 464.
[9] A. E. Reed, L. A. Curtiss, F. Weinhold, *Chem. Rev.* **1988**, *88*, 899.
[10] H.-J. Werner, P. J. Knowles, F. R. Manby, M. Schütz, P. Celani, G. Knizia, T. Korona, R. Lindh, A. Mitrushenkov, G. Rauhut, T. B. Adler, R. D. Amos, A. Bernhardsson, A. Berning, D. L. Cooper, M. J. O. Deegan, A. J. Dobbyn, F.Eckert, E. Goll, C. Hampel, A. Hesselmann, G. Hetzer, T. Hrenar, G. Jansen, C. Köppl, Y. Liu, A. W. Lloyd, R. A. Mata, A. J. May, S. J. McNicholas, W. Meyer, M. E. Mura, A. Nicklass, P. Palmieri, K. Pflüger, R. Pitzer, M. Reiher, T. Shiozaki, H. Stoll, A. J. Stone, R. Tarroni, T. Thorsteinsson, M. Wang, A. Wolf, MOLPRO, version 2010.1, a package of ab initio programs; molpro, **2010**.
[11] A. J. Stone, A. J. Misquitta, *Chem. Phys. Lett.* **2009**, *473*, 201.
[12] I. Dąbkowska, P. Jurečka, P. Hobza, *J. Chem. Phys.* **2005**, *122*, 204 322.
[13] A. Halkier, T. Helgaker, P. Jorgensen, W. Klopper, H. Koch, J. Olsen, A. K. Wilson, *Chem. Phys. Lett.* **1998**, *286*, 243.
[14] K. E. Riley, M. Pitonak, P. Jurecka, P. Hobza, *Chem. Rev.* **2010**, *110*, 5023.
[15] A. J. Stone, A. Dullweber, O. Engkvist, E. Fraschini, M. P. Hodges, A. W. Meredith, D. R. Nutt, P. L. A. Popelier, D. J. Wales, Orient, version 4.5, *A*

Program for Studying Interactions Between Molecules, Cambridge, **2002**; enquiries to A. J. Stone, ajs1@cam.ac.uk.
[16] A. J. Stone, *The Theory of Intermolecular Forces. International Series of Monographs in Chemistry*, Clarendon, Oxford, **1996**.
[17] A. J. Stone, *J. Chem. Phys. Lett.* **1981**, *83*, 233.
[18] A. J. Stone, M. Anderton, *Mol. Phys.* **1985**, *56*, 1047.
[19] A. J. Stone, *J. Chem. Theory Comput.* **2005**, *1*, 1128.
[20] Gaussian 09, Revision A.1, M. J. Frisch, G. W. Trucks, H. B. Schlegel, G. E. Scuseria, M. A. Robb, J. R. Cheeseman, G. Scalmani, V. Barone, B. Mennucci, G. A. Petersson, H. Nakatsuji, M. Caricato, X. Li, H. P. Hratchian, A. F. Izmaylov, J. Bloino, G. Zheng, J. L. Sonnenberg, M. Hada, M. Ehara, K. Toyota, R. Fukuda, J. Hasegawa, M. Ishida, T. Nakajima, Y. Honda, O. Kitao, H. Nakai, T. Vreven, J. A. Montgomery, Jr., J. E. Peralta, F. Ogliaro, M. Bearpark, J. J. Heyd, E. Brothers, K. N. Kudin, V. N. Staroverov, R. Kobayashi, J. Normand, K. Raghavachari, A. Rendell, J. C. Burant, S. S. Iyengar, J. Tomasi, M. Cossi, N. Rega, J. M. Millm, M. Klene, J. E. Knox, J. B. Cross, V. Bakken, C. Adamo, J. Jaramillo, R. Gomperts, R. E. Stratmann, O. Yazyev, A. J. Austin, R. Cammi, C. Pomelli, J. W. Ochterski, R. L. Martin, K. Morokuma, V. G. Zakrzewski, G. A. Voth, P. Salvador, J. J. Dannenberg, S. Dapprich, A. D. Daniels, O. Farkas, J. B. Foresman, J. V. Ortiz, J. Cioslowski, D. J. Fox, Gaussian, Inc., Wallingford, CT, **2009**.
[21] A. G. H. Barbosa, A. M. Barcelos, *Theor. Chem. Acc.* **2009**, *122*, 51.
[22] W. Klopper, J. G. C. M. van Dujineveldt-van de Rijdt, F. B. van Dujineveldt, *Phys. Chem. Chem. Phys.* **2000**, *2*, 2227.
[23] P. Auffinger, F. A. Hays, E. Westhof, P. S. Ho, *Proc. Natl. Acad. Sci. USA* **2004**, *101*, 16789.
[24] S. Karthikeyan, R. Sedlak, P. Hobza, *J. Phys. Chem. A*, **2011**, *115*, 9422.

Received: June 14, 2011
Published online on October 13, 2011

THE JOURNAL OF PHYSICAL CHEMISTRY A

Article

pubs.acs.org/JPCA

Why Is the L-Shaped Structure of $X_2 \cdots X_2$ (X = F, Cl, Br, I) Complexes More Stable Than Other Structures?

Robert Sedlak,[†,§] Palanisamy Deepa,[†,§] and Pavel Hobza*[,†,‡]

[†]Institute of Organic Chemistry and Biochemistry, Academy of Sciences of the Czech Republic, Flemingovo nám. 2, 166 10 Prague 6, Czech Republic

[‡]Regional Centre of Advanced Technologies and Materials, Department of Physical Chemistry, Palacky University, 771 46 Olomouc, Czech Republic

Supporting Information

ABSTRACT: Five different structures (L- and T-shaped (LS, TS), parallel (P), parallel-displaced (PD), and linear (L)) of $(X_2)_2$ dimers (X = F, Cl, Br, I, N) have been investigated at B97-D3, M06-2X, DFT-SAPT, and CCSD(T) levels. The Q_{zz} component of the quadrupole moment of all dihalogens, which coincides with the main rotational axis of the symmetry of the molecule, has been shown to be positive, whereas that of dinitrogen is negative. All of these values correlate well with the most positive value of the electrostatic potential, which, for dihalogens, reflects the magnitude of the σ-hole. The LS structure is the most stable structure for all dihalogen dimers. This trend is the most pronounced in the case of iodine and bromine; for dinitrogen dimer, the LS, TS, and PD structures are comparably stable. The dominant stabilization energy for dihalogen dimers is dispersion energy, followed by Coulomb energy. In the case of dinitrogen dimer, it is only the dispersion energy. At short distances, the Coulomb (polarization) energy for dihalogen dimers is more attractive for the LS structure; at larger distances, the TS structure is more favorable, as dispersion and induction energies are systematically more stable for the TS structure. For all dimers and all distances, the long-range electrostatic energy covering the interactions of multipole moments is the most attractive for the TS structure. In the case of dihalogen dimers, the preference of the LS structure over the others, resulting from the concert action of Coulomb, dispersion, and induction energies, is explained by the presence of a σ-hole. In the case of dinitrogen, comparable stability of LS, TS, and PD structures is obtained, as all are dominantly stabilized by dispersion energy.

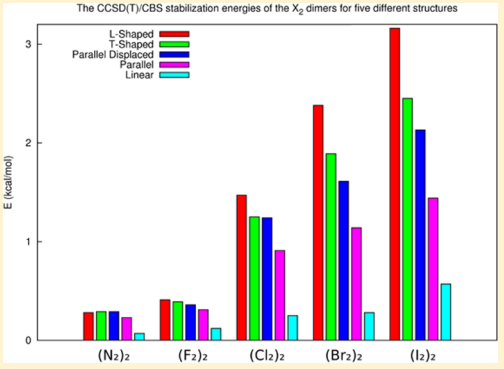

INTRODUCTION

The first nonzero electric multipole moment of dihalogens (X_2, X = F, Cl, Br, I) is the quadrupole moment (Q_{zz}), which is positive for all of these systems. In a simplified notation, these quadrupole moments may be written as + − − +. The quadrupole moment of other diatomics such as dinitrogen is negative and the simplified notation is − + + −. The explanation of the different signs of quadrupole moments of the dihalogens and dinitrogen is not easy because both halogens and nitrogen bear lone electron pairs and pair, respectively. This is in accord with the sign of the quadrupole moment of dinitrogen but not with that of dihalogens.[1,2] To our knowledge, no easy explanation of this fact was available until the recent introduction of the σ-hole, which has been used to explain the origin of the attraction in the halogen bond.[3]

The existence of halogen bonding, described as an attractive interaction between a bound halogen and an electronegative atom, seems counterintuitive, given that an attractive noncovalent interaction is not expected to exist between two atoms that have high electronegativity, that is, possess a partial negative charge. The reason for the attractive noncovalent interaction that occurs in halogen bonds is the presence of a region of a positive electrostatic potential (σ-hole) along the extension of the C−X bond (X is most typically bound to carbon), which interacts electrostatically with an electron donor.[4,5] Here, we present the recent IUPAC definition of the halogen bonding: "A halogen bond occurs when there is evidence of a net attractive interaction between an electrophilic region associated with a halogen atom in a molecular entity and a nucleophilic region in another, or the same, molecular entity."[6,7]

The existence of the positive σ-hole explains positive quadrupole moments in dihalogens; similarly, the nonexistence of the σ-hole in dinitrogen explains its negative quadrupole moment. Are the two concepts fully equivalent? In other words, do they both lead to the same structure prediction? Certainly, such a comparison is limited to systems where the first nonvanishing multipole moment is the quadrupole moment. In other cases (i.e. for systems with dipole moments), the concept of the σ-hole is clearly the only applicable explanation. We

Received: March 17, 2014
Revised: May 5, 2014
Published: May 5, 2014

   dx.doi.org/10.1021/jp502648e | J. Phys. Chem. A 2014, 118, 3846−3855

should mention a study done by Duarte et al.,[8] in which analyses of atomic quadrupole moments of halogens were performed for halogen bonded complexes.

The aim of the present paper is to investigate different structures of the (X_2, X = F, Cl, Br, I, N) complexes.

CALCULATIONS

The electrostatic potential (ESP)[9−12] computed for all subsystems at the B97/def2-QZVP,[13,14] HF/aug-cc-pVTZ,[15−19] PBE0/aug-cc-pVTZ,[20−22] MP2/aug-cc-pVTZ,[23] and CISD/aug-cc-pVTZ[24] levels was determined on the 0.001 au (e^-/Bohr^3) isodensity surface, as proposed by Bader et al.[25] The point on the 0.001 au isodensity surface, which lies on the main rotational axis of the X_2 molecule, is referred to here as $V_{s,max}$ (Figures S1 and S2, Supporting Information). In the case of dihalogens, this point possesses the most positive value of the ESP (the local maximum). The angular dependence of the ESP was also investigated. The angle α, at which the ESP becomes negative when moving from the $V_{s,max}$ point on the 0.001 isodensity surface, was evaluated. The $V_{s,max}$ and α quantities are the magnitude and the size of the σ-hole and have been defined by Kolář et al.[26] For more details concerning $V_{s,max}$ and α, see the Supporting Information or ref 26.

The benchmark stabilization energies were obtained from CCSD(T)/CBS calculations. The DFT-SAPT method has been shown to provide a reliable estimation of the stabilization energies of various noncovalent interactions including the halogen bond.[27−38] Hence, the DFT-SAPT calculations were used for the decomposition of the total interaction energy.

The relativistic effects were included by considering the pseudopotentials (PPs).[39,40] Specifically, for bromine and iodine at the HF, PBE0, MP2, CCSD(T)/CBS, DFT-SAPT, and CISD levels, PPs consistent with respective correlation consistent basis sets (aug-cc-pVXZ-PP) were applied. At the B97-D3/def2-QZVP level, the PPs were considered only for iodine.

Five different structures of the $(X_2)_2$ dimers (L-shaped (LS), T-shaped (TS), parallel (P), parallel-displaced (PD), and linear (L)) were considered, and the respective energy minima were determined by an unrelaxed potential energy scan along the main intermolecular coordinates (Figure 1). The scans were performed on the grid with a point-to-point distance of 0.1 Å. The geometries of the X_2 molecules considered for all calculations were calculated at the B97-D3/def2-QZVP level of theory.

The benchmark interaction energies were evaluated at the CCSD(T) level and extrapolated to the complete basis set (CBS) limit. Specifically, the CCSD(T)/CBS interaction energy was constructed as the sum of HF/CBS interaction energy and the correlation part of the MP2/CBS interaction energy. Both were determined by the two-point extrapolation scheme of Halkier from aug-cc-pVTZ and aug-cc-pVQZ basis sets.[41,42] The CCSD(T) correction term ($\Delta E^{CCSD(T)} - \Delta E^{MP2}$) was evaluated utilizing the aug-cc-pVTZ basis set.[43−46] Besides CCSD(T), two variants of the DFT method were applied. The M06-2X functional[47] was recommended for calculations of halogen-bonded complexes.[48] Therefore, this functional in combination with the aug-cc-pVTZ basis set was used in the present study along with the DFT-D (B97-D3/def2-QZVP) method.[49] The Grimme's empirical dispersion correction (D3) was calculated employing Becke−Johnson damping.[50]

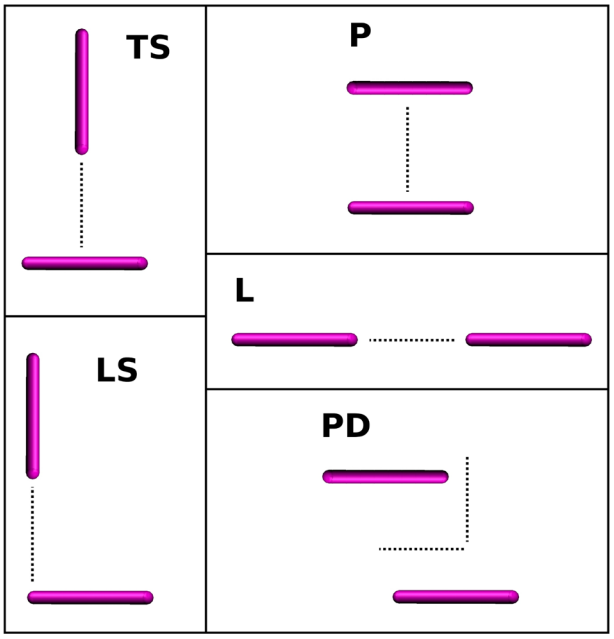

Figure 1. The five conformers that were considered for each homodimer. The intermolecular coordinate along which the unrelaxed scan was performed is also depicted. LS, TS, P, PD, and L stand for L-shaped, T-shaped, parallel, parallel-displaced, and linear, respectively.

The decomposition of stabilization energy was obtained by using the SAPT method,[51] specifically the DFT-SAPT technique. The subsystems were treated via the DFT approach, utilizing the asymptotically corrected LPBE0AC exchange-correlation functional[52,57] and the aug-cc-pVTZ basis set for nitrogen, fluorine, and chlorine. In the case of bromine and iodine, the aug-cc-pVTZ-PP basis set was used to account for relativistic effects.[39,40] The DFT-SAPT total interaction energy is given as the sum of the first- (E_1) and second-order (E_2) perturbation energy terms and δHF energy terms, specifically Coulomb (E_1^{Pol}), induction (E_2^{I}), and dispersion (E_2^{D}), together with exchange-repulsion terms (E_1^{Ex}, $E_2^{Ex\text{-}I}$, $E_2^{Ex\text{-}D}$). The exchange-induction and exchange-dispersion terms are merged into the respective induction and dispersion terms. Further, the δHF term, which represents higher than second-order terms covered by the Hartree−Fock approach, is also included in the induction energy.

$$E_{int} = E_1^{Pol} + E_1^{Ex} + E_2^{I} + E_2^{Ex\text{-}I} + \delta HF + E_2^{D} + E_2^{Ex\text{-}D} = E_1^{Pol} + E_1^{Ex} + E_2^{Ind} + E_2^{Disp} \quad (1)$$

More details about the DFT-SAPT calculations can be found in refs 53−59.

Finally, the long-range electrostatic interaction energy between two subsystems covering interactions of multipoles was calculated using the distributed multipole analysis of Stone.[60−62] The multipole moments were calculated on the basis of the PBE0/aug-cc-pVTZ wave function using the GDMA program.[63] Subsequently, the electrostatic interactions between molecules were calculated via the Orient program.[64] The diatomic molecule was represented by three sites. Two of these sites coincide with X atoms, and the third one was located in the middle of the X−X bond. Each site was constituted by the multipole moments up to the hexadecupole. For the technical details of the distributed multipole moment analysis, see ref 62.

dx.doi.org/10.1021/jp502648e | J. Phys. Chem. A 2014, 118, 3846−3855

All of the post Hartree−Fock calculations (MP2, CCSD(T), and DFT-SAPT) were carried out using the MOLPRO 2010 software package.[65] The convergence threshold imposed on the change in energy and root-mean-square deviation (RMSD) of the density matrix between consecutive SCF iterations was set to 10^{-9} and 10^{-6} au, respectively. The CCSD convergence criteria were set to 10^{-8} au for the energy change and 10^{-8} au for the square sum of the changes of the CC amplitudes. The DFT-based methods, excluding M06-2X, were applied utilizing the TURBOMOLE 6.3 software package.[66] The TURBOMOLE grid m3 was consistently used for integral evaluation in all the calculations. The convergence criteria were set to 10^{-7} and 10^{-6} au for the energy change and RMSD of the density matrix, respectively. The M06-2X and population analysis[67] calculations were carried out using the Gaussian 09 software package,[68] employing default convergence criteria and a default fine grid for integral evaluation. All of the interaction energy calculations were corrected for the basis set superposition error employing counterpoise correction.[69] A full description of the material can be found in the Supporting Information.

RESULTS AND DISCUSSION

Isolated Systems. Table 1 summarizes the geometries, quadrupole moments, and size (α) and magnitude ($V_{s,max}$)[26] of

Table 1. Geometries, Quadrupole Moments, and $V_{s,max}$ for all Monomers Calculated at the B97/def2-QZVP Level of Theory

systems	geometries (Å)	quadruple moment[a]	$V_{s,max}$ (au)[b]
I_2	2.703	3.402	0.0474
Br_2	2.322	2.362	0.0443
Cl_2	2.013	1.574	0.0389
F_2	1.410	0.436	0.0243
N_2	1.116	−0.774	−0.0140

[a]The Q_{zz} component in ea_o^2. [b]Calculated at the 0.001 au isodensity surface.

σ-holes calculated for all subsystems at the B97/def2-QZVP level of theory. The electrostatic potential for all subsystems is visualized in Figure 2. Clearly, the quadrupole moments of all dihalogens are positive, while the quadrupole moment of dinitrogen is negative. The same is valid for the magnitudes of the σ-holes ($V_{s,max}$). The negative value of $V_{s,max}$ for dinitrogen

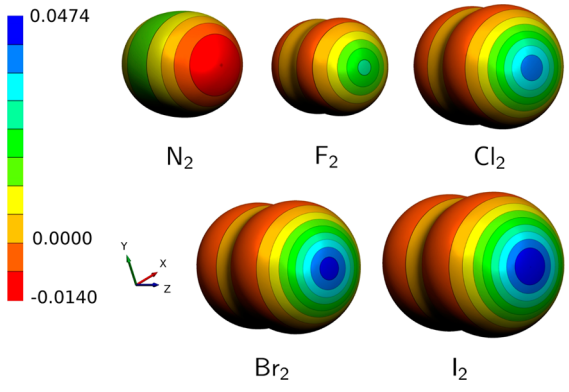

Figure 2. Electrostatic potential (in au) mapped on the 0.001 au isodensity surface for all monomers calculated at the B97/def2-QZVP level of theory. The z axis coincides with the main rotational axis of the molecule (the X−X bond direction).

indicates that the positive σ-hole is not present. The largest absolute value of both characteristics (quadrupole moments and $V_{s,max}$) was found for diiodine, and the smallest positive one was found for difluorine (the smallest $V_{s,max}$ was calculated for dinitrogen); quadrupole moments and $V_{s,max}$ correlate very well (R^2 = 0.849) for all systems.

This finding is important because it shows that at least for the systems studied (and similar systems for which the first nonzero multipole moment is quadrupole) their nontrivial electronic structure is described already by the classical concept of electric quadrupoles and that the recently introduced new concept of the σ-hole is not bringing any new information.

Table S1 (Supporting Information) compares the quadrupole moments (Q_{zz}) calculated at the B97/def2-QZVP, PBE0/aug-cc-pVTZ, HF/aug-cc-pVTZ, MP2/aug-cc-pVTZ, and CISD/aug-cc-pVTZ (as reference) levels of theory. We have done these calculations to verify the reliability of the DFT methods in providing accurate electrostatic properties because our further discussions are based on DFT calculations. The DFT and MP2 methods provide reliable values of quadrupole moments for all the molecules with respect to the reference CISD data (Table S1, Supporting Information). The only exception is the large underestimation of the quadrupole moment at the HF level for the F_2 molecule. This failure of the HF method to provide an accurate quadrupole moment for the F_2 molecule has already been discussed in the literature, see ref 1 and the references therein. It is attributed to the extremely compact character of the valence orbitals of the F_2 molecule.[1] However, in the case of the DFT (PBE0, B97) methods, no such discrepancy has been observed for this anomalous molecule. This is encouraging and serves as a proof that the use of the DFT methods for these purposes is legitimate.

Table S2 (Supporting Information) materials lists $V_{s,max}$ and the qaudrupole-moment (Q_{zz}) values for all diatomics at all the levels of theory mentioned. The high correlation between these two quantities can be observed for all of the methods tested. The correlation coefficient (R^2) amounts to 0.838, 0.849, 0.852, 0.858, and 0.869 for MP2, B97, CISD, PBE0, and HF, respectively. These results only support the already stated conclusion about the close relation between Q_{zz} and $V_{s,max}$.

Table 2 presents the X−X bond orbital analysis together with the occupancy of the p-type valence natural atomic orbitals (NAOs) and $V_{s,max}$ values. It further lists the size (angle α) and magnitude ($V_{s,max}$) of the σ-hole. The angle α varies between 59° (F_2) and 65°(I_2). When one moves from difluorine toward heavier dihalogens, the slight increase of α is in correlation with the significant increase of $V_{s,max}$. The small variation of the size of the σ-hole can be interpreted using the natural-bond orbital (NBO) analysis.[67]

First, the hybridization between s and p orbitals, in the case of the X−X natural-bond orbital, is negligible, not exceeding 6% (dichlorine). Second, the occupancy of p-type valence NAOs does not differ much between different halogens. Specifically, the valence p_z occupancy varies between 1.022 (I_2) and 1.043 (Cl_2). Moreover, the occupancy of the p_x and p_z orbitals is essentially constant. Finally, it is clear that the hybridization state and the occupancy of NAO are more or less constant for all dihalogens. Consequently, we conclude that the angular redistribution of the valence electrons is very similar for all dihalogens. Hence, marginal differences in the size of the σ-hole are observed. On the other hand, the possible explanation for the relatively large increase of the $V_{s,max}$ value (Table 1) can be seen as a consequence of the decreasing ability of the electron

Table 2. Hybridization State (%) of the Natural Hybrid Orbital (NHO) of Atom X in the Natural X−X Bonding Orbital, Occupancies of the p-Type Valence Natural Atomic Orbitals of Atom X, $V_{s,max}$, and the Size of the σ-hole (α)[a]

	NHOs of X−X NBOs					NAOs of p-type valence				
X	s	p	d	f	g	p_x	p_y	p_z[b]	$V_{s,max}$ (au)[c]	α (deg)[c]
F	4.9	94.9	0.2	0.1	0.0	1.999	1.999	1.038	0.0243	59
Cl	6.2	92.5	1.0	0.3	0.0	1.992	1.992	1.043	0.0389	62
Br	4.3	94.8	0.6	0.2	0.0	1.994	1.994	1.029	0.0443	64
I	3.5	95.6	0.5	0.3	0.0	1.994	1.994	1.022	0.0474	65
N	36.6[d]	62.9[d]	0.5[d]	0.0[d]	0.0[d]	0.996	0.996	1.325	−0.0140	
	0.0[e]	99.6[e]	0.4[e]	0.0[e]	0.0[e]					

[a]All data correspond to the B97/def2-QZVP densities and B97-D3/def2-QZVP geometries of X_2 molecules. [b]The z axis coincides with the X−X bond. [c]Calculated at the 0.001 au isodensity surface. For more details, see the Supporting Information. [d]The numbers correspond to s-type NBOs. [e]The numbers correspond to p-type NBOs.

Table 3. Interaction Energies (kcal/mol) Calculated at the B97-D3, M062X, CCSD(T)/CBS, and DFT-SAPT Levels of Theory for L-Shaped (LS), T-Shaped (TS), Parallel (P), Parallel-Displaced (PD), and Linear (L) Structures[a]

		R/R'	B97-D3	R/R'	M06-2X	R/R'	CCSD(T)/CBS	DFT-SAPT
LS	I_2	3.5/5.0	−4.77 (−3.44)	3.6/5.1	−2.96	3.6/5.1	−3.16	−3.64
	Br_2	3.3/4.6	−2.86 (−2.68)	3.3/4.6	−2.31	3.4/4.7	−2.38	−2.47
	Cl_2	3.3/4.4	−1.58 (−1.94)	3.2/4.3	−1.18	3.3/4.4	−1.47	−1.20
	F_2	3.2/4.0	−0.30 (−0.23)	2.9/3.7	−0.39	2.8/3.6	−0.41	−0.30
	N_2	3.7/4.3	−0.47 (−0.46)	3.8/4.4	−0.21	3.6/4.2	−0.28	−0.26
TS	I_2	4.1/5.2	−3.04 (−3.23)	4.0/5.1	−2.27	4.1/5.2	−2.45	−2.61
	Br_2	3.9/4.9	−1.96 (−2.25)	3.7/4.7	−1.61	3.7/4.7	−1.89	−1.93
	Cl_2	3.7/4.6	−1.25 (−1.69)	3.5/4.4	−0.87	3.6/4.5	−1.25	−1.05
	F_2	3.2/3.8	−0.29 (−0.24)	3.0/3.6	−0.38	3.0/3.6	−0.39	−0.31
	N_2	3.7/4.2	−0.48 (−0.45)	3.8/4.3	−0.21	3.6/4.1	−0.29	−0.27
P	I_2	4.5/4.5	−2.22 (−3.36)	4.4/4.4	−0.53	4.5/4.5	−1.44	−1.46
	Br_2	4.2/4.2	−1.50 (−2.39)	4.2/4.2	−0.37	4.2/4.2	−1.14	−1.08
	Cl_2	4.1/4.1	−1.04 (−1.49)	4.0/4.0	−0.40	3.9/3.9	−0.91	−0.78
	F_2	3.6/3.6	−0.26 (−0.22)	3.1/3.1	−0.36	3.2/3.2	−0.31	−0.25
	N_2	3.8/3.8	−0.51 (−0.57)	4.0/4.0	−0.20	3.7/3.7	−0.23	−0.22
PD	I_2	4.5/4.5	−2.82 (−3.85)	4.3/4.3	−1.73	4.4/4.4	−2.13	−2.26
	Br_2	4.2/4.2	−1.83 (−2.64)	4.0/4.0	−1.19	4.0/4.0	−1.61	−1.58
	Cl_2	3.9/3.9	−1.23 (−2.08)	3.7/3.7	−0.89	3.8/3.8	−1.24	−1.02
	F_2	3.6/3.6	−0.26 (−0.25)	3.3/3.3	−0.34	3.2/3.2	−0.36	−0.28
	N_2	3.9/3.9	−0.55 (−0.60)	4.4/4.4	−0.20	4.0/4.0	−0.31	−0.29
L	I_2	4.2/6.9	−0.72 (−1.61)	3.8/6.5	−0.18	3.9/6.6	−0.57	−0.44
	Br_2	4.1/6.4	−0.43 (−1.01)	3.5/5.8	0.17	3.7/6.0	−0.28	−0.15
	Cl_2	3.8/5.8	−0.34 (−0.81)	4.1/6.1	0.02	3.5/5.5	−0.25	−0.11
	F_2	3.3/4.7	−0.11 (−0.13)	3.0/4.4	−0.14	2.9/4.3	−0.12	−0.11
	N_2	3.9/5.0	−0.13 (−0.20)	4.0/5.1	−0.09	3.7/4.8	−0.07	−0.07

[a]The numbers in parentheses correspond to dispersion energy. R and R' correspond to the closest X···X and center of mass distances (in Å), respectively.

shell to shield the nucleus. In other words, the shielding of the nucleus charge is more significant in the case of the compact electron shell (e.g., fluorine, chlorine) than in the case of the diffuse one (e.g., bromine, iodine).

The character of the electron redistribution is entirely different for the dinitrogen molecule when compared with dihalogens. The triple bond is represented by two π- and one σ-bond orbitals within the NBO analysis (Table 2).

The sign of the $V_{s,max}$ value, which is positive in the case of dihalogens and negative for dinitrogen, can be interpreted by means of the relative occupancy of the NAOs of the valence p type.[2] In the case of dihalogens, the lack of electron density is observed in the z axis, which coincides with the X−X bond when compared with the x and y axes. In the case of dinitrogen, the opposite is true (Table 2).

Complexes. The total interaction energies of all dihalogen dimers determined by the B97-D3, M06-2X, CCSD(T), and DFT-SAPT techniques are given in Table 3. The numbers in parentheses listed with the B97-D3 energies correspond to the respective empirical dispersion energies. In the case of DFT-SAPT calculations presented in Table 3, the potential-energy scans were not made, and the values correspond to the structures, which represent the CCSD(T)/CBS energy minima.

Stabilization energies evaluated at different levels of theory correlate well with reference CCSD(T) stabilization energies. Specifically, correlation coefficient (R^2) amounts to 0.95, 0.92, and 0.99 for the B97-D3, M06-2X, and DFT-SAPT method. The general performance of listed methods, which can be judged on the basis of the value of the root-mean-square deviation (RMSD) with respect to reference data, is following. The most accurate method is DFT-SAPT followed by M06-2X

dx.doi.org/10.1021/jp502648e | J. Phys. Chem. A 2014, 118, 3846−3855

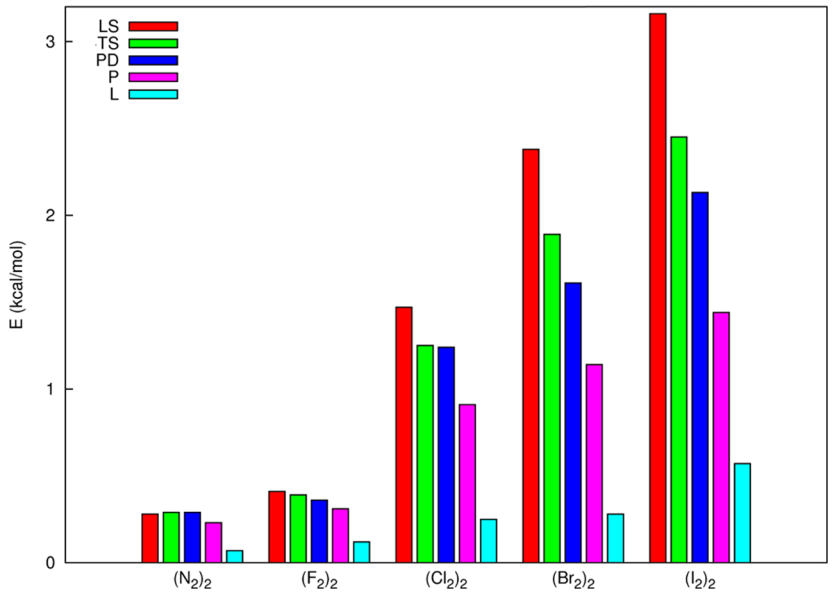

Figure 3. CCSD(T)/CBS stabilization energies (in kcal/mol) for all complexes. LS, TS, P, PD, and L stand for L-shaped, T-shaped, parallel, parallel-displaced, and linear, respectively.

and B97-D3. Corresponding RMSD values are 0.15, 0.34, and 0.44 kcal/mol.

Specifically, the B97-D3 interaction energies are mostly the largest ones and are, especially for the heavier dihalogens, strongly overestimated (with respect to the CCSD(T)/CBS benchmark values). The average absolute (relative) errors for chlorine, bromine, and iodine are −0.06 (11), −0.26 (25), and −0.76 kcal/mol (38%), respectively. The same feature of overestimation is observed for nitrogen. Error amounts to −0.19 kcal/mol (85%). However, in the case of fluorine, the interaction energies are underestimated. The average absolute (relative) error is 0.07 kcal/mol (−21%).

The M06-2X method exhibits opposite trends. In the case of fluorine, the interaction energies are overestimated. The absolute (average) error is −0.03 kcal/mol (12%), whereas the average absolute (relative) errors for chlorine, bromine, iodine, and nitrogen are 0.34 (−47), 0.38 (−53), 0.42 (−33), and 0.05 kcal/mol (−13%), respectively.

DFT-SAPT energies match closely with the benchmark data. The relatively low overestimation for iodine complexes is −0.13 kcal/mol (1%). The underestimation is observed for the rest of the complexes and varies from 0.01 kcal/mol (−5%) for nitrogen up to 0.19 kcal/mol (−25%) for chlorine.

Investigating the reference CCSD(T)/CBS stabilization energies of dihalogen complexes, we found that the LS structure corresponds with the most stable structure (i.e., the global minimum), followed by the TS, PD, P, and L structures. For heavier dihalogens, the LS and TS structures are more stable than other structures; in the case of difluorine, all the structures, except linear (L), are comparably stable (Figure 3). This finding is surprising because it was long believed that the TS structure of dihalogens, stabilized by quadrupole−quadrupole electrostatic interaction, corresponds to the global minimum. Moreover, Table 3 (the last column labeled as R/R') shows that the intermolecular distances between the centers of mass for the optimized LS and TS structures are similar.

The DFT-SAPT total interaction energies of all dihalogen dimers are the most negative for the LS structure (Table 3). Analyzing the DFT-SAPT energy components (Figure 4), we found that this is mainly caused by the Coulomb E_1^{Pol} energies. The other attractive energies (dispersion and induction) are also the largest for the LS structure, but the absolute difference with respect to other structures (TS, PD, P, and L) is much smaller. This can be interpreted as a consequence of the higher orientation dependence of the Coulomb interaction, in contrast with induction and dispersion. However, it should be stressed that the largest attractive contribution for all structures (including LS and TS) comes from dispersion energy, followed by Coulomb energy.

To exclude the overlap effects (see below), we evaluate the total interaction energies at the DFT-SAPT level for the two most stable structures (LS and TS) and for larger intermolecular distances. These scans are performed for the diiodine dimer and will be discussed in the following paragraphs. Figure 5 shows the distance dependence of the total DFT-SAPT as well as Coulomb (E_1^{Pol}) energies for the LS and TS structures of the diiodine dimer. At short distances, the Coulomb energy is evidently more attractive for the LS structure, while the opposite is true at larger distances. On the other hand, the total DFT-SAPT energy is systematically larger for the LS structure. This finding can be easily explained on the basis of penetration energy.[51] The systematically attractive penetration energy, which is included in the DFT-SAPT Coulomb energy, is overlap-dependent. The overlap in the LS structure is clearly larger than that in the TS structure because of a closer X···X contact in the former structure. At large distances, the penetration of both molecules becomes negligible and the DFT-SAPT Coulomb energy is exclusively represented by long-range electrostatic energy. The long-range electrostatic energy covering all the interactions between the multipole moments is less attractive for the L-shaped structure than for the T-shaped structure (Figure 6).

We should summarize the previous findings. In the whole range of distances, the stabilization energy of the LS structure is larger than that of the TS structure, while the opposite is true for the long-range electrostatic energy. The Coulomb energy is larger for the LS structure only at short distances. The question

dx.doi.org/10.1021/jp502648e | J. Phys. Chem. A 2014, 118, 3846−3855

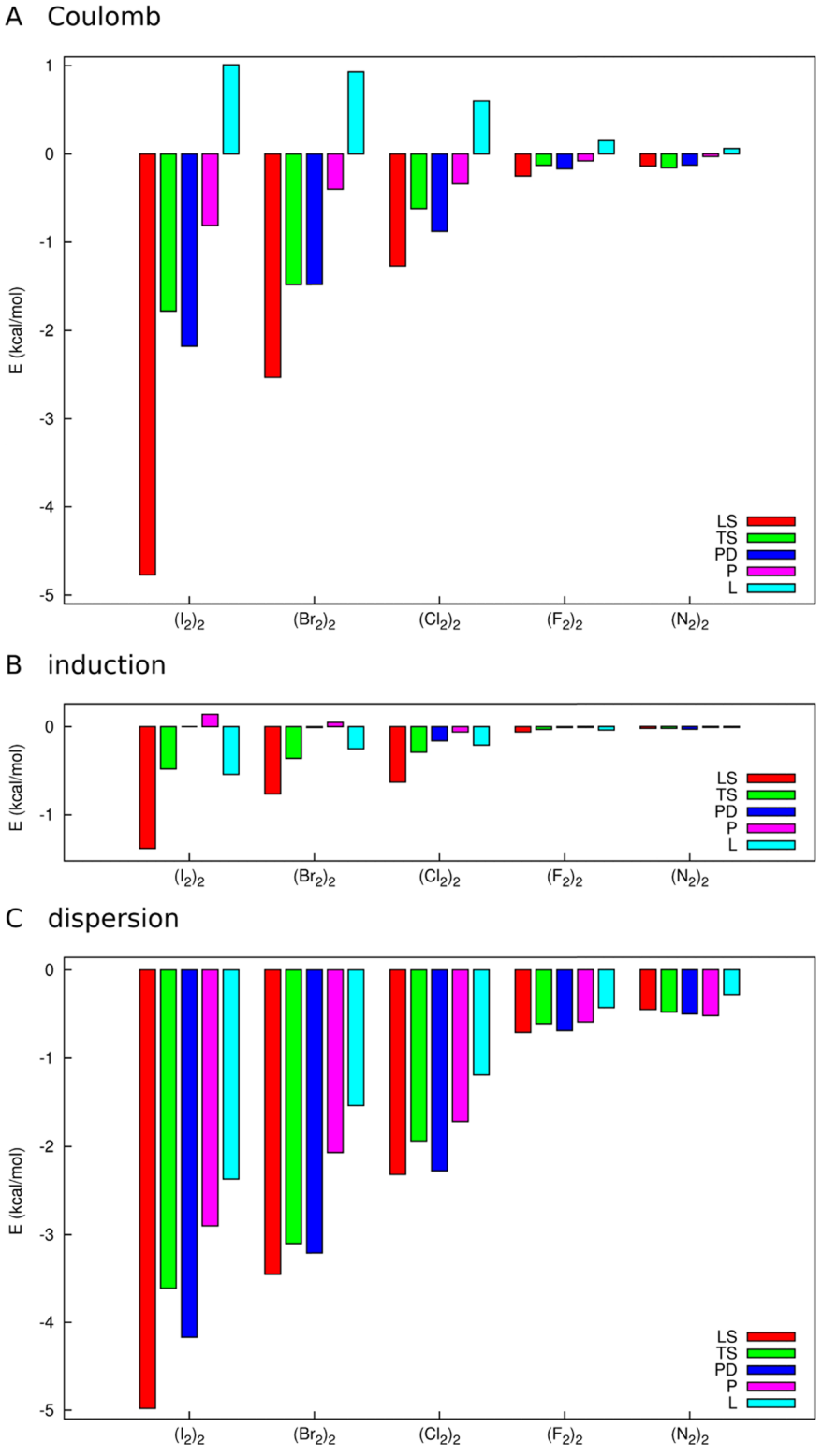

Figure 4. Coulomb E_1^{Pol} (A), induction E_2^{Ind} (B), and dispersion E_2^{Disp} (C) components of the DFT-SAPT interaction energy (in kcal/mol), listed for all five structures of each complex. For exact definitions of Coulomb, induction, and dispersion, see the Calculations section.

is how to explain the larger stabilization energy in the L-shaped structure. Figure 7 shows the distance dependence of the remaining attractive energy terms, dispersion (E_2^{Disp}) and induction (E_2^{Ind}). It is evident that both energies are systematically more attractive for the LS structure. This was also observed for equilibrium geometries (see above). The reason for this is again the shorter interatomic distances for the LS structure. The preference of the LS structure in the entire distance region cannot be explained by either electrostatic or Coulomb energies. It is a result of the concert action of all three attractive energies, Coulomb, dispersion and induction.

The interaction interpreted via quadrupoles prefers the T-shaped structure, but the full QM treatment leads to the L-shaped structure. An alternative description of the monomers is

dx.doi.org/10.1021/jp502648e | J. Phys. Chem. A 2014, 118, 3846−3855

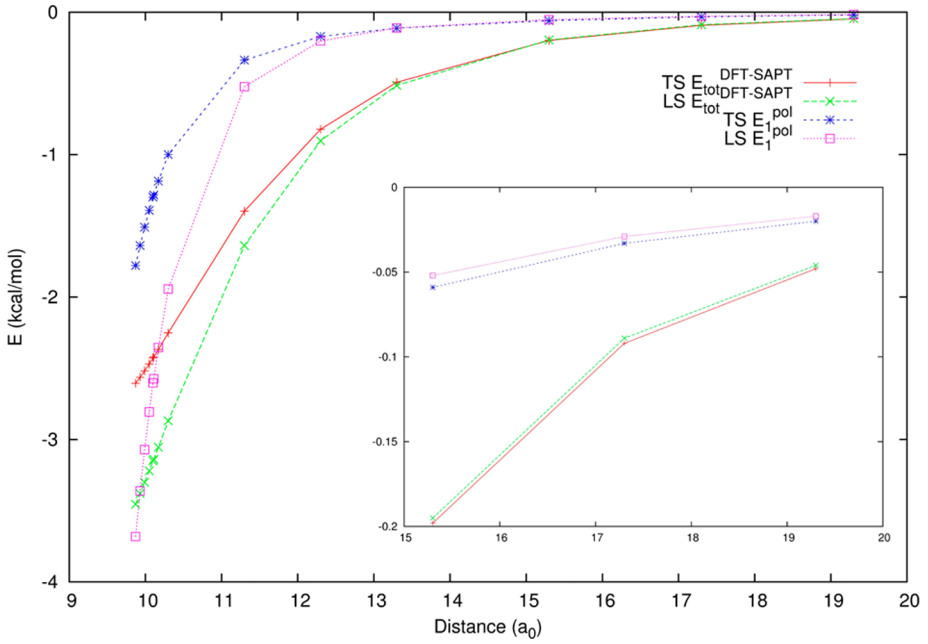

Figure 5. Distance dependence of the total interaction ($E_{tot}^{DFT\text{-}SAPT}$) and Coulomb ($E_1^{Pol}$) energies for LS and TS structures of the diiodine dimer calculated at DFT-SAPT/aug-cc-pVTZ-PP level of theory. All energies are listed in kilocalories per mole (kcal/mol).

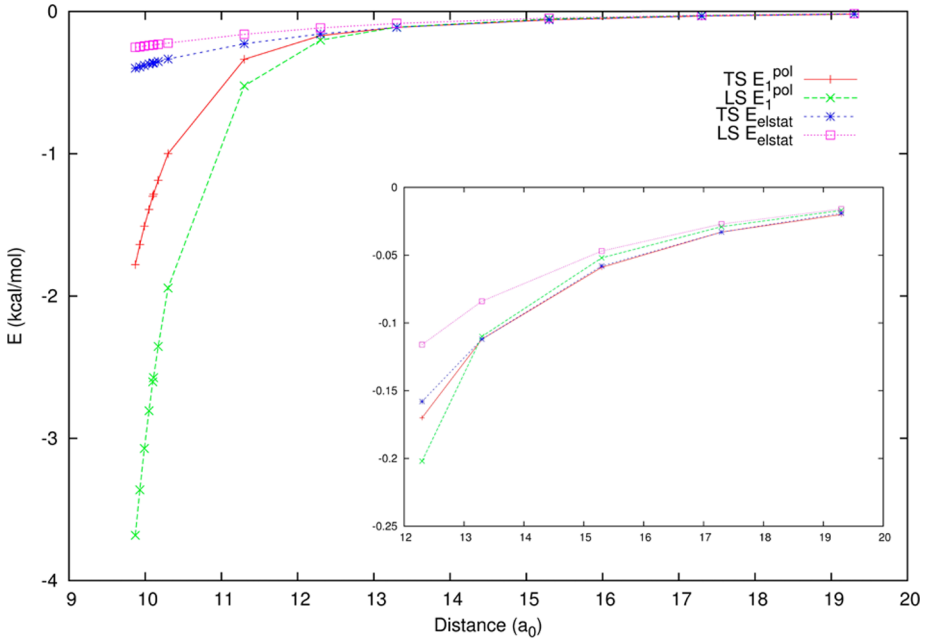

Figure 6. Distance dependence of electrostatic (E_{elstat}) and Coulomb (E_1^{Pol}) energies for the LS and TS structures of the diiodine dimer calculated using distributed multipole analysis[57−59] and the DFT-SAPT/aug-cc-pVTZ-PP level of theory, respectively. All energies are listed in kilocalories per mole (kcal/mol).

provided by the concept of electrostatic potential, for example, the σ-hole (see above). The question arises whether the interaction of two dihalogens, each possessing the σ-hole, can be explained or at least schematically interpreted on the basis of the monomer electrostatic potential. Another question is whether it would be possible to explain the preferential binding of the L-shaped structure within this concept. Figure 8 schematically shows the LS and TS structures together with the ESP of isolated molecules. Evidently, the first structure exhibits a strong attractive electrostatic interaction between the most positive σ-hole of the upper (vertical) dihalogen and the less positive belt of the lower (horizontal) one (the so-called dihalogen bond). Such an interaction is not expressed as strongly in the T-shaped structure. Thus, it is possible to conclude that the preferential binding of the LS structure in all the dihalogen dimers investigated can be interpreted by the dihalogen bonding. The classical concept of electric multipoles cannot be used because it leads to preferential binding in the TS structure.

The situation with dinitrogen not possessing the σ-hole is different. Here, the total stabilization energy at the CCSD(T)/CBS level is comparable for the LS, TS, and PD structures. The

dx.doi.org/10.1021/jp502648e | J. Phys. Chem. A 2014, 118, 3846−3855

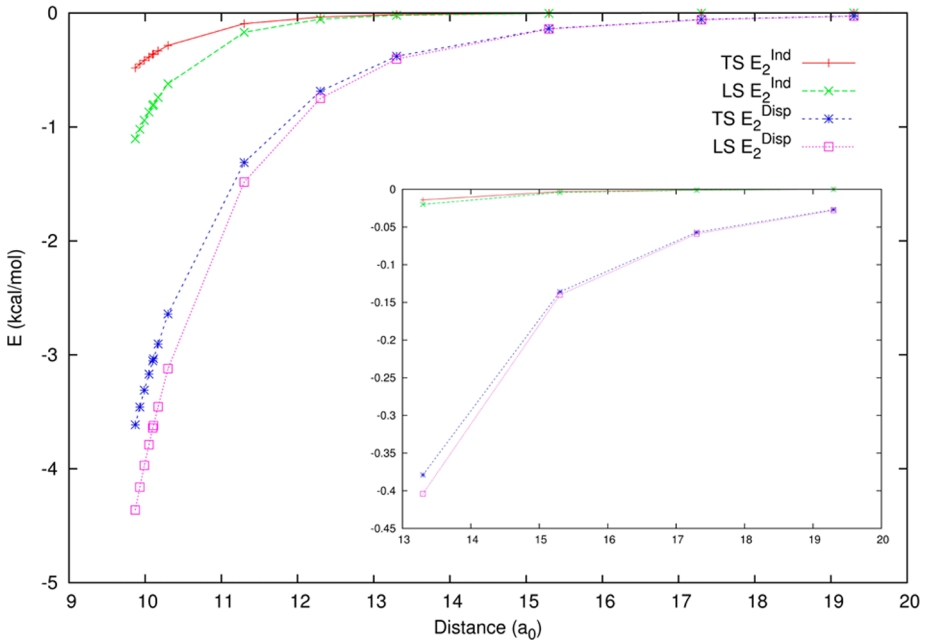

Figure 7. Distance dependence of induction (E_2^{Ind}) and dispersion (E_2^{Disp}) energies for the LS and TS structures of the diiodine dimer calculated at the DFT-SAPT/aug-cc-pVTZ-PP level of theory. All energies are listed in kilocalories per mole (kcal/mol).

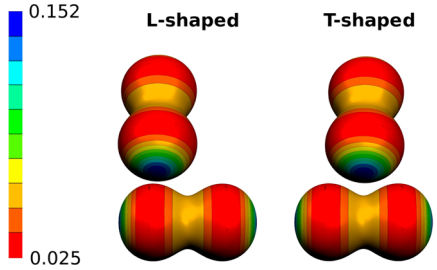

Figure 8. L-shaped (left) and T-shaped (right) structures of the X_2 dimer. A schematic interpretation of the electrostatic interaction based on the electrostatic potentials (ESP, in au) of isolated monomers. The ESP is mapped on the 0.01 au isodensity surface to prevent the overlap of the electron densities.

L and P structures are less stable (Figure 3). Analyzing the DFT-SAPT energies, we found that dispersion energy is clearly a dominant stabilization term for all five conformers (Figure 4), while Coulomb energy is marginal. It could thus be concluded that the preference of the LS structure found in dihalogen dimers arises from the presence of the σ-hole, or, in other words, the presence of the dihalogen bond. In this case, Coulomb energy is important. On the other hand, when the σ-hole is absent, Coulomb energy is negligible, and dispersion energy becomes clearly dominant.

CONCLUSIONS

The most stable structure among the complexes of homodiatomics possessing the σ-hole is the LS structure. For dinitrogen dimer (a system without the σ-hole), it is TS structure. The stabilization in the former case results from the existence of a dihalogen bond having comparable Coulomb and dispersion energies. The TS structure of dinitrogen dimer is stabilized dominantly by dispersion energy.

ASSOCIATED CONTENT

Supporting Information

Schematic representation of the grid orientation of the X_2 molecule; definition of the σ-hole size; and $V_{s,max}$ (in au) and quadrupole moment (Q_{zz} in au) values for all diatomics (F_2, Cl_2, Br_2, I_2 and N_2). This material is available free of charge via the Internet at http://pubs.acs.org.

AUTHOR INFORMATION

Corresponding Author

*E-mail: pavel.hobza@uochb.cas.cz.

Author Contributions

§Both authors have contributed equally and can be considered as the first author.

Notes

The authors declare no competing financial interest.

ACKNOWLEDGMENTS

This work was part of the Research Project RVO: 61388963 of the Institute of Organic Chemistry and Biochemistry, Academy of Sciences of the Czech Republic. This work was also supported by the Czech Science Foundation (P208/12/G016) and the operational program Research and Development for Innovations of the European Social Fund (CZ 1.05/2.1.00/03/0058).

REFERENCES

(1) Barbosa, A. G. H.; Barcelos, A. M. The Electronic Structure of the F_2, Cl_2, Br_2 Molecules: The Description of Charge-Shift Bonding within the Generalized Valence Bond Ansatz. *Theor. Chem. Acc.* **2009**, *122*, 51−66.

(2) Munusamy, E.; Sedlak, R.; Hobza, P. On The Nature of the Stabilization of Benzene···Dihalogen and Benzene···Dinitrogen Complexes: CCSD(T)/CBS and DFT-SAPT Calculations. *ChemPhysChem* **2011**, *12*, 3253−3261.

(3) Politzer, P.; Murray, J. S.; Clark, T. Halogen Bonding: An Electrostatically Driven Highly Directional Noncovalent Interaction. *Phys. Chem. Chem. Phys.* **2010**, *12*, 7748−7757.
(4) Clark, T.; Hennemann, M.; Murray, J. S.; Politzer, P. Halogen Bonding: The σ-Hole. *J. Mol. Model.* **2007**, *13*, 291−296.
(5) Politzer, P.; Lane, P.; Concha, M. C.; Ma, Y.; Murray, J. S. An Overview of Halogen Bonding. *J. Mol. Model.* **2007**, *13*, 305−311.
(6) Desiraju, G. R.; Shing Ho, P.; Kloo, L.; Legon, A. C.; Marquardt, R.; Metrangolo, P.; Politzer, P.; Resnati, G.; Rissanen, K. Definition of the Halogen Bond. *Pure Appl. Chem.* **2013**, *85*, 1711−1713.
(7) Muller, P. Glossary of Terms Used in Physical Organic Chemistry. *Pure Appl. Chem.* **1994**, *66*, 1077−1184.
(8) Duarte, D. J. R.; Angelina, E. L.; Peruchena, N. M. On the Strength of the Halogen Bonds: Mutual Penetration, Atomic Quadrupole Moment and Laplacian Distribution of the Charge Density Analysis. *Comput. Theor. Chem.* **2012**, *998*, 164−172.
(9) Politzer, P.; Laurence, P. R.; Jayasuriya, K. Molecular Electrostatic Potentials: An Effective Tool for the Elucidation of Biochemical Phenomena. *Environ. Health Perspect.* **1985**, *61*, 191−202.
(10) Murray, J. S.; Politzer, P. Statistical Analysis of the Molecular Surface Electrostatic Potential: An Approach to Describing Noncovalent Interactions in Condensed Phases. *J. Mol. Struct.: THEOCHEM* **1998**, *425*, 107−114.
(11) Politzer, P.; Murray, J. S. Representation of Condensed Phase Properties in Terms of Molecular Surface Electrostatic Potentials. *Trends Chem. Phys.* **1999**, *7*, 157−168.
(12) Politzer, P.; Murray, J. S.; Peralta-Inga, Z. Molecular Surface Electrostatic Potentials in Relation to Noncovalent Interactions in Biological Systems. *Int. J. Quantum Chem.* **2001**, *85*, 676−684.
(13) Becke, A. D. Density-Functional Thermochemistry. V. Systematic Optimization of Exchange-correlation Functionals. *J. Chem. Phys.* **1997**, *107*, 8554−8560.
(14) Schmider, H. L.; Becke, A. D. Optimized Density Functionals from the Extended G2 Test Set. *J. Chem. Phys.* **1998**, *108*, 9624−9631.
(15) Hartree, D. R. The Wave Mechanics of an Atom with a Non-Coulomb Central Field. Part I. Theory and Methods. *Math. Proc. Cambridge Philos. Soc.* **1928**, *24*, 89−110. Fock, V. Näherungsmethode zur Lösung des quantenmechanischen Mehrkörperproblems. *Z. Phys.* **1930**, *61*, 126−148.
(16) Dunning, T. H., Jr. Gaussian Basis Sets for Use in Correlated Molecular Calculations. I. The Atoms Boron Through Neon and Hydrogen. *J. Chem. Phys.* **1989**, *90*, 1007−1023.
(17) Davidson, E. R. Comment on Comment on Dunning's Correlation-Consistent Basis Sets. *Chem. Phys. Lett.* **1996**, *260*, 514−518.
(18) Kendall, R. A.; Dunning, T. H., Jr.; Harrison, R. J. Electron Affinities of the First-Row Atoms Revisited. Systematic Basis Sets and Wave Functions. *J. Chem. Phys.* **1992**, *96*, 6796−6806.
(19) Woon, D. E.; Dunning, T. H., Jr. Gaussian-Basis Sets for Use in Correlated Molecular Calculations. 3. The Atoms Aluminum Through Argon. *J. Chem. Phys.* **1993**, *98*, 1358−1371.
(20) Perdew, J. P.; Burke, K.; Ernzerhof, M. Generalized Gradient Approximation Made Simple. *Phys. Rev. Lett.* **1996**, *77*, 3865−68.
(21) Perdew, J. P.; Burke, K.; Ernzerhof, M. Errata: Generalized Gradient Approximation Made Simple. *Phys. Rev. Lett.* **1997**, *78*, 1396.
(22) Adamo, C.; Barone, V. Toward Reliable Density Functional Methods without Adjustable Parameters: The PBE0 Model. *J. Chem. Phys.* **1999**, *110*, 6158−6169.
(23) Møller, C.; Plesset, M. S. Note on an Approximation Treatment for Many-Electron Systems. *Phys. Rev.* **1934**, *46*, 618−622.
(24) Pople, J. A.; Seeger, R.; Krishnan, R. Variational Configuration Interaction Methods and Comparison with Perturbation Theory. *Int. J. Quantum Chem.* **1977**, *12* (Suppl. S11), 149−163.
(25) Bader, R. F. W.; Carroll, M. T.; Cheeseman, J. R.; Chang, C. Properties of Atoms in Molecules: Atomic Volumes. *J. Am. Chem. Soc.* **1987**, *109*, 7968−7979.
(26) Kolář, M.; Hostaš, J.; Hobza, P. The Strength and Directonality of the Halogen Bond Are Co-Determined by the Magnitude and Size of the σ-Hole. *Phys. Chem. Chem. Phys.* **2014**, *16*, 9987−9996.
(27) Pitonak, M.; Riley, K. E.; Neogrady, P.; Hobza, P. Highly Accurate CCSD(T) and DFT−SAPT Stabilization Energies of H-Bonded and Stacked Structures of the Uracil Dimer. *ChemPhysChem* **2008**, *9*, 1636−1644.
(28) Zierkiewicz, W.; Michalska, D.; Hobza, P. Adenine Ribbon Stabilized by Watson−Crick and Hoogsteen Hydrogen Bonds: WFT and DFT Study. *Phys. Chem. Chem. Phys.* **2010**, *12*, 2888−2894.
(29) Rezac, J.; Hobza, P. Extrapolation and Scaling of the DFT-SAPT Interaction Energies toward the Basis Set Limit. *J. Chem. Theory Comput.* **2011**, *7*, 685−689.
(30) Ran, J.; Hobza, P. Nature of Bonding in Nine Planar Hydrogen-Bonded Adenine···Thymine Base Pairs. *J. Phys. Chem. B* **2009**, *113*, 2933−2936.
(31) Riley, K. E.; Pitonak, M.; Cerny, J.; Hobza, P. On the Structure and Geometry of Biomolecular Binding Motifs (Hydrogen-bonding, Stacking, X−H···π): WFT and DFT Calculations. *J. Chem. Theory Comput.* **2010**, *6*, 66−80.
(32) Riley, K. E.; Hobza, P. Noncovalent Interactions in Biochemistry. *Wiley Interdiscip. Rev.: Comput. Mol. Sci.* **2011**, *1*, 3−17.
(33) Sponer, J.; Riley, K. E.; Hobza, P. Nature and Magnitude of Aromatic Stacking of Nucleic Acid Bases. *Phys. Chem. Chem. Phys.* **2008**, *10*, 2595−2610.
(34) Sedlak, R.; Jurecka, P.; Hobza, P. Density Functional Theory-Symmetry Adapted Perturbation Treatment Energy Decomposition of Nucleic Acid Base Pairs Taken from DNA Crystal Geometry. *J. Chem. Phys.* **2007**, *127*, 075104−075106.
(35) Hesselmann, A.; Korona, T. On the Accuracy of DFT-SAPT, MP2, SCS-MP2, MP2C, and DFT+Disp Methods for the Interaction Energies of Endohedral Complexes of the C_{60} Fullerene with a Rare Gas Atom. *Phys. Chem. Chem. Phys.* **2011**, *13*, 732−743.
(36) Karthikeyan, S.; Sedlak, R.; Hobza, P. On the Nature of Stabilization in Weak, Medium, and Strong Charge-Transfer Complexes: CCSD(T)/CBS and SAPT Calculations. *J. Phys. Chem. A* **2011**, *115*, 9422−9428.
(37) Sedlak, R.; Hobza, P.; Patwari, G. N. Hydrogen-Bonded Complexes of Phenylacetylene with Water, Methanol, Ammonia, and Methylamine. The Origin of Methyl Group-Induced Hydrogen Bond Switching. *J. Phys. Chem. A* **2009**, *113*, 6620−6625.
(38) Munusamy, E.; Sedlak, R.; Hobza, P. On the Nature of the Stabilization of Benzene···Dihalogen and Benzene···Dinitrogen Complexes: CCSD(T)/CBS and DFT-SAPT Calculations. *ChemPhysChem* **2011**, *12*, 3253−3261.
(39) Peterson, K. A.; Figgen, D.; Goll, E.; Stoll, H.; Dolg, M. Systematically Convergent Basis Sets with Relativistic Pseudopotentials. II. Small-core Pseudopotentials and Correlation Consistent Basis Sets for the Post-*d* Group 16−18 Elements. *J. Chem. Phys.* **2003**, *119*, 11113−11123.
(40) Peterson, K. A. Systematically Convergent Basis Sets With Relativistic Pseudopotentials. I. Correlation Consistent Basis Sets for the Post-*d* Group 13−15 Elements. *J. Chem. Phys.* **2003**, *119*, 11099−11112.
(41) Halkier, A.; Helgaker, T.; Jorgensen, P.; Klopper, W.; Olsen, J. Basis-set Convergence of the Energy in Molecular Hartree−Fock Calculations. *Chem. Phys. Lett.* **1999**, *302*, 437−446.
(42) Halkier, A.; Helgaker, T.; Jorgensen, P.; Klopper, W.; Koch, H.; Olsen, J.; Wilson, A. K. Basis-set Convergence in Correlated Calculations on Ne, N_2, and H_2O. *Chem. Phys. Lett.* **1998**, *286*, 243−252.
(43) Jurecka, P.; Sponer, J.; Cerny, J.; Hobza, P. Benchmark Database of Accurate (MP2 and CCSD(T) Complete Basis Set Limit) Interaction Energies of Small Model Complexes, DNA Base Pairs, and Amino Acid Pairs. *Phys. Chem. Chem. Phys.* **2006**, *8*, 1985−1993.
(44) Hobza, P.; Sponer, J. Toward True DNA Base-Stacking Energies: MP2, CCSD(T), and Complete Basis Set Calculations. *J. Am. Chem. Soc.* **2002**, *124*, 11802−11808.
(45) Jurecka, P.; Hobza, P. On the Convergence of the (Delta-E CCSD(T)-Delta-E-MP2) Term for Complexes with Multiple H-bonds. *Chem. Phys. Lett.* **2002**, *365*, 89−94.

(46) Dabkowska, I.; Jurecka, P.; Hobza, P. On Geometries of Stacked and H-bonded Nucleic Acid Base Pairs Determined at Various DFT, MP2 and CCSD(T) Levels up to the CCSD(T)/Complete Basis Set Limit Level. *J. Chem. Phys.* **2005**, *122*, 204322−204329.
(47) Zhao, Y.; Truhlar, D. G. The M06 Suite of Density Functionals for Main Group Thermochemistry, Thermochemical Kinetics, Noncovalent Interactions, Excited States, and Transition Elements: Two New Functionals and Systematic Testing of Four M06-class Functionals and 12 Other Functionals. *Theor. Chem. Acc.* **2008**, *120*, 215−241.
(48) Kozuch, S.; Martin, J. M. L. Halogen Bonds: Benchmarks and Theoretical Analysis. *J. Chem. Theory Comput.* **2013**, *9*, 1918−1931.
(49) Grimme, S.; Antony, J.; Ehrlich, S.; Krieg, H. A Consistent and Accurate ab initio Parametrization of Density Functional Dispersion Correction (DFT-D) for the 94 Elements H-Pu. *J. Chem. Phys.* **2010**, *132*, 154104−154123.
(50) Grimme, S.; Ehrlich, S.; Goerigk, L. Effect of the Damping Function in Dispersion Corrected Density Functional Theory. *J. Comput. Chem.* **2011**, *32*, 1456−1465.
(51) Jeziorski, B.; Moszynski, R.; Szalewicz, K. Perturbation Theory Approach to Intermolecular Potential Energy Surfaces of van der Waals Complexes. *Chem. Rev.* **1994**, *94*, 1887−1930.
(52) Grüning, M.; Gritsenko, O. V.; van Gisbergen, S. J. A.; Baerends, E. J. Shape Corrections to Exchange-Correlation Potentials by Gradient-Regulated Seamless Connection of Model Potentials for Inner and Outer Region. *J. Chem. Phys.* **2001**, *114*, 652−660.
(53) Hesselmann, A.; Jansen, G. First-order Intermolecular Interaction Energies from Kohn−Sham Orbitals. *Chem. Phys. Lett.* **2002**, *357*, 464−470.
(54) Hesselmann, A.; Jansen, G. Intermolecular Induction and Exchange-induction Energies from Coupled-perturbed Kohn−Sham Density Functional Theory. *Chem. Phys. Lett.* **2002**, *362*, 319−325.
(55) Hesselmann, A.; Jansen, G. Intermolecular Dispersion Energies from Time-dependent Density Functional Theory. *Chem. Phys. Lett.* **2003**, *367*, 778−784.
(56) Hesselmann, A.; Jansen, G. The Helium Dimer Potential from a Combined Density Functional Theory and Symmetry-adapted Perturbation Theory Approach Using an Exact Exchange−Correlation Potential. *Phys. Chem. Chem. Phys.* **2003**, *5*, 5010−5014.
(57) Hesselmann, A.; Jansen, G.; Schütz, M. Density-Functional Theory-Symmetry-Adapted Intermolecular Perturbation Theory with Density Fitting: A New Efficient Method to Study Intermolecular Interaction Energies. *J. Chem. Phys.* **2005**, *122*, 014103−014119.
(58) Jansen, G.; Hesselmann, A. Comment on: Using Kohn−Sham Orbitals in Symmetry-Adapted Perturbation Theory to Investigate Intermolecular Interactions. *J. Phys. Chem. A* **2001**, *105*, 11156−11157.
(59) Misquitta, A. J.; Szalewicz, K. Intermolecular Forces from Asymptotically Corrected Density Functional Description of Monomers. *Chem. Phys. Lett.* **2002**, *357*, 301−306.
(60) Stone, A. J. Distributed Multipole Analysis, or How to Describe a Molecular Charge Distribution. *Chem. Phys. Lett.* **1981**, *83*, 233−239.
(61) Stone, A. J.; Alderton, M. Distributed Multipole Analysis Methods and Applications. *Mol. Phys.* **1985**, *56*, 1047−1064.
(62) Stone, A. J. Distributed Multipole Analysis: Stability for Large Basis Sets. *J. Chem. Theory Comput.* **2005**, *1*, 1128−1132.
(63) Stone, A. J. *GDMA: Distributed Multipoles from Gaussian 98 Wavefunctions*, version 2.2.04; Tech. Rep., University of Cambridge, 1998.
(64) Stone, A. J.; Dullweber, A.; Engkvist, O.; Fraschini, E.; Hodges, M. P.; Meredith, A. W.; Nutt, D. R.; Popelier, P. L. A.; Wales, D. J. *Orient: A Program for Studying Interactions Between Molecules*, version 4.6.16; University of Cambridge, Cabmridge, U.K., 2002; Enquiries to Stone, A. J. ajs1@cam.ac.uk.
(65) Werner, H.-J.; Knowles, P. J.; Manby, F. R.; Schütz, M.; Celani, P.; Knizia, G.; Korona, T.; Lindh, R.; Mitrushenkov, A.; Rauhut, G.; et al. *MOLPRO, A Package of ab initio Programs*, version 2010.1; 2010; http://www.molpro.net.
(66) TURBOMOLE V6.3 2011, A Development of the University of Karlsruhe and the Forschungszentrum Karlsruhe GmbH, 1989−2007; TURBOMOLE GmbH, since 2007; available from http://www.turbomole.com.
(67) Reed, A. E.; Curtiss, L. A.; Weinhold, F. Intermolecular Interactions from a Natural Bond Orbital, Donor-Acceptor Viewpoint. *Chem. Rev.* **1988**, *88*, 899−926.
(68) Frisch, M. J.; Trucks, G. W.; Schlegel, H. B.; Scuseria, G. E.; Robb, M. A.; Cheeseman, J. R.; Scalmani, G.; Barone, V.; Mennucci, B.; Petersson, G. A.; et al. *Gaussian 09*, Revision D.01; Gaussian, Inc.: Wallingford, CT, 2009.
(69) Boys, S. F.; Bernardi, F. The Calculation of Small Molecular Interactions by the Differences of Separate Total Energies. Some Procedures with Reduced Errors. *Mol. Phys.* **1970**, *19*, 553−566.

PCCP

PAPER

View Article Online
View Journal | View Issue

Cite this: *Phys. Chem. Chem. Phys.*, 2014, **16**, 6679

On the origin of the substantial stabilisation of the electron-donor 1,3-dithiole-2-thione-4-carboxyclic acid$\cdots I_2$ and DABCO$\cdots I_2$ complexes†

Palanisamy Deepa,[a] Robert Sedlak[a] and Pavel Hobza*[ab]

Received 6th January 2014,
Accepted 5th February 2014

DOI: 10.1039/c4cp00055b

www.rsc.org/pccp

The stabilisation energies of the crystal structures of 1,3-dithiole-2-thione-4-carboxyclic acid$\cdots I_2$ and DABCO$\cdots I_2$ complexes determined by the CCSD(T)/CBS method are very large and exceed 8 and 15 kcal mol^{-1}, respectively. The DFT-D method (B97-D3/def2-QZVP) strongly overestimates these stabilisation energies, which support the well-known fact that the DFT-D method is not very applicable to the study of charge-transfer complexes. On the other hand, the M06-2X/def2-QZVP method provides surprisingly reliable energies. A DFT-SAPT analysis has shown that a substantial stabilisation of these complexes arises from the charge-transfer energy included in the induction energy and that the respective induction energy is much larger than that of other non-covalently bound complexes. The total stabilisation energies of the complexes mentioned as well as of those where iodine has been replaced by lighter halogens (Br_2 and Cl_2) or by hetero systems (IF, ICH_3, N_2) correlate well with the magnitude of the σ-hole ($V_{s,max}$ value) as well as with the LUMO energy. The nature of the stabilisation of all complexes between both electron donors and X_2 (X = I, Br, Cl, N) systems is explained by the magnitude of the σ-hole but surprisingly also by the values of the electric quadrupole moment of these systems. Evidently, the nature of the stabilisation of halogen-bonded complexes between electron donors and systems where the first non-zero electric multipole moment is the quadrupole moment can be explained not only by the recently introduced concept of the σ-hole but also by the classical concept of electric quadrupole moments.

Introduction

Complexes containing halogens participating in halogen bonding (X-bonding) are characterised by large stability, mostly comparable with the stabilisation of similar H-bonded complexes. Indeed, accurate CCSD(T)/CBS stabilisation energies of complexes with halogens (X40 dataset[1]) and H-bonded complexes from the S66 dataset[2,3] are well comparable. In both cases, energy decomposition is similar, with electrostatic energy playing a dominant role. A counterintuitive electrostatic attraction in the case of a X–Y$\cdots$D halogen bond, where Y is Cl, Br or I, X is an electronegative atom (mostly carbon) and D is an electron donor like oxygen, nitrogen or sulphur, is explained by the existence of a positive σ-hole on top of the halogen atom.[4–6] The electrostatic attraction thus occurs between the positive σ-hole and a negative electron donor. In the case of an X–H$\cdots$D hydrogen bond,[7,8] the electrostatic attraction is caused by the interaction between a positively charged hydrogen and a negatively charged electron donor. A comparison of other energy contributions reveals that dispersion energy is more negative in X-bonds than in H-bonds, which is explained by the fact that halogen and electron donors, both having large polarisability, are close to each other. The last attractive energy, induction energy, is mostly smaller than dispersion energy; in X- and H-bonds, it is comparable. Induction energy in a broader sense of the SAPT[9–17] also contains, apart from exchange induction, the δHF term, which covers higher-order terms. The induction energy thus contains not only classical multiple-induced multiple induction energy but also charge-transfer energy. The charge-transfer energy becomes important only if an electron donor effectively interacts with an electron acceptor. This means that besides the highest-occupied molecular orbital (HOMO) of the donor and the lowest-unoccupied molecular orbital (LUMO) of the acceptor, there must also be a favourable overlap between these orbitals.

In our recent study,[18] we investigated the crystal structures containing iodine; among them, we found one structure (1,3-dithiole-2-thione-4-carboxyclic acid (DTCA)$\cdots I_2$), for which we obtained a surprisingly large stabilisation energy exceeding 10 kcal mol^{-1}. Then we searched in the literature[19] and found a

[a] *Institute of Organic Chemistry and Biochemistry, Academy of Sciences of the Czech Republic, Flemingovo nám. 2, 166 10 Prague 6, Czech Republic. E-mail: pavel.hobza@uochb.cas.cz*

[b] *Regional Centre of Advanced Technologies and Materials, Department of Physical Chemistry, Palacky University, 771 46 Olomouc, Czech Republic*

† Electronic supplementary information (ESI) available. See DOI: 10.1039/c4cp00055b

similar complex (DABCO$\cdots$I$_2$) with an even larger stabilisation energy close to 20 kcal mol^{-1}. Since both calculations were made at a lower theoretical level, it is not clear whether these surprising numbers are correct. If they are, where does this large stabilisation come from? Is it only caused by halogen bonding with heavy iodine or does charge transfer play an important role here?

The aim of the present study is to investigate in detail the nature of the interactions in the above-mentioned complexes. To elucidate the role of I_2, we will also study complexes where I_2 is replaced by lighter halogens (Br_2, Cl_2), hetero dihalogen (IF) as well as other systems (ICH_3, N_2). The benchmark stabilisation energies will be evaluated at the CCSD(T)/CBS level[1,2] and the energy components will be obtained from SAPT calculations.[20]

Calculations

The electrostatic potentials were computed on molecular surfaces, with a surface being defined as the 0.001 a.u. (electrons per bohr^3) outer contour of the electron density, as proposed by Bader *et al.*[21] The most positive value of the potentials at the halogen (the local maximum) is referred to as $V_{s,max}$. Here, the electrostatic potentials as well as the geometries of electron acceptors and their electric quadrupole moments were calculated at the B97-D3/def2-QZVP level.[22–24]

The benchmark stabilisation energies were evaluated using the CCSD(T)/CBS method. Specifically, these stabilisation energies were constructed as the sum of HF/CBS and MP2/CBS interaction energies. Both CBS energies were obtained *via* 2 point Helgaker extrapolation from aug-cc-pVDZ and aug-cc-pVTZ basis sets.[25,26] The CCSD(T) correction term ($\Delta E^{CCSD(T)} - \Delta E^{MP2}$) was evaluated using an aug-cc-pVDZ basis set. The theoretical level used for benchmark calculation represents a compromise between accuracy and economy. A more detailed description of the present procedure can be found in our previous paper.[1,2] The M06-2X functional was recommended[27] for calculations of halogen-bonded complexes and it was also used in the present study. Besides DFT-D (B97-D3/def2-QZVP), M06-2X/def2-QZVP calculations[28] were also performed. All interaction energy calculations were corrected for the basis set superposition error (BSSE) utilizing counterpoise correction.[29]

Energy decomposition of the stabilisation energies of all complexes was obtained by using the DFT-SAPT method.[9–17] The DFT part was treated using an asymptotically corrected PBE0AC exchange–correlation functional and an aug-cc-pVDZ basis set. The total interaction energy in the DFT-SAPT is given as the sum of the first- (E_1) and second-order (E_2) perturbation energy terms and δHF energy terms, specifically electrostatic (E_1^{Pol}), induction (E_2^{ind}) and dispersion (E_2^{disp}) energy terms together with exchange–repulsion terms (E_1^{Ex}, $E_2^{ex\text{-}ind}$ and $E_2^{ex\text{-}disp}$). The exchange-induction and exchange-dispersion terms are merged into the respective induction (E_2^{Ind}) and dispersion terms (E_2^{Disp}); furthermore, the δHF term, which represents higher than second-order electrostatic and induction terms covered by the Hartree–Fock approach, was calculated separately, utilizing the aug-cc-pVDZ basis set. The δHF term is defined as a difference between the HF stabilization energy and the sum of E_1^{Pol}, E_1^{Ex}, E_2^{ind} and $E_2^{ex\text{-}ind}$ energies calculated at the HF-SAPT level. The δHF term is also included in the induction energy (E_2^{Ind}).

$$E_{int} = E_1^{Pol} + E_1^{Ex} + E_2^{ind} + E_2^{ex\text{-}ind} + E_2^{disp} + E_2^{ex\text{-}disp} + \delta HF$$
$$= E_1^{Pol} + E_1^{Ex} + E_2^{Ind} + E_2^{Disp} \quad (1)$$

The greatest improvement of the DFT-SAPT method over the original SAPT is the acceleration of the calculations by one order of magnitude.[9–17] The intramolecular treatment is conducted using DFT and therefore suffers from inaccurate energies of the virtual orbitals. This drawback is corrected before the actual SAPT treatment by a gradient-controlled shift procedure, which uses the difference between the exact vertical ionisation potential (IP) and the energy of the HOMO.[13] In this work, PBE0/aug-cc-pVTZ and PBE0/aug-cc-pVDZ calculations were carried out to obtain the respective HOMO values of the IP.

All the post Hartree–Fock calculations (including DFT-SAPT) were carried out using the Molpro 2010 package.[30] The DFT based methods, excluding M062X, were done utilizing the Turbomole 6.3 package.[31] The M062X calculations were carried out using the Gaussian 09 package.[32]

Structures

The coordinates of heavy atoms for both the I_2 complexes were taken from X-ray structures.[18,19] Afterwards, hydrogen atoms were manually added using the Molden program[33] and subsequently optimized at the B97-D3/def2-QZVP level of theory, while keeping the coordinates of the heavy atoms frozen (*cf.* Fig. 1).

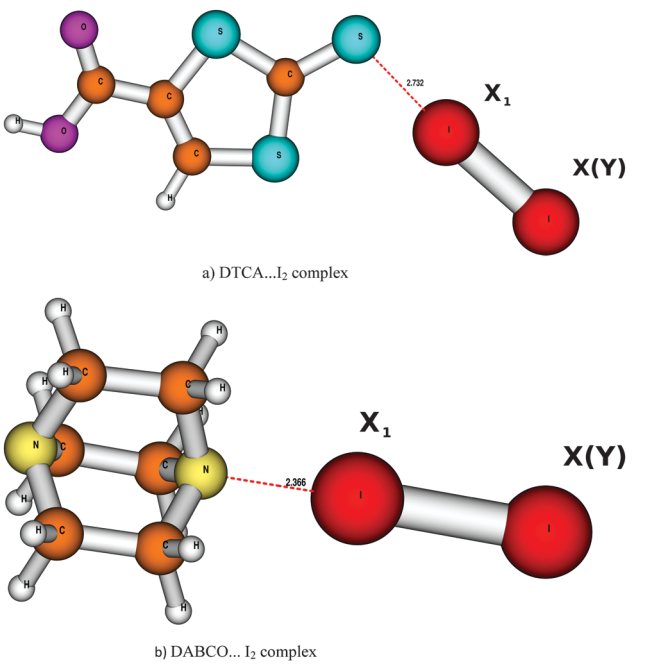

Fig. 1 Crystal structures of complexes investigated shown with halogen bond lengths (Å). Red colour represents iodine, magenta oxygen, blue sulphur, pale yellow nitrogen, orange carbon and white hydrogen.

When constructing the geometries of other binary complexes, the following procedure was utilized. Firstly, the coordinates of the DTCA and DABCO molecules were taken from structures of the respective I_2 complexes. Secondly, when the I_2 molecule was replaced from the corresponding I_2 complex structure by X_2 (X = Br, Cl, N) or XY (Y = F, CH_3) systems, the closer halogen atom X_1 coincides with the closer iodine atom (*cf.* Fig. 1). Finally, the rest of the electron acceptor molecule was constructed using the optimized geometry of the isolated acceptor, which was calculated at the B97-D3/def2-QZVP level of theory (*cf.* Fig. 1).

Results and discussion

Isolated systems

The geometries of all electron donors as well as electron acceptors taken from X-ray crystal structures or optimised structures are collected in Table S1 of the ESI.†

The LUMO energies of the acceptors are summarised in Table 1, which also contains the $V_{s,max}$ values and the quadrupole moment of all electron acceptors. The electrostatic potentials of selected monomers are visualised in Fig. 2.

Investigating the LUMO values, we find that IF, I_2 and Br_2 are the best acceptors. The Cl_2 systems are slightly worse and the N_2 molecule has the LUMO at higher energies, which agrees with the fact that N_2 is not an electron acceptor. The same is true for ICH_3 systems. The HOMO value for the electron donors DTCA and DABCO is −0.199 and −0.144 a.u., respectively; this means that DABCO is a better electron donor.

As expected, the magnitude of the σ-hole (see the $V_{s,max}$ value) for I_2 is larger than that of Br_2 and Cl_2. When the iodine was replaced by the more electronegative fluorine, the $V_{s,max}$ value increased considerably. The $V_{s,max}$ for N_2 is negative, which provides evidence that the positive σ-hole does not exist here. Comparing the quadrupoles of X_2 molecules, we find that they have different signs for halogens (I_2, Br_2, Cl_2) and nitrogen. The quadrupoles of the halogens can thus be schematically written as + − − + while that of the nitrogen as − + + −. Evidently, the schematic notations reflect the concept of the σ-hole. The correlation between the $V_{s,max}$ and the quadrupole moment for the X_2 systems is shown in Fig. 3a and, evidently, it is very high (R^2 = 0.902). This finding is surprising, because it tells us that for the explanation of the different binding of the halogens (Cl_2, Br_2, I_2) and the nitrogen to electron donors like O or N, it is not necessary to introduce a concept of the σ-hole, but it is enough to consider classical quadrupole moments. The electron donors with halogens exhibit attraction while the electron donors with nitrogen repulsion. This can be easily explained by the values of $V_{s,max}$ but comparably easily by quadrupole moments. Clearly, this is valid only for the X_2 systems where the first non-vanishing electric multipole moment is quadrupole. In the case of XY systems, such as IF, the first non-vanishing electric multipole moment is the dipole moment and here the bonding of this system to an electron donor can only be explained by using the σ-hole.

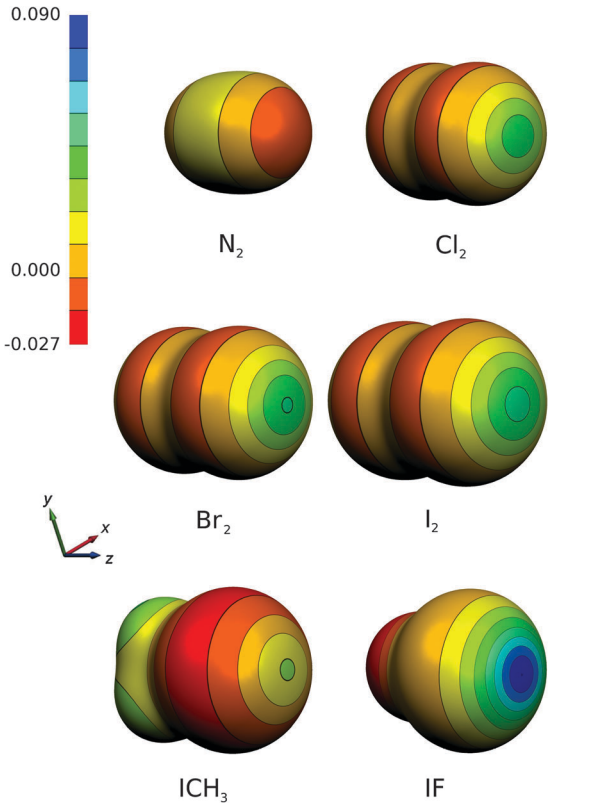

Fig. 2 Electrostatic potential (a.u.) for all the monomers: I_2, Br_2, Cl_2, N_2, IF and ICH_3. Here the blue and red colour indicates the positive and negative region, respectively.

Table 1 The Q_{zz} component of the quadrupole moment (a.u.), LUMO (a.u.) and $V_{s,max}$ at the 0.001 a.u. isodensity surface for selected monomers calculated at the B97-D3/def2-QZVP level of theory. $V_{s,max}$ value corresponds to the cusp/pick point of the halogen atom

	Quadruple moment	LUMO	$V_{s,max}$
I_2	3.402	−0.168	0.0474
Br_2	2.362	−0.173	0.0443
Cl_2	1.574	−0.162	0.0389
N_2	−0.774	−0.076	−0.0140
IF	0.273	−0.183	0.0896
ICH_3	3.217	−0.076	0.0214

Complexes

Table 2 contains interaction energies determined for all complexes investigated using various computational techniques. The B97-D3 stabilization energies for the complexes with halogens are very large; for DABCO complexes, they are even 40–70% larger. The larger stabilisation of the DABCO complexes can be easily explained by the fact that DABCO is a better electron acceptor (see above). In both complexes, dispersion energy (shown in Table 2, 1st column in parentheses) is an important stabilisation component, but it is not dominant. For further energy decomposition, see the SAPT calculations. As mentioned in the Introduction, the DFT stabilisation energies for the charge-transfer complexes could be overestimated due to an unrealistic description of the virtual space. The benchmark stabilisation energies are produced by the CCSD(T)/CBS calculations, as seen from Table 2,

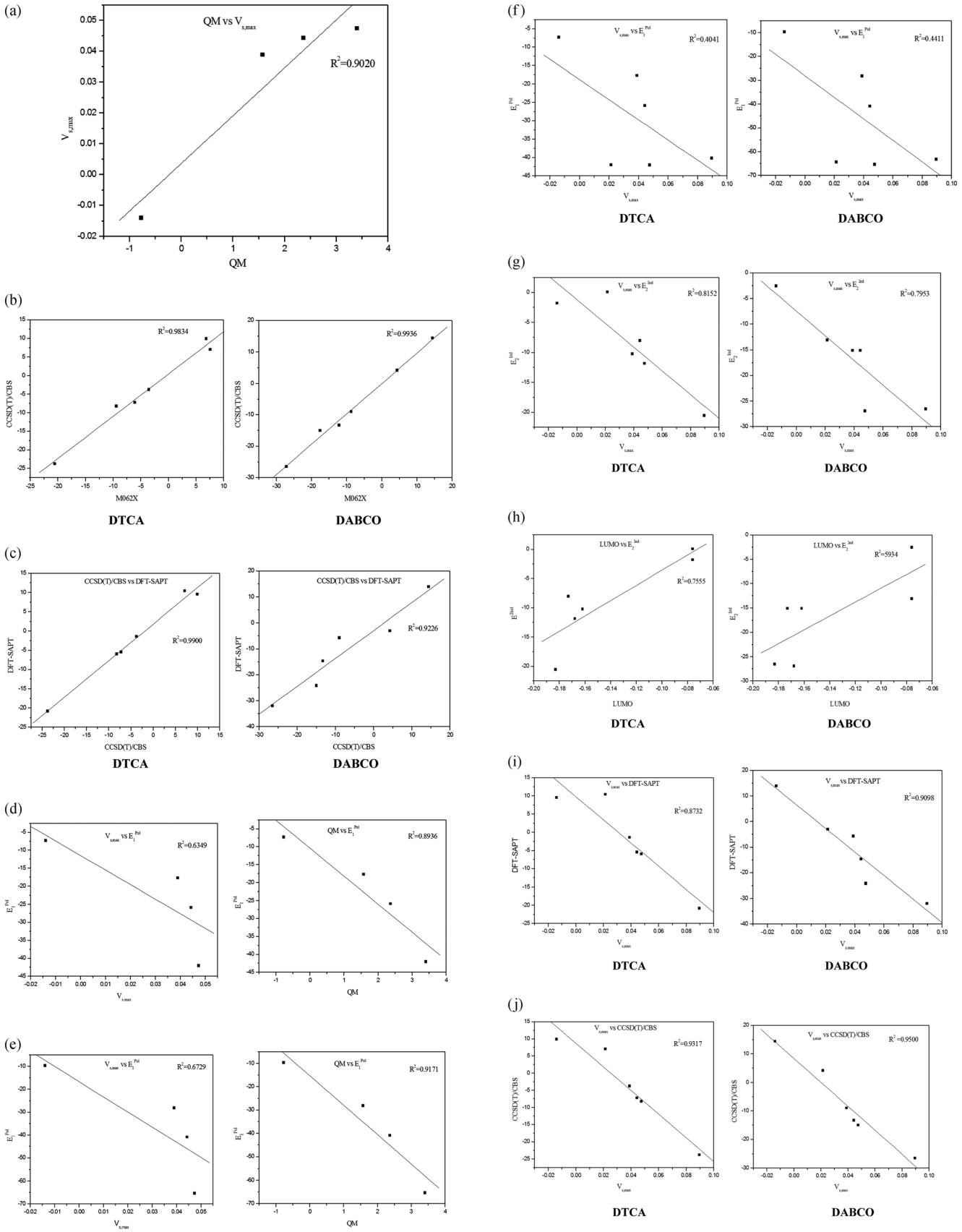

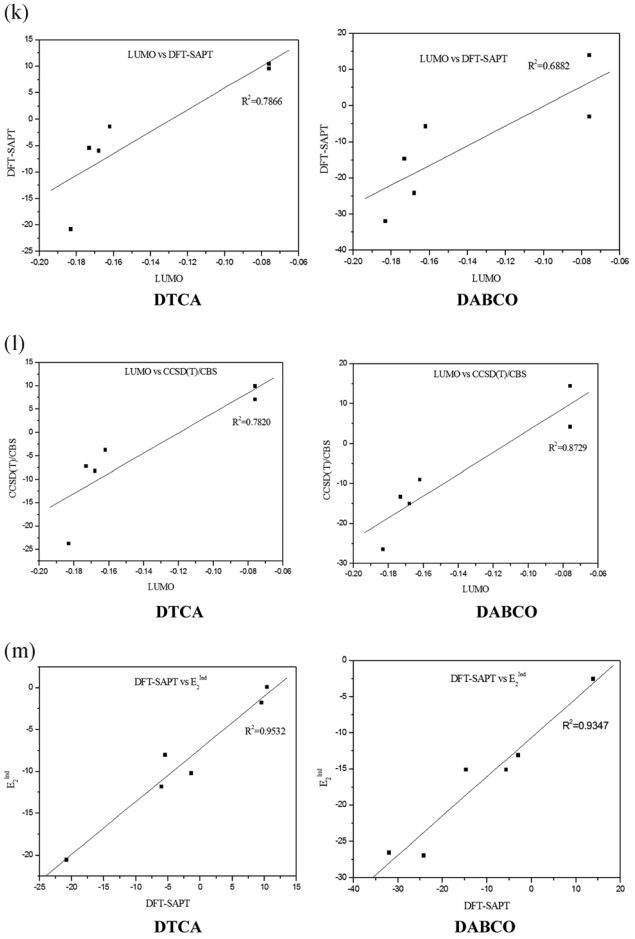

Fig. 3 (a) Correlation between QM and $V_{s,max}$ for I_2, Br_2, Cl_2, N_2 molecules (in all subsequent plots of Fig. 3, QM stands for quadrupole moment and the following units are used: [$V_{s,max}$] = a.u., [QM] = a.u. and all interaction energy values are listed in kcal mol^{-1}). (b) Correlation between M062X and CCSD(T)/CBS interaction energies for the DTCA (left) and DABCO (right) set of complexes. (c) Correlation between CCSD(T)/CBS and DFT-SAPT interaction energies for the DTCA (left) and DABCO (right) set of complexes. (d) Correlation between $V_{s,max}$ and E_1^{Pol} (left); QM and E_1^{Pol} (right) for I_2, Br_2, Cl_2, and $N_2\cdots$DTCA complexes. (e) Correlation between $V_{s,max}$ and E_1^{Pol} (left); QM and E_1^{Pol} (right) for I_2, Br_2, Cl_2, and $N_2\cdots$DABCO complexes. (f) Correlation between $V_{s,max}$ and E_1^{Pol} for the DTCA (left) and DABCO (right) set of complexes. (g) Correlation between $V_{s,max}$ and E_2^{Ind} for the DTCA (left) and DABCO (right) set of complexes. (h) Correlation between LUMO and E_2^{Ind} for the DTCA (left) and DABCO (right) set of complexes. (i) Correlation between $V_{s,max}$ and DFT-SAPT for the DTCA (left) and DABCO (right) set of complexes. (j) Correlation between $V_{s,max}$ and CCSD(T)/CBS for the DTCA (left) and DABCO (right) set of complexes. (k) Correlation between LUMO and DFT-SAPT for the DTCA (left) and DABCO (right) set of complexes. (l) Correlation between LUMO and CCSD(T)/CBS for the DTCA (left) and DABCO (right) set of complexes. (m) Correlation between DFT-SAPT and E_2^{Ind} for the DTCA (left) and DABCO (right) set of complexes.

these energies are considerably smaller than the DFT ones. Considering all the complexes with attractive interaction, we found that the CCSD(T)/CBS stabilisation energy forms on average 62% of the DFT-D stabilisation energy for the DTCA complexes and 79% for the DABCO complexes. The CCSD(T)/CBS stabilisation energies of the DABCO complexes are larger than those of the DTCA complexes (by 11–139%). Surprisingly accurate

Table 2 The stabilization energies ($-E_{int}$; in kcal mol^{-1}) calculated at the DFT-D (B97-D3/def2-QZVP), M062X/def2-QZVP, CCSD(T)/CBS and DFT-SAPT/aug-cc-pVDZ levels of theory. In all the cases, the intermolecular distances of X···S and X···N contacts amount to 2.73 Å and 2.37 Å, respectively. The numbers in the round brackets correspond to the dispersion energy (in kcal mol^{-1})

Systems	B97-D3/def2-QZVP	M062X/def2-QZVP	CCSDT/CBS	DFT-SAPT/aug-cc-pVDZ	MP2/CBS
DTCA···I_2	13.80 (−5.38)	8.81	8.20	5.98	12.36
DTCA···Br_2	11.25 (−4.45)	6.97	7.21	5.42	10.27
DTCA···Cl_2	8.34 (−3.82)	3.40	3.75	1.36	6.01
DTCA···N_2	−10.11 (−2.61)	−10.03	−9.93	−9.57	−9.11
DTCA···IF	29.27 (−5.01)	25.10	23.77	20.81	27.21
DTCA···ICH_3	−4.33 (−5.20)	−8.12	−7.08	−10.43	−3.98
DABCO···I_2	18.97 (−8.33)	17.18	15.01	24.19	20.31
DABCO···Br_2	16.72 (−6.58)	13.04	13.31	14.68	17.21
DABCO···Cl_2	13.79 (−5.39)	8.47	8.98	5.68	11.72
DABCO···N_2	−14.55 (−3.44)	−14.40	−14.40	−13.92	−14.02
DABCO···IF	28.22 (−8.03)	26.94	26.49	31.98	30.29
DABCO···ICH_3	−2.69 (−8.19)	−4.90	−4.21	−3.01	−0.89

numbers are obtained using the M06-2X functional and the respective correlations (R^2 = 0.983, R^2 = 0.994) between the M06-2X and the CCSD(T)/CBS energies for both complexes are shown in Fig. 3b. The MP2/CBS stabilization energies are systematically overestimated with respect to CCSD(T)/CBS values. The average overestimation for the DABCO and the DTCA complexes evaluates to 32% and 37%, respectively. The DFT-SAPT calculations provide stabilisation energies smaller than the benchmark CCSD(T)/CBS values, but the correlation between both energies is quite close (R^2 = 0.990 and R^2 = 0.923, see Fig. 3c). The underestimation of the SAPT energies arises from the use of a small aug-cc-pVDZ basis set. Among various energies, dispersion energy is the most underestimated.[14] We, however, use the SAPT not for generating accurate total stabilisation energies but for a mere decomposition of the total stabilisation energies.

Passing from iodine to chlorine, the stabilisation energies of both complexes decrease, the drop between iodine and bromine is moderate, but it becomes larger between bromine and chlorine. The stabilisation energies of chlorine complexes are considerably smaller than those of iodine complexes, but they are still substantial. A dramatic increase of the stabilisation energies of both complexes occurs when I_2 is replaced (at the same geometry) by IF. The electronegative fluorine withdraws electrons from iodine, which results in a much larger magnitude of the σ-hole (see Table 1 and Fig. 2). Consequently, the total stabilisation energies also increase. On the other hand, when one iodine atom in the iodine molecule is replaced by an electron-pushing CH_3 group, the $V_{s,max}$ decreases and the total stabilisation energy decreases dramatically and even becomes repulsive. Very large stabilisation energies of complexes with IF are also caused due to the fact that this molecule is the best electron acceptor among all the systems investigated (see Table 1). The replacement of an iodine molecule with a nitrogen molecule also results in larger repulsive interaction energy. Here again, a certain role is played by both effects (nitrogen is not a good electron acceptor and does not contain a

Table 3 The DFT-SAPT/aug-cc-pVDZ interaction energies (in kcal mol^{-1}). For the exact definition of particular terms *cf.* subsection calculations

Complex/term	E_{tot}	E_1^{Pol}	E_1^{Ex}	$E_2^{ind}+E_2^{ex\text{-}ind}$	E_2^{Disp}	δHF	E_2^{Ind}
DTCA acid$\cdots$I$_2$	−5.98	−42.06	59.00	−67.07	−11.11	55.25	−11.82
DTCA$\cdots$Br$_2$	−5.42	−25.82	36.97	−22.09	−8.54	14.05	−8.03
DTCA$\cdots$Cl$_2$	−1.36	−17.68	33.34	−4.37	−6.79	−5.86	−10.23
DTCA$\cdots$N$_2$	9.57	−7.28	23.01	−0.33	−4.39	−1.45	−1.78
DTCA$\cdots$IF	−20.81	−40.19	49.97	−66.41	−10.05	45.86	−20.55
DTCA$\cdots$ICH$_3$	10.43	−42.01	63.60	−66.01	−11.25	66.10	0.09
DABCO$\cdots$I$_2$	−24.19	−65.36	83.02	−93.51	−14.91	66.57	−26.94
DABCO$\cdots$Br$_2$	−14.68	−40.81	52.52	−31.82	−11.29	16.73	−15.09
DABCO$\cdots$Cl$_2$	−5.68	−28.10	46.47	−7.20	−8.95	−7.91	−15.11
DABCO$\cdots$N$_2$	13.92	−9.65	31.82	−0.71	−5.71	−1.82	−2.54
DABCO$\cdots$IF	−31.98	−63.24	71.35	−90.82	−13.55	64.28	−26.54
DABCO$\cdots$ICH$_3$	−3.01	−64.32	89.58	−92.07	−15.17	78.97	−13.10

positive σ-hole). These findings indicate that electrostatic and charge-transfer energies play an important role in the complexes investigated.

To understand the nature of the stabilisation of both complexes, we performed a SAPT decomposition, and the single-energy terms are shown in Table 3. From Table 3, it becomes clear that SAPT energies are determined as a sum of differently large numbers. The largest energy (in the absolute value) is exchange–repulsion energy E_1^{Ex}, which indicates short intermolecular distances. Indeed, this finding is supported by the intermolecular distances shown in Fig. 1. Among attractive terms, the largest energy is electrostatic energy E_1^{Pol}. In both complexes, dispersion energy E_2^{Disp} is large but induction energy E_2^{Ind} (the sum of induction, exchange-induction and δHF energies) is comparable or in some cases even larger. This is clearly a new phenomenon in all of our previous studies[34–59] on non-covalent complexes including X-bonded complexes, the induction energy was systematically the smallest attractive term.

In this paragraph we will discuss the magnitude of the dispersion interaction, electrostatic and induction will follow in the next. Comparing the value of E_2^{Disp} from DFT-SAPT and D3 from B97-D3 (*cf.* Table 2) it is obvious that E_2^{Disp} term is systematically more negative. The E_2^{Disp} term is larger (in absolute value) on average by 94% and 73% for DTCA and DABCO complexes, respectively. This is in contrast to magnitudes of whole stabilization energies (as discussed above). This counter-intuitive result can be understood as a consequence of the vagueness, when defining the dispersion interaction within the framework of the DFT. Grimme's empirical correction to dispersion interaction (D3) tries to remove one of the most important drawbacks of the exchange–correlation functional in DFT, which is its inability to reproduce the dispersion interaction, but not only at the asymptotic region ($1/R^6$ dependence) but in the whole range of distances. However, we should keep in mind that the "local" or "semi-local" functional, such as B97, can cover some part of the dispersion interaction. When describing the medium-range attractive non-covalent interaction at the van der Waals distances, the intermolecular overlap is not negligible. Hence, we stress that Grimme's D3 correction represents only a part of the dispersion. On the other hand, the E_2^{Disp} term from DFT-SAPT, which is based on second order perturbation theory, represents a better approximation to exact dispersion. That is why, the E_2^{Disp} term covers a bigger portion of dispersion (*i.e.* more negative) than the empirical D3 correction. Finally, we would like to point out that the presented difference between the E_2^{Disp} term and the D3 dispersion correction is underestimated. This follows from the fact that the aug-cc-pVDZ basis set does not provide a sufficiently converged value of the E_2^{Disp} term. This term is underestimated roughly by 10–20% at this level.[14]

Now we will try to explain the magnitude of electrostatic and induction energies. First, we will investigate the correlation between electrostatic energy and the values of $V_{s,max}$ on the one hand and the quadrupole moment of X_2 molecules on the other. Evidently, both correlations (DTCA: 0.635, 0.894; DABCO 0.673, 0.917; Fig. 3d and e) are high, showing again that the σ-hole as well as the quadrupole moment explain the significant electrostatic stabilisation in X-bonded complexes. When going from X_2 molecules to other electron acceptors (IF, ICH_3) for which the first non-zero multipole moment is the dipole moment, the concept of quadrupole moment cannot be used any more. The correlation between electrostatic energy and $V_{s,max}$ for all six electron acceptors and both electron donors is, however, not very high (DTCA 0.404; DABCO 0.441; Fig. 3f) and it is slightly better for the correlations between induction energy and $V_{s,max}$ (DTCA 0.815, DABCO 0.795; Fig. 3g). Evidently, electrostatic as well as induction energies depend on more variables than only on the magnitude of the σ-hole. As mentioned above, induction energy contains a charge-transfer term which depends on the ability of an electron donor to donate electrons and an electron acceptor to accept electrons. The correlations between the induction energy and the LUMO energy of the electron acceptors for DTCA and DABCO are comparable (0.756 and 0.593; Fig. 3h). This tells us that charge-transfer energy plays a dominant role in induction energy. We have seen above that the $V_{s,max}$ value does not correlate tightly with either electrostatic or induction energies. However, the correlation between the SAPT interaction energy and the $V_{s,max}$ value (0.873 and 0.910; Fig. 3i) as well as between the CCSD(T)/CBS interaction energy and the $V_{s,max}$ value (0.932 and 0.950; Fig. 3j) is much higher. Little worse correlation has been found between the SAPT interaction energy and the LUMO energy of the acceptor (0.787 and 0.688; Fig. 3k) and the CCSD(T)/CBS interaction energy and the LUMO energy of the acceptor (0.782 and 0.873; Fig. 3l). It is thus possible to conclude that the $V_{s,max}$ value as well as the LUMO energy of the electron acceptor provide almost complete information on the stabilisation of the complexes investigated.

We should further investigate the composition of the total SAPT interaction energy. The SAPT energy correlates best with the total induction energy (0.953 and 0.935; Fig. 3m), whereas the correlation with electrostatic and dispersion energies is considerably worse. Putting together this and previous conclusions, we can state that within all the complexes investigated, the charge-transfer energy included in the SAPT induction energy represents the most important energy term. Among the single

characteristics of the acceptor, the $V_{s,max}$ value as well as the LUMO energy of the acceptor correlate best with the total interaction energies.

Conclusions

(i) The CCSD(T)/CBS stabilisation energies of the DTCA$\cdots$$I_2$ and DABCO$\cdots$$I_2$ charge-transfer complexes are very large, exceeding 8 and 15 kcal mol^{-1}, respectively. The B97-D3/def2-QZVP stabilisation energies of these complexes are strongly overestimated while the M062X/def2-QZVP energies agree with the benchmark values very well. DFT-SAPT stabilisation energies are smaller than the benchmark values, which arise from the use of the aug-cc-pVDZ basis set which underestimates the dispersion interaction.

(ii) The stabilisation energies of both complexes decrease when passing from iodine to chlorine and dramatically increase when iodine is replaced by IF. When replacing halogen electron acceptors with ICH_3 or nitrogen, the stabilisation energy strongly decreases and becomes repulsive. All of these findings support the charge-transfer character of the mentioned complexes.

(iii) The total stabilisation energies correlate well with the induction energy including the charge-transfer energy as well as with the $V_{s,max}$ value and the LUMO energy, and the induction energy is the most important attractive term. It should be mentioned again that in all our previous studies[35–59] on non-covalent complexes including X-bonded complexes, the induction energy was systematically the smallest attractive term.

(iv) The halogen bond in the mentioned complexes is thus stabilised mainly by induction (charge-transfer) energy and to a lesser extent by electrostatic energy.

Acknowledgements

This work was part of the Research Project RVO: 61388963 of the Institute of Organic Chemistry and Biochemistry, Academy of Sciences of the Czech Republic. This work was also supported by the Czech Science Foundation [P208/12/G016] and the operational program Research and Development for Innovations of the European Social Fund (CZ 1.05/2.1.00/03/0058).

References

1 J. Rezac, K. E. Riley and P. Hobza, *J. Chem. Theory Comput.*, 2012, **8**, 4285–4292.
2 J. Rezac, K. E. Riley and P. Hobza, *J. Chem. Theory Comput.*, 2011, **7**, 2427–2438.
3 L. F. Molnar, X. He, B. Wang and K. M. Merz Jr, *J. Chem. Phys.*, 2009, **131**, 065102.
4 T. Clark, M. Hennemann, J. S. Murray and P. Politzer, *J. Mol. Model.*, 2007, **13**, 291–296.
5 P. Politzer, J. S. Murray and T. Clark, *Phys. Chem. Chem. Phys.*, 2013, **15**, 11178–11189.
6 P. Politzer and J. S. Murray, *ChemPhysChem*, 2013, **14**, 278–294.
7 E. Arunan, G. R. Desiraju, R. A. Klein, J. Sadlej, S. Scheiner, I. Alkorta, D. C. Clary, R. H. Crabtree, J. J. Dannenberg, P. Hobza, H. G. Kjaergaard, A. C. Legon, B. Mennucci and D. J. Nesbitt, *Pure Appl. Chem.*, 2011, **83**, 1619–1636.
8 E. Arunan, G. R. Desiraju, R. A. Klein, J. Sadlej, S. Scheiner, I. Alkorta, D. C. Clary, R. H. Crabtree, J. J. Dannenberg, P. Hobza, H. G. Kjaergaard, A. C. Legon, B. Mennucci and D. J. Nesbitt, *Pure Appl. Chem.*, 2011, **83**, 1637–1641.
9 A. Hesselmann and G. Jansen, *Chem. Phys. Lett.*, 2002, **357**, 464–470.
10 A. Hesselmann and G. Jansen, *Chem. Phys. Lett.*, 2002, **362**, 319–325.
11 J. Misquitta and K. Szalewicz, *Chem. Phys. Lett.*, 2002, **357**, 301–306.
12 G. Jansen and A. Hesselmann, *J. Phys. Chem. A*, 2001, **105**, 11156–11157.
13 A. Hesselmann and G. Jansen, *Chem. Phys. Lett.*, 2003, **367**, 778–784.
14 A. Hesselmann, G. Jansen and M. Schütz, *J. Chem. Phys.*, 2005, **122**, 014103–014119.
15 A. Hesselmann, G. Jansen and M. Schütz, *J. Am. Chem. Soc.*, 2006, **128**, 11730–11731.
16 R. Podeszwa, R. Bukowski and K. Szalewicz, *J. Phys. Chem. A*, 2006, **110**, 10345–10354.
17 H. L. Williams and C. F. Chabalowski, *J. Phys. Chem. A*, 2001, **105**, 646–659.
18 P. Deepa, B. V. Pandiyan, P. Kolandaivel and P. Hobza, *Phys. Chem. Chem. Phys.*, 2014, **16**, 2038–2047.
19 A. Peuronen, A. Valkonen, M. Kortelainen, K. Rissanen and M. Lahtinen, *Cryst. Growth Des.*, 2012, **12**, 4157–4169.
20 B. Jeziorski, R. Moszynski and K. Szalewicz, *Chem. Rev.*, 1994, **94**, 1887–1930.
21 R. F. Bader, M. T. Carroll, J. R. Cheeseman and C. Chang, *J. Am. Chem. Soc.*, 1987, **109**, 7968–7979.
22 D. Becke, *J. Chem. Phys.*, 1997, **107**, 8554–8560.
23 H. L. Schmider and A. D. Becke, *J. Chem. Phys.*, 1998, **108**, 9624–9631.
24 S. Grimme, S. Ehrlich and L. Goerigk, *J. Comput. Chem.*, 2011, **32**, 1456–1465.
25 A. Halkier, T. Helgaker, P. Jorgensen, W. Klopper and J. Olsen, *Chem. Phys. Lett.*, 1999, **302**, 437–446.
26 A. Halkier, T. Helgaker, P. Jorgensen, W. Klopper, H. Koch, J. Olsen and A. K. Wilson, *Chem. Phys. Lett.*, 1998, **286**, 243–252.
27 S. Kozuch and J. M. Martin, *J. Chem. Theory Comput.*, 2013, **9**, 1918–1931.
28 Y. Zhao and D. G. Truhlar, *Theor. Chem. Acc.*, 2008, **120**, 215–241.
29 S. F. Boys and F. Bernardi, *Mol. Phys.*, 1970, **19**, 553–557.
30 H.-J. Werner, P. J. Knowles, F. R. Manby, M. Schuetz, P. Celani, G. Knizia, T. Korona, R. Lindh, A. Mitrushenkov, G. Rauhut, T. B. Adler, R. D. Amos, A. Bernhardsson, A. Berning, D. L. Cooper, M. J. O. Deegan, A. J. Dobbyn, F. Eckert, F. Goll, C. Hampel, A. Hesselmann, G. Hetzer, T. Hrenar, G. Jansen, C. Koeppl, Y. Liu, A. W. Lloyd, R. A. Mata, A. J. May, S. J. McNicholas, W. Meyer, M. E. Mura, A. Nicklass,

P. Palmieri, K. Pflueger, K. Pitzer, M. Reiher, T. Shiozaki, H. Stoll, A. J. Stone, R. Tarroni, T. Thorsteinsson, M. Wang and A. Wolf, *MOLPRO, version 2010.1, a package of ab initio programs*, 2010, see http://www.molpro.net.

31 TURBOMOLE V6.3 2011, a development of University of Karlsruhe and Forschungszentrum Karlsruhe GmbH, 1989–2007, TURBOMOLE GmbH, since 2007; available from http://www.turbomole.com.

32 M. J. Frisch, G. W. Trucks, H. B. Schlegel, G. E. Scuseria, M. A. Robb, J. R. Cheeseman, G. Scalmani, V. Barone, B. Mennucci, G. A. Petersson, H. Nakatsuji, M. Caricato, X. Li, H. P. Hratchian, A. F. Izmaylov, J. Bloino, G. Zheng, J. L. Sonnenberg, M. Hada, M. Ehara, K. Toyota, R. Fukuda, J. Hasegawa, M. Ishida, T. Nakajima, Y. Honda, O. Kitao, H. Nakai, T. Vreven, J. A. Montgomery, Jr., J. E. Peralta, F. Ogliaro, M. Bearpark, J. J. Heyd, E. Brothers, K. N. Kudin, V. N. Staroverov, R. Kobayashi, J. Normand, K. Raghavachari, A. Rendell, J. C. Burant, S. S. Iyengar, J. Tomasi, M. Cossi, N. Rega, N. J. Millam, M. Klene, J. E. Knox, J. B. Cross, V. Bakken, C. Adamo, J. Jaramillo, R. Gomperts, R. E. Stratmann, O. Yazyev, A. J. Austin, R. Cammi, C. Pomelli, J. W. Ochterski, R. L. Martin, K. Morokuma, V. G. Zakrzewski, G. A. Voth, P. Salvador, J. J. Dannenberg, S. Dapprich, A. D. Daniels, O. Farkas, J. B. Foresman, J. V. Ortiz, J. Cioslowski and D. J. Fox, *Gaussian 09, Revision D.01*, Gaussian, Inc., Wallingford, CT, 2009.

33 G. Schaftenaar and J. H. Noordik, Molden: a pre- and post-processing program for molecular and electronic structures, *J. Comput.-Aided Mol. Des.*, 2000, **14**, 123–134.

34 M. Pitonak, K. E. Riley, P. Neogrady and P. Hobza, *ChemPhysChem*, 2008, **9**, 1636–1644.

35 W. Zierkiewicz, D. Michalska and P. Hobza, *Phys. Chem. Chem. Phys.*, 2010, **12**, 2888–2894.

36 E. Munusamy, R. Sedlak and P. Hobza, *ChemPhysChem*, 2011, **12**, 3253–3261.

37 R. Sedlak, P. Jurecka and P. Hobza, *J. Chem. Phys.*, 2007, **127**, 075104–075106.

38 J. Rezac and P. Hobza, *J. Chem. Theory Comput.*, 2011, **7**, 685–689.

39 R. Sedlak, J. Fanfrlík, D. Hnyk, P. Hobza and M. Lepsík, *J. Phys. Chem. A*, 2010, **114**, 11304–11311.

40 S. Karthikeyan, R. Sedlak and P. Hobza, *J. Phys. Chem. A*, 2011, **115**, 9422–9428.

41 W. Wang and P. Hobza, *ChemPhysChem*, 2008, **9**, 1003–1009.

42 R. Sedlak, P. Hobza and G. N. Patwari, *J. Phys. Chem. A*, 2009, **113**, 6620–6625.

43 S. Maity, R. Sedlak, P. Hobza and G. N. Patwari, *Phys. Chem. Chem. Phys.*, 2009, **11**, 9738–9743.

44 J. Ran and P. Hobza, *J. Phys. Chem. B*, 2009, **113**, 2933–2936.

45 L. Biedermannova, K. E. Riley, K. Berka, P. Hobza and J. Vondrasek, *Phys. Chem. Chem. Phys.*, 2008, **10**, 6350–6359.

46 M. Kolar, K. Berka, P. Jurecka and P. Hobza, *ChemPhysChem*, 2010, **11**, 2399–2408.

47 C. A. Morgado, P. Jurecka, D. Svozil, P. Hobza and J. Sponer, *Phys. Chem. Chem. Phys.*, 2010, **12**, 3522–3534.

48 J. Cerny and P. Hobza, *Phys. Chem. Chem. Phys.*, 2007, **9**, 5291–5303.

49 K. Berka, P. Hobza and J. Vondrasek, *ChemPhysChem*, 2009, **10**, 543–548.

50 K. E. Riley, M. Pitonak, J. Cerny and P. Hobza, *J. Chem. Theory Comput.*, 2010, **6**, 66–80.

51 K. E. Riley and P. Hobza, *Wiley Interdiscip. Rev.: Comput. Mol. Sci.*, 2011, **1**, 3–17.

52 L. Bendova, P. Jurecka, P. Hobza and J. Vondrasek, *J. Phys. Chem. B*, 2007, **111**, 9975–9979.

53 J. Ran and P. Hobza, *J. Chem. Theory Comput.*, 2009, **5**, 1180–1185.

54 S. Maity, G. N. Patwari, R. Sedlak and P. Hobza, *Phys. Chem. Chem. Phys.*, 2011, **13**, 16706–16712.

55 J. Sponer, K. E. Riley and P. Hobza, *Phys. Chem. Chem. Phys.*, 2008, **10**, 2595–2610.

56 M. Zgarbova, M. Otyepka, J. Sponer, P. Hobza and P. Jurecka, *Phys. Chem. Chem. Phys.*, 2010, **12**, 10476–10493.

57 W. Zierkiewicz, R. Wieczorek, P. Hobza and D. Michalska, *Phys. Chem. Chem. Phys.*, 2011, **13**, 5105–5113.

58 K. Pluhackova, P. Jurecka and P. Hobza, *Phys. Chem. Chem. Phys.*, 2007, **9**, 755–760.

59 U. Adhikari and S. Scheiner, *Chem. Phys. Lett.*, 2012, **532**, 31–35.

THE JOURNAL OF PHYSICAL CHEMISTRY A

Article

pubs.acs.org/JPCA

Differences in the Sublimation Energy of Benzene and Hexahalogenbenzenes Are Caused by Dispersion Energy

Jakub Trnka,[†] Robert Sedlak,[†,‡] Michal Kolář,[†,‡] and Pavel Hobza*[,†,§]

[†]Institute of Organic Chemistry and Biochemistry, Academy of Sciences of the Czech Republic, Flemingovo nam 2, 166 10 Prague, Czech Republic

[‡]Department of Physical and Macromolecular Chemistry, Faculty of Science, Charles University in Prague, Albertov 6, 128 43 Prague, Czech Republic

[§]Regional Center of Advanced Technologies and Materials, Department of Physical Chemistry, Palacky University, 771 46 Olomouc, Czech Republic

Supporting Information

ABSTRACT: The crystals of benzene and hexahalogenbenzenes have been studied by means of the density functional theory augmented by an empirical dispersion correction term as well as by the symmetry-adapted perturbation theory. In order to elucidate the nature of noncovalent binding, pairwise interactions have been investigated. It has been demonstrated that the structures of dimers with the highest stabilization energy differ notably along the crystals. It has been shown that the differences in the experimental sublimation energies might be attributed to the dispersion interaction. To our surprise, the dihalogen bonding observed in the hexachloro- and hexabromobenzenes plays a rather minor role in structure stabilization because it is energetically comparable with the other binding motifs. However, the dihalogen bond is by far the most frequent binding motif in hexachloro- and hexabromobenzenes.

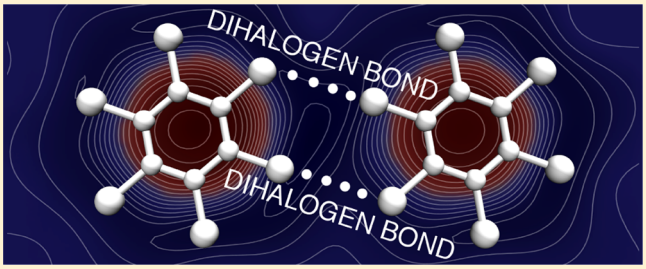

1. INTRODUCTION

The benzene dimer is one of the most studied aromatic molecular clusters, which arises among other things from the importance of the stacking $\pi\cdots\pi$ interaction.[1−5] Two dimer structures are supposed to coexist at the respective potential energy surface, the T-shaped, or nearly T-shaped, structure and the parallel-displaced (PD) structure. The parallel C_{2h} structure, which was expected to be the global minimum (because of the maximal overlap), is actually penalized by the quadrupole−quadrupole (Q−Q) electrostatic interaction, which is repulsive here.[6] The Q−Q interaction becomes less repulsive or attractive in the case of PD and T-shaped structures, respectively. Evidently, the electrostatic energy plays an important role in the interaction of benzene molecules not only in the benzene dimer but also in crystalline and plastic-crystalline phases.[7,8]

It is thus not surprising that there have been attempts to interpret the sublimation energy of the benzene crystal only in terms of electrostatic quadrupole energy,[9] although there are certainly higher electric multipoles presented. The resulting sublimation energy of 10.7 kcal/mol agreed exactly with the respective experimental value.[9]

When passing to hexahalogenbenzenes, the quadrupole moment remains the first nonzero multipole moment, and it is hence possible to expect that the sublimation energies of hexahalogenbenzenes will be determined dominantly also by the electrostatic Q−Q interaction.

Table 1 shows the z-components of quadrupole moments Q, polarizabilities α, and sublimation energies E^{sub} of benzene and hexahalogenbenzenes. In the case of benzene, the x- and y-components are positive, while in the cases of hexafluoro- (C_6F_6) and hexachlorobenzenes (C_6Cl_6), these quadrupole components are negative. Hexabromobenzene has again the components with the same sign as benzene. The quadrupole orientations correspond to the electrostatic potential (ESP) maps in Figure 1. While the benzene ring is negatively charged in its center, the halogen atoms withdraw the electrons from the π-system, making the ring either positive (C_6F_6 and C_6Cl_6)

Table 1. z-Component of Quadrupole Moments (Q, au), Polarizabilities (α, Å^3), and Sublimation Energies (E^{sub}, kcal/mol) of the C_6X_6 (X = H, F, Cl, Br) Systems

	Q	α	E^{sub}
C_6H_6	−6.59	56.23	10.7
C_6F_6	7.89	57.24	11.8
C_6Cl_6	0.25	120.63	23.8
C_6Br_6	−4.72	152.93	

Received: February 25, 2013
Revised: April 24, 2013
Published: April 25, 2013

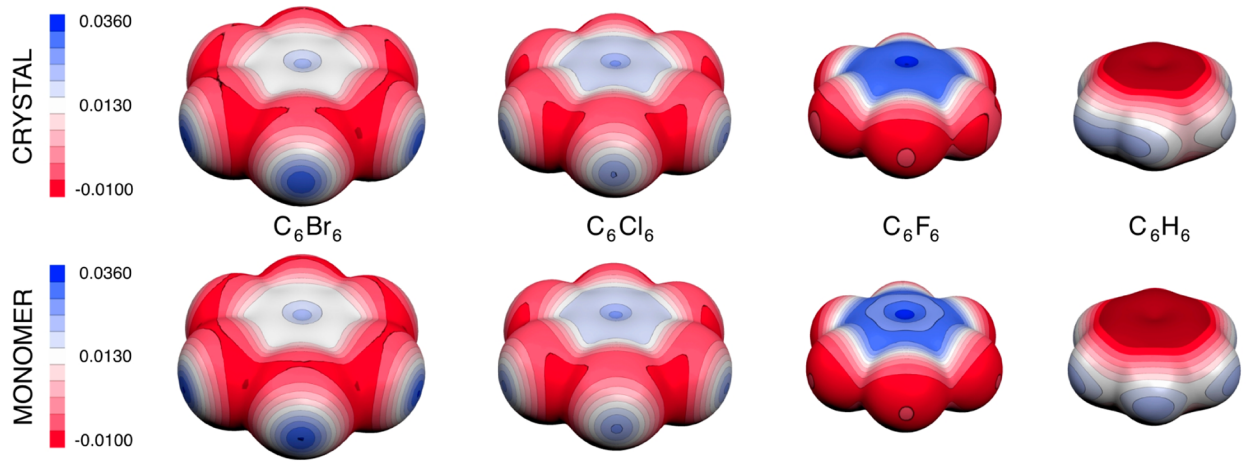

Figure 1. The electrostatic potential mapped on the 0.001 e/bohr^3 electron isodensity surface of C_6X_6 (X = H, F, Cl, Br). The maps were determined at the B3LYP/TZVPP level for the central reference molecule of the crystal model and for B3LYP/6-311+G*-optimized monomers. The color scale is in au.

or slightly negative (C_6Br_6). The overall contribution of the hexadecapole interactions is however negligible, indeed.

A quick inspection of the quadrupole moments and the respective sublimation energies in Table 1 reveals no correlation between them. The quadrupole moments of hexafluorobenzene and benzene have the opposite sign, but their absolute values are similar (the former is slightly larger). With respect to this fact, we could expect the sublimation energy of the C_6F_6 to be slightly larger than that of the benzene, which actually holds true (cf. Table 1). When passing from hexafluorobenzene to hexachlorobenzene, the situation is dramatically changed, and the quadrupole moment of the latter molecule is more than an order of magnitude smaller. The sublimation energy of C_6Cl_6, however, has increased. Evidently, the assumption that the sublimation energy of hexahalogenbenzenes is determined by the electrostatic quadrupole energy is not fulfilled, and other energy terms may also have their contribution. In Table 1, we can find a close correlation between the polarizabilities and the sublimation energies, which tells us that the dispersion energy plays an important role in the interaction between hexahalogenbenzenes because there is a direct connection between the molecular polarizability and dispersion forces.

In the case of benzene dimer (or the crystal), both the electrostatic and dispersion energies are dominant attractive energy terms, while the induction term (quadrupole-induced dipole) is much smaller. These two terms are thus responsible for the structure determination, and the relevant dimer structures should be localized in the crystal structure. The situation is exactly the same in the case of hexafluorobenzene. With hexachloro- and hexabromobenzenes, this is no longer valid because a new interaction motif appears here.

Specifically, the dihalogen bond is formed between two molecules of hexachlorobenzenes or hexabromobenzenes, namely, between a halogen, X_1 (Cl, Br, I), which is covalently bound to a less electronegative atom (e.g., carbon), and another halogen, X_2 ($C{-}X_1{\cdots}X_2$).[10,11] This counterintuitive interaction is explained by the fact that a halogen atom is not isotropically negatively charged but it has a region with a positive electrostatic potential located on its top. This region is usually called a σ-hole;[12] it is depicted in Figure 1 as the blue disk on the halogens in C_6Cl_6 and C_6Br_6. Generally, in a $R_1{-}X_1{\cdots}X_2{-}R_2$ complex when the $R_1X_1X_2$ and $X_1X_2R_2$ angles are both close to 180°, the interaction of two positive σ-holes is repulsive, resulting from the Coulomb law. However, when one of the respective angles is about 90° while the other remains at 180°, the positive σ-hole interacts with the negatively charged ring of the atom, and the resulting interaction energy is attractive. The strength of the dihalogen bond is expected to increase with the atomic number of the halogens; in other words, the C−Cl···Cl dihalogen bond is weaker than the C−Br···Br or C−I···I bonds. The σ-hole also exists at fluorine covalently bound to carbon, but this is typical only for small inorganic compounds such as NCF and not for aromatic species.[13,14] Consequently, the C−F···F dihalogen bonds between two C_6F_6 are mostly impossible to form. It has to be added that in the case of the dihalogen bond, the dominant energy term is dispersion energy followed by electrostatic energy.[15] The important contribution of dispersion energy can be easily explained by the short distance between two heavy halogens possessing high polarizabilities.

The array of the σ-holes is also manifested by higher electric multipoles. While there are no differences in the electric octapole moments, which is almost zero, there is a decrease of nonzero hexadecapole components when passing from C_6H_6 to C_6Br_6 (i.e., it is the most negative for C_6Br_6).

The aim of the present study is to examine the nature of noncovalent binding within the crystals of C_6X_6 benzenes (X = H, F, Cl, Br). Specifically, we focused on identification of the binding motifs in various dimer structures appearing in these crystals. An attempt is made to correlate the experimental sublimation energy with the total interaction energies calculated for the crystal structures.

2. METHODS

2.1. Structure Preparation. The X-ray structures of the hexahalogenbenzene crystals were obtained from the Cambridge Structural Database.[16,17] The X-ray structure of the benzene crystal[18] was obtained from the Crystallography Open Database (21000348.cif).[19] Subsequently, it was processed using the JMol program.[20]

Within each crystal, the pairwise interactions were identified in the following manner: a reference molecule was chosen arbitrarily, and 20 pairs were created. Each pair contains the reference molecule and one of the 20 nearest neighbors (cf. Figure S1 in the Supporting Information).

dx.doi.org/10.1021/jp401961g | J. Phys. Chem. A 2013, 117, 4331−4337

2.2. Computations. The interaction energies for various dimers and for a large cluster, consisting of 21 molecules, were evaluated at the DFT (B3LYP-D3) level using the TZVPP basis set and the empirical pairwise dispersion contribution.[21] No deformation energy nor counterpoise correction was included. The interaction energy (ΔE) for a pair was determined as the difference between the energy of the dimer and the energies of both monomers (eq 1)

$$\Delta E_{AB} = E(AB) - E(A) - E(B) \quad (1)$$

The energy of the central reference molecule $E(1)$ and the energy of the cluster containing all but the central molecule $E(20)$ were subtracted from the energy of the entire cluster $E(21)$, providing the total interaction energy ΔE_{tot} (eq 2)

$$\Delta E_{tot} = E(21) - E(1) - E(20) \quad (2)$$

Finally, the average interaction energy (ΔE_{aver}) was evaluated according to eq 3

$$\Delta E_{aver} = \frac{[E(21) - 21 \cdot E(1)]}{21} \quad (3)$$

where $E(21)$ stands for the energy of the entire cluster and $E(1)$ is the energy of the central reference molecule. The energy decomposition for all of the dimers was found by the DFT-SAPT method using the aug-cc-pVDZ basis set.[22,23] The SAPT interaction energy (E_{INT}) was constructed as a sum of electrostatic (ES), induction (IND), dispersion (DISP), and exchange−repulsion (EXCH) terms. The exchange−induction and exchange−dispersion terms were added to the induction and dispersion energies, and finally, the δ(HF) term was added to the induction energy. More details about the DFT-SAPT method can be found elsewhere.[24]

It is a known fact that using the DFT-SAPT decomposition with an aug-cc-pVDZ basis set provides an unconverged dispersion (DISP) contribution, while the other contributions are converged, indeed, when compared with the complete basis set limit values.[24] Hence, the dispersion contribution was scaled by a factor that was calculated as follows. For the most stable dimers, we performed calculations with the aug-cc-pVTZ and aug-cc-pVDZ basis sets, and the scaling coefficients were obtained as the ratio between the dispersion term with the aug-cc-pVTZ and aug-cc-pVDZ basis sets. The coefficients are 1.42, 1.09, 1.09, and 1.12 for benzene, C_6F_6, C_6Cl_6, and C_6Br_6. For more details, see Table S1 in the Supporting Information.

The calculations were carried out with Gaussian,[25] Molpro,[26] and Grimme's DFT-D3[21] program packages.

3. RESULTS AND DISCUSSION

3.1. Interaction Energies. The total DFT-D3 interaction energies of the central reference molecule with the 20 neighboring molecules (cf. Figure S1, Supporting Information) evaluated for 4 molecular crystals are presented in Table 2. Besides the total interaction energies, likewise, their DFT and dispersion components are shown. Table 2 also shows the average interaction energies, and also here, their DFT and dispersion components are presented.

The total interaction energies of benzene and C_6F_6 are almost equal, and also, the DFT and dispersion components are roughly comparable. These results are not surprising regarding the molecular properties (cf. Table 1). However, the relatively large difference between the average interaction energies of C_6H_6 and C_6F_6 is surprising. This discrepancy may arise from the differences in the symmetry of particular crystal structures. This issue will be addressed in more details below.

Table 2. Interaction Energies (in kcal/mol) of the Central Molecule with the 20 Neighboring Molecules (the total columns) and the Average Interaction Energies (the average columns) for the Clusters[a]

	total			average		
	$\Delta E_{DFT+Disp}$	ΔE_{DFT}	ΔE_{Disp}	$\Delta E_{DFT+Disp}$	ΔE_{DFT}	ΔE_{Disp}
C_6H_6	−27.6	4.6	−32.2	−6.0	1.0	−7.0
C_6F_6	−27.9	1.0	−28.8	−10.5	−2.5	−8.0
C_6Cl_6	−45.6	19.3	−64.9	−13.5	5.5	−19.0
C_6Br_6	−61.6	24.3	−85.9	−17.6	7.3	−24.9

[a]The DFT and dispersion components are provided.

When passing from C_6F_6 to C_6Cl_6 and C_6Br_6, a significant increase of the total stabilization energy and roughly the same increase of the average stabilization energy were found. In both cases, the dispersion contribution is much larger than that in the previous two crystals, and it is responsible for the total stabilization energy increase. Let us add that for all four crystals, the DFT energy component is repulsive. The decomposition of the total interaction energy presented in Table 2 does not say anything about the nature of the stabilization of the particular pairs.

Table 3 shows the interaction energies for various pairs of benzene and hexahalogenbenzenes. The interaction energy is systematically determined using DFT-D3 and DFT-SAPT approaches, and various pairs are ordered along decreasing stabilization energy; only the pairs with the stabilization energy higher than 1.0 kcal/mol are presented. All pair interaction energies are provided in the Supporting Information in Table S2. DFT-D3 stabilization energies are in all cases larger than the DFT-SAPT ones. This overestimation is the largest for hexafluorobenzene and benzene (39 and 31%), while that for hexachloro- and hexabromobenzenes is considerably smaller (5 and 9%). Evidently, the DFT-SAPT stabilization energies evaluated with the aug-cc-pVTZ basis set are more reliable and will be considered in the following text when analyzing the pair interactions.

First, a quick inspection of the DFT-SAPT energies from Table 3 reveals a feature valid for almost all listed pair interactions. Not surprisingly, all dimers are mainly stabilized by dispersion and electrostatic interactions. Second, by comparing the pair interaction energies of C_6H_6 and C_6F_6 with those of C_6Cl_6 and C_6Br_6, we found an important difference. The stabilization energies for the most and least attractive pairs differ for the former two systems only marginally (by less than 1.2 kcal/mol), while this difference is much more pronounced for the latter two systems (8.1 and 9.4 kcal/mol, respectively). This difference can be documented also with the corresponding relative numbers. The relative increase of interaction from the weakest to the strongest dimer is 83% 100, 506, and 448% for C_6H_6, C_6F_6, C_6Cl_6, and C_6Br_6, respectively.

3.2. Relative Importance of Energy Terms. We calculated the ratios of the dispersion and interaction energies ($DISP/E_{INT}$) as well as of the electrostatic and interaction energies (ES/E_{INT}). They provide a picture on the balance between the two most important attractive forces. The ES/E_{INT} ratios averaged over the pairs with stabilization higher than 1 kcal/mol are 0.51, 0.54, 0.68, and 0.89 for C_6H_6, C_6F_6, C_6Cl_6, and C_6Br_6, respectively. Clearly, the relative importance of the

dx.doi.org/10.1021/jp401961g | J. Phys. Chem. A 2013, 117, 4331−4337

Table 3. DFT-D3 and DFT-SAPT Pair Interaction Energies (ΔE and E_{INT}) for the Energetically Most Favorable Pairs[a]

			DFT-D3	DFT-SAPT			
molecule	bind. motif	deg.	$-\Delta E$	−ES	−IND	−DISP	$-E_{INT}$
C_6H_6	T-shape	3	2.8 (3.3)	1.2	0.1	3.3	2.2
	distorted T-shape	3	2.0 (2.4)	1.0	0.0	2.4	1.5
	L-shape	3	1.6 (2.0)	0.4	0.0	1.9	1.2
C_6F_6	PD	1	3.3 (2.9)	1.4	0.1	3.7	2.4
	distant PD	0	3.3 (2.7)	1.7	0.1	3.7	2.4
	distorted T-shape	0	3.0 (2.8)	1.0	0.1	3.6	2.3
	distorted T-shape	0	2.7 (2.9)	1.0	0.1	3.7	1.9
	distorted T-shape	0	2.5 (2.4)	1.1	0.1	3.2	1.8
	distorted T-shape	0	2.4 (2.2)	1.1	0.1	2.9	1.7
	distorted T-shape	1	2.0 (1.7)	0.5	0.0	2.0	1.6
	distorted T-shape	1	1.9 (2.1)	0.7	0.0	2.8	1.2
C_6Cl_6	PD	1	11.5 (16.6)	6.0	0.4	19.6	9.7
	dihalogen bonded	1	2.0 (2.6)	1.2	0.1	3.8	2.1
	distorted T-shape	3	1.9 (2.4)	1.2	0.1	3.4	1.9
	distant PD	1	1.9 (2.9)	1.1	0.0	3.7	1.7
	distorted T-shape	3	1.6 (2.3)	1.3	0.1	3.4	1.6
C_6Br_6	PD	1	14.1 (20.9)	8.3	0.5	22.8	11.5
	dihalogen bonded	1	3.0 (3.8)	2.3	0.3	5.3	2.9
	distorted T-shape	3	2.7 (3.4)	2.3	0.3	4.8	2.7
	distorted T-shape	3	2.1 (3.1)	2.4	0.3	4.8	2.2
	distant PD	1	2.6 (4.1)	1.8	0.1	4.6	2.1

[a]The numbers in parentheses refer to the absolute value of the dispersion component of the DFT-D3 energy, and besides the total DFT-SAPT interaction energy (E_{INT}), also its components electrostatic (ES), induction (IND), and dispersion (DISP) are presented; all energies are listed in kcal/mol. The table shows only pairs with the DFT-SAPT stabilization energy larger than 1.0 kcal/mol; deg stands for the degeneracy level of the particular structure (deg. = n means that n + 1 identical structures exist).

electrostatic contribution increases with the atomic number of the halogen. However, the value of neither the quadrupole (cf. Table 1) nor the quadrupole−quadrupole electrostatic interaction can interpret these ratios. An important increase of this ratio when passing from C_6H_6 and C_6F_6 to C_6Cl_6 and C_6Br_6 could be connected with the fact that a new binding motif is created in the latter group of crystals. Selected dimers of C_6Cl_6 and C_6Br_6 are stabilized by dihalogen bonds that do not exist in the former two crystals. The value of the ES/E_{INT} ratio for the dihalogen-bonded dimers of the C_6Cl_6 and C_6Br_6 molecules is even more pronounced. The values of 0.70 and 0.94 support our previous statement. Hence, the mere formation of dihalogen bonds in selected dimers of C_6Cl_6 and C_6Br_6 can explain the increase of the ES/E_{INT} ratios for the C_6Cl_6 and C_6Br_6 dimers. The different electrostatic potentials of C_6Cl_6 and C_6Br_6 with respect to the other two molecules, which is the reason for the formation of dihalogen-bond structures, may potentially be responsible for the increased value of the ES/E_{INT} ratio. A more detailed view of the electrostatic potentials of all four molecules will be presented below. In Table 3, other relatively interesting features can be observed. The PD structure is either the most stable or one of the most stable dimer structures. When investigating the ES DFT-SAPT energies for this structure, we found its dramatic increase for hexachloro- and hexabromobenzenes, which contradicts the decrease of the quadrupole moment when passing from C_6H_6 and C_6F_6 to C_6Cl_6 and C_6Br_6. Visualizing the PD structures of all crystals (Figure 2), we found that monomers in C_6Cl_6 and C_6Br_6 PD dimers are much closer to each other than those in the C_6F_6 dimer; the distance between the centers of mass of the C_6F_6, C_6Cl_6, and C_6Br_6 crystals amounts to 5.76, 3.76, and 3.95 Å, respectively. A closer contact in the C_6Cl_6 and C_6Br_6 PD structures (which contradicts the larger vdW radii of Cl and Br than that of F) is clearly due to a very large dispersion energy (cf. Table 3), which pushes monomers together. The penetration energy, defined as a difference between the SAPT electrostatic energy and multipole−multipole electrostatic energy, is negligible at the distances larger than equilibrium and becomes important (attractive) at shorter distances. Large SAPT electrostatic energies for the C_6Cl_6 and C_6Br_6 dimers are thus due to attractive penetration energies and have no connection with the quadrupole−quadrupole electrostatic energy.

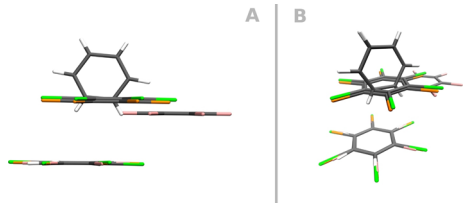

Figure 2. The most stable pair structures for benzene, hexafluorobenzene, hexachlorobenzene, and hexabrombenzene; silver = C, white = H, pink = F, orange = Cl, and green =Br; (A) side view; (B) perspective view.

The DISP/E_{INT} ratios averaged over the pairs with stabilization higher than 1 kcal/mol are 1.56, 1.69, 2.00, and 1.99 for C_6H_6, C_6F_6, C_6Cl_6, and C_6Br_6, respectively. Unsurprisingly, the relative importance of the dispersion contribution is the lowest for C_6H_6 and the highest for C_6Cl_6 and C_6Br_6.

3.3. Structural Analysis. The binding motifs between the central and neighboring molecules in our cluster models as well as the geometrical parameters of the individual dimers are discussed in the following subsection.

dx.doi.org/10.1021/jp401961g | J. Phys. Chem. A 2013, 117, 4331−4337

The differences in the binding motifs themselves, along with the different energetic degeneracy for all four molecular crystals, reveal that the relative arrangement of the molecules in the cluster models is different (cf. Table 3).

The highest degree of the energetic as well as binding motif degeneracy is exhibited by the benzene crystal. The 12 closest molecules that surround the central molecule are grouped into three structural motifs, each including four dimers (cf. the first part of Table 3 and Figure S1, Supporting Information). Several structural motifs can be recognized, T-shape, distorted T-shape, and L-shape (Figure 3).

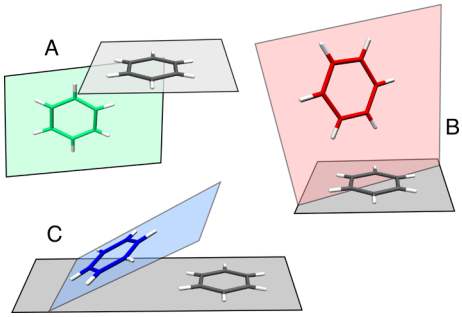

Figure 3. Structural motifs of benzene pairs found in the crystal. (A) L-shape, (B) T-shape, and (C) distorted T-shape.

The crystal of C_6F_6 possesses the lowest degree of structural motif and energetic degeneracy. The 11 neighboring molecules are divided into 8 groups (cf. the second part of Table 3 and Figure S1, Supporting Information). The three most stable dimers correspond to the PD structures. The structures of the remaining eight dimers can be classified as T-shape or distorted T-shape structures. The least stable dimer (with stabilization < 1 kcal/mol) with the planar molecular structure is rare in the cluster model.

The crystals of C_6Cl_6 and C_6Br_6 are almost identical, hence possessing similar energetic and structural characteristics. The 14 neighboring molecules are divided into 5 groups. The most stable are two PD structures followed by two planar structures with two dihalogen bonds. As already mentioned above, dimers with dihalogen bonds are considerably less stable than the PD structures. Another two dimers represent a distant PD structure. The eight least stable dimers were included in the category of distorted halogen-bonded structures. However, they represent two distinct stabilization levels (cf. the third and fourth parts of Table 3 and Figures 4 and S1, Supporting Information).

One could expect that the similarity or the dissimilarity in the mutual arrangement of the neighboring molecules in the molecular crystals can be predicted for different chemical species based on the values of molecular properties, such as permanent multipole moments, polarizabilities, and so forth. However, the crystal structure analysis showed that such an assumption would lead to wrong interpretations. The structural differences between the crystals of C_6H_6 and C_6F_6 are remarkable, while the opposite is true when the crystals of C_6Cl_6 and C_6Br_6 are compared. Nevertheless, in the first example, the values of molecular properties are very similar, whereas in the second, there are significant differences (cf. Table 1). This leads us to the statement that more sophisticated approaches are necessary for the interpretation of the structural motif among noncovalently bound clusters.

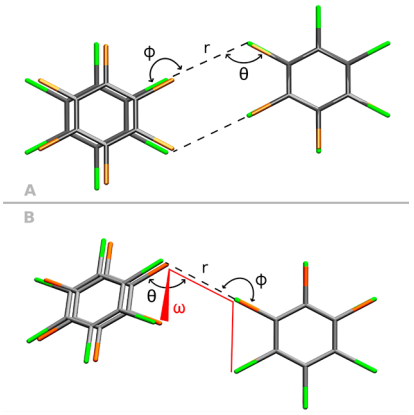

Figure 4. (A) Structures of the planar dihalogen-bonded dimer of hexachloro- and hexabromobenzene, with two ("cyclic") dihalogen bonds: $\varphi = 171°$, $\theta = 123°$, $r = 3.7$ Å and $\varphi = 173°$, $\theta = 123°$, $r = 3.8$ Å for C_6Cl_6 and C_6Br_6, respectively; the top view. (B) Structures of the distorted dihalogen-bonded dimer of hexachloro- and hexabromobenzene, with one dihalogen bond: $\varphi = 175°$, $\theta = 117°$, $\omega = 35°$, $r = 3.4$ Å and $\varphi = 174°$, $\theta = 115°$, $\omega = 35°$, $r = 3.5$ Å for C_6Cl_6 and C_6Br_6, respectively; the perspective view. Silver = C, orange = Cl, and green = Br.

In the next paragraphs, the geometrical parameters of individual dimers will be discussed. The most attractive pair of C_6H_6 is represented by the T-shape structure, while the distorted T-shape and L-shaped structures are considerably less stable (by 29 and 43%, respectively). The situation with the remaining three hexahalogenbenzenes is different, and here, the most attractive pairs correspond to the PD structures. However, while the stabilization of the PD structure of C_6F_6 is comparable to that of the remaining structures, in the case of the other halogenbenzenes, the difference is significant. A comparison of the PD structures of hexahalogenbenzenes brings quantitative differences. For C_6F_6, the distance between the centers of mass is 5.8 Å (Figure 2). On the other hand, in the case of chloro- and bromoderivates, the equivalent distance ranges between 3.8 and 4.0 Å, respectively. Hence, in the case of C_6F_6, the electrostatic and dispersion terms are much smaller. While for C_6Cl_6 and C_6Br_6 the PD structure is significantly more stable than the other structures, the situation for C_6F_6 is different, and here, the stability of PD and other structures (see below) differs only marginally. A further comparison of the most attractive PD structure for the three studied halogenbenzenes leads to the electrostatic term being larger for C_6Cl_6 and C_6Br_6 (than that for C_6F_6) by 4.6 and 6.9 kcal/mol, respectively. This difference is, however, significantly larger (by 14.6 and 17 kcal/mol) for the dispersion contribution. Consequently, it is mostly the dispersion energy for the PD structures that makes the total stabilization energy of C_6Cl_6 and C_6Br_6 much larger than that of C_6F_6 (cf. the polarizabilities of hexahalogenbenzenes presented in Table 1).

Investigating other less stable pairs, we again found more pronounced differences between C_6H_6, C_6F_6, C_6Cl_6, and C_6Br_6. The three most stable structures of the second crystal possess a PD structure, while all of the others have a T-shaped structure.

The crystals of hexachloro- and hexabromobenzenes differ from the crystals of benzene and hexafluorobenzene by the presence of structures possessing dihalogen bonds (cf. Figure 3). There are two structures with two ("cyclic") dihalogen bonds for each crystal with stabilization energies of 2.1 and 2.9 kcal/mol for C_6Cl_6 and C_6Br_6, respectively. The $C_1X_1X_2$ angle

dx.doi.org/10.1021/jp401961g | J. Phys. Chem. A 2013, 117, 4331−4337

(φ) in these structures is, as it should be, almost linear (171 and 173° for C_6Cl_6 and C_6Br_6, respectively), and the $X_1\cdots X_2$ distance is 3.7 and 3.8 Å. The $X_1X_2C_2$ angle (θ) is 123° for C_6Cl_6 and C_6Br_6 (cf. Figure 4). Other dimer structures, named distorted dihalogen bonds, are not planar. One molecule is distorted from the imaginary plane (cf. Figure 4B); hence, the structure contains only one dihalogen bond. The arrangement of the CX_1X_2 atoms is almost identical as in the case of structures with two (cyclic) dihalogen bonds. Originally, we expected that due to this rather short distance between heavy halogens, the stabilization energy of the structures with dihalogen bonds will be significantly higher. From the Table 3, it is, however, evident that these stabilization energies are only slightly larger than the stabilization energies of other structures.

Investigating different structures of hexafluorobenzene, whose stabilization energy exceeds 1 kcal/mol, we found neither planar nor distorted structures with a difluoro noncovalent bond. This is caused by the fact that fluorine covalently bound to an aromatic ring usually does not exhibit a σ-hole, which is a prerequisite for the existence of halogen bonding (cf. Figure 1). This significant difference between the electrostatic potential of C_6F_6 and C_6Cl_6 (together with C_6Br_6) crystals can be seen as the reason for the significant differences in the crystal structures (cf. Figure 1). The region of the positive electrostatic potential (σ-hole), present at the top of each chlorine and bromine atom in a hexahalogenbenzene molecule (cf. Figure 1), is the moiety via which the intermolecular interaction is realized (cf. Figure 4).

Nevertheless, the stabilization energies of various hexafluorobenzene structures mostly having the T-shaped structure without a direct X···X interaction are comparable to the stabilization energies of the structures possessing dihalogen bonds.

It must be emphasized that no σ-hole$\cdots\pi$ interactions were found in the crystals. The positive σ-hole could be attracted by the negative π-electrons of the aromatic rings, but this is not the case of the C_6X_6 crystals, which are composed of one type of monomer only. According to Figure 1, due to its positive charge, the π-system of C_6Cl_6 and C_6Br_6 is a poor σ-hole-acceptor. For mixed crystals, however, the σ-hole$\cdots\pi$ interactions could play a role.

3.4. Discussion. Similar total interaction energies (1 + 20) of benzene and hexafluorobenzene agree with similar sublimation energies of these two crystals, and the much larger total interaction energy of hexachlorobenzene again agrees with its much larger sublimation energy. The relatively large difference in the average interaction energy of C_6H_6 and C_6F_6 (of as much as 75%) can be interpreted as a consequence of a different spatial orientation of the pairs within the clusters considered. Comparing the entire cluster model of the C_6H_6 and C_6F_6 (cf. Figure S1, Supporting Information) crystals, it is evident that the former one is spherically less symmetric than the latter one, which means that the molecules around the central one are ordered less compactly. Hence, the average stabilization energy of the C_6H_6 molecule is substantially smaller.

The significant differences between the binding motif of the most stable dimer of C_6H_6 and C_6F_6 crystals (T-shape and PD structure) can be seen as a consequence of a subtle difference in the electrostatic potential. In the case of the C_6H_6 molecule, where the hydrogen atom regions are represented by a continuously increased positive potential (cf. Figure 1), the T-shape conformer is energetically more preferred. On the other hand, the electrostatic potential of C_6F_6 in the regions of fluorine atoms does not show the same properties. Even though the fluorine atoms are surrounded by a negative region of the potential, an increase of the potential on top of each fluorine can be observed. This is a consequence of a mutual electron repulsion; hence, the T-shape structure is not as preferred as the PD structure.

4. CONCLUSIONS

Both the total and the average interaction energies increase when passing from benzene through hexafluorobenzene over hexachlorobenzene, and this increase is proportional to the increase of sublimation energy.

The most favorable pair structure with benzene corresponds to the T-shaped structure, while that for hexahalogenbenzenes corresponds systematically to the PD structure. Because of the much higher polarizability of the hexachloro- and hexabromobenzene, the dispersion energy in this structure is also much higher than that in the hexafluorobenzene. The significant increase in the total interaction energy as well as that in the experimental sublimation energy when passing from hexafluorobenzene to hexachloro- and hexabromobenzene is thus mainly caused by the increase in dispersion energy. Indeed, the DFT-SAPT decomposition shows that the dominant part of the interaction energy originates in the dispersion energy. Nevertheless, the relative importance of the electrostatic contribution increases when passing to heavier halogens; in the case of hexabromobenzene, it is at the expense of the dispersion term.

The new structural type, found in the crystals of hexachloro- and hexabromobenzenes, is stabilized by dihalogen bonds. However, the stabilization energies of these structures do not differ much from the stabilization energies of other, mainly T-shaped structures of hexahalogenbenzene. The existence of the structures with dihalogen bonds thus cannot be responsible for the higher total interaction and sublimation energies of hexachloro- and hexabromobenzene. However, the presence of dihalogen bonds in hexachloro- and hexabromobenzenes has a crucial role for the determination of geometries of their crystals.

■ ASSOCIATED CONTENT

Supporting Information

The *xyz* coordinates of the clusters, the details of the DFT-SAPT dispersion contribution, the interaction energies and decompositions for all of the pairs, and the depiction of the cluster models are provided. This material is available free of charge via the Internet at http://pubs.acs.org.

■ AUTHOR INFORMATION

Notes

The authors declare no competing financial interest.

■ ACKNOWLEDGMENTS

This work was part of the Research Project RVO: 61388963 of the Institute of Organic Chemistry and Biochemistry, Academy of Sciences of the Czech Republic. This work was also supported by the Czech Science Foundation [P208/12/G016] and the operational program Research and Development for Innovations of the European Social Fund (CZ 1.05/2.1.00/03/0058).

REFERENCES

(1) Watson, J. D.; Crick, H. C. D. Molecular Structure of Nucleic Acids — A Structure for Deoxyribose Nucleic Acid. *Nature* **1953**, *171*, 737−738.

(2) Lerman, L. S. Structure of DNA−Acridine Complex. *J. Mol. Biol.* **1961**, *3*, 18−20.

(3) Burley, S. K.; Petsko, G. A. Aromatic−Aromatic Interaction — A Mechanism of Protein-Structure Stabilization. *Science* **1985**, *229*, 23−28.

(4) Hunter, C. A.; Singh, J.; Thornton, J. M. $\pi-\pi$ Interactions — The Geometry and Energetics of Phenylalanine Phenylalanine Interactions in Proteins. *J. Mol. Biol.* **1991**, *218*, 838−846.

(5) McGaughey, G. B.; Gagne, M.; Rappe, A. K. π-Stacking Interactions — Alive and Well in Proteins. *J. Biol. Chem.* **1998**, *273*, 15458−15463.

(6) Battaglia, M. R.; Buckingham, A. D.; Williams, J. H. The Electric Quandrupole-Moments of Benzene and Hexafluorobenzene. *Chem. Phys. Lett.* **1981**, *78*, 421−423.

(7) Shahin, M.; Murthy, S. S. N.; Singh, L. P. Glass Transition Phenomena in Two-Component Plastic Crystals: Study of Hexasubstituted Benzenes. *J. Phys. Chem. B* **2006**, *110*, 18573−18582.

(8) Cansell, F.; Fabre, D.; Petitet, J. P. Phase Transitions and Chemical Transformations of Benzene up to 550 °C and 30 GPa. *J. Chem. Phys.* **1993**, *99*, 7300−7304.

(9) Sen, P.; Basu, S. Sublimation Energy of Benzene. *J. Chem. Phys.* **1968**, *48*, 4075−4076.

(10) Politzer, P.; Murray, J. S.; Concha, M. C. σ-Hole Bonding between Like Atoms: A Fallacy of Atomic Charges. *J. Mol. Model.* **2008**, *14*, 659−665.

(11) Politzer, P.; Riley, K. E.; Bulat, F. A.; Murray, J. S. Perspectives on Halogen Bonding and Other σ-Hole Interactions: Lex Parsimoniae (Occam's Razor). *Comput. Theor. Chem.* **2012**, *998*, 2−8.

(12) Clark, T.; Hennemann, M.; Murray, J. S.; Politzer, P. Halogen Bonding: The σ-Hole. *J. Mol. Model.* **2007**, *13*, 291−296.

(13) Politzer, P.; Lane, P.; Concha, M.; Ma, Y.; Murray, J. σ-Hole Bonding: Molecules Containing Group VI Atoms. *J. Mol. Model.* **2007**, *13*, 305−311.

(14) Metrangolo, P.; Murray, J. S.; Pilati, T.; Politzer, P.; Resnati, G.; Terraneo, G. Fluorine-Centered Halogen Bonding: A Factor in Recognition Phenomena and Reactivity. *Cryst. Growth Des.* **2011**, *11*, 4238−4246.

(15) Riley, K. E.; Hobza, P. Investigations into the Nature of Halogen Bonding Including Symmetry Adapted Perturbation Theory Analyses. *J. Chem. Theory Comput.* **2008**, *4*, 232−242.

(16) Boden, N.; Davis, P. P.; Stam, C. H.; Wesselink, G. A. Solid Hexafluorobenzene 1. Crystal-Structure at 120 K. *Mol. Phys.* **1973**, *25*, 81−86.

(17) Reddy, C. M.; Kirchner, M. T.; Gundakaram, R. C.; Padmanabhan, K. A.; Desiraju, G. R. Isostructurality, Polymorphism and Mechanical Properties of Some Hexahalogenated Benzenes: The Nature of Halogen···Halogen Interactions. *Chem.—Eur. J.* **2006**, *12*, 2222−2234.

(18) Budzianowski, A.; Katrusiak, A. Pressure-Frozen Benzene I Revised. *Acta Crystallogr., Sect. B* **2006**, *62*, 94−101.

(19) *Crystallography Open Database*. http://www.crystallography.net (2013).

(20) *JMOL: an Open-Source Java Viewer for Chemical Structures in 3D*. http://www.jmol.org/ (2013).

(21) Grimme, S.; Antony, J.; Ehrlich, S.; Krieg, H. A Consistent and Accurate Ab Initio Parametrization of Density Functional Dispersion Correction (DFT-D) for the 94 Elements H−Pu. *J. Chem. Phys.* **2010**, *132*, 154104−154120.

(22) Jeziorski, B.; Moszynski, R.; Szalewicz, K. Perturbation-Theory Approach to Intermolecular Potential-Energy Surfaces of van-Der-Waals Complexes. *Chem. Rev.* **1994**, *94*, 1887−1930.

(23) Williams, H. L.; Chabalowski, C. F. Using Kohn−Sham Orbitals in Symmetry-Adapted Perturbation Theory to Investigate Intermolecular Interactions. *J. Phys. Chem. A* **2001**, *105*, 646−659.

(24) Haselmann, A.; Jansen, G.; Schütz, M. Density-Functional Theory-Symmetry-Adapted Intermolecular Perturbation Theory with Density Fitting: A New Efficient Method to Study Intermolecular Interaction Energies. *J. Chem. Phys.* **2005**, *122*, 014103−014119.

(25) Frisch, M. J.; Trucks, G. W.; Schlegel, H. B.; Scuseria, G. E.; Robb, M. A.; Cheeseman, J. R.; Scalmani, G.; Barone, V.; Mennucci, B.; Petersson, G. A.; et al. *Gaussian 09*, revision A.1; Gaussian, Inc.: Wallingford, CT, 2009.

(26) Werner, H.-J.; Knowles, P. J.; Manby, F. R.; Schuetz, M.; Celani, P.; Knizia, G.; Korona, T.; Lindh, R.; Mitrushenkov, A.; Rauhut, G.; et al. *MOLPRO*, version 2010.1, a package of ab initio programs; MOLPRO, 2010.

Interactions of Boranes and Carboranes with Aromatic Systems: CCSD(T) Complete Basis Set Calculations and DFT-SAPT Analysis of Energy Components†

Róbert Sedlák,‡ Jindřich Fanfrlík,‡ Drahomír Hnyk,§ Pavel Hobza,*,‡,∥ and Martin Lepšík*,‡

Center for Biomolecules and Complex Systems and Institute of Organic Chemistry and Biochemistry, 16610, Prague 6, Institute of Inorganic Chemistry, 250 68, Rez near Prague, Academy of Sciences of the Czech Republic, and Department of Physical Chemistry, Palacky University, 771 46, Olomouc, Czech Republic

Received: May 14, 2010; Revised Manuscript Received: August 23, 2010

The noncovalent interactions of heteroboranes with aromatic systems have only recently been acknowledged as a source of stabilization in supramolecular complexes. The physical basis of these interactions has been studied in several model complexes using advanced computational methods. The highly accurate CCSD(T)/complete basis set (CBS) value of the interaction energy for the model diborane···benzene complex in a stacking geometry exhibiting a $B_2H\cdots\pi$ hydrogen bond was calculated to be -4.0 kcal·mol^{-1}. The DFT-SAPT/CBS approach, which is shown to reproduce the CCSD(T)/CBS data reliably asserted that the major stabilizing component was dispersion, followed by electrostatics. Furthermore, the effect of the benzene heteroatom- and exosubstitutions was studied and found to be small. Next, when aromatic molecules were changed to cyclic aliphatic ones, van der Waals complexes stabilized by the dispersion term only were formed. As the last step, interactions of two larger icosahedral borane cages with benzene were explored. The complex of the monoanionic $CB_{11}H_{12}^-$ exhibited two minima: the first stacked above the plane of the benzene ring with a $C-H\cdots\pi$ hydrogen bond and the second planar, in which the carborane cage bound to benzene via five $B-H\cdots H-C$ dihydrogen bonds. The DFT-SAPT/CBS calculations revealed that both of these binding motifs were stabilized by dispersion followed by electrostatic terms, with the planar complex being 1.4 kcal·mol^{-1} more stable than the stacked one. The dianionic $B_{12}H_{12}^{2-}$ interacted with benzene only in the planar geometry, similarly as smaller anions do. The large stabilization energy of 11.0 kcal·mol^{-1} was composed of dominant attractive dispersion and slightly smaller electrostatic and induction terms. In summary, the borane/carborane···aromatic interaction is varied both in the complex geometries and in the stabilizing energy components. The detailed insight derived from high-level quantum chemical computations can help us understand such important processes as host−guest complexation or carborane···biomolecule interactions.

Introduction

Heteroboranes (substituted boron hydrides) can form two types of noncovalent interactions. The first are the thoroughly studied dihydrogen bonds (DHB) of the $B-H\cdots H-X$ type,[1,2] which underlie their binding to biomolecules[3] or stabilize noncovalent complexes of substituted boranes in crystals.[4−8] The second type of interaction is stacking, that is, boranes and carboranes are located above aromatic rings while pointing their positively charged hydrogen to the center of the ring, thus forming a $B-H\cdots\pi$/$C-H\cdots\pi$ type of interaction. Such a structural motif has been observed in a few dicarba-borane nanostructures[9,10] and in a recent crystal structure of the *n*-$B_{18}H_{22}$···benzene complex.[11]

This "stacking" arrangement was subsequently studied computationally in a model diborane···benzene complex (Figure 1A).[12−14] The authors asserted that this $B_2H\cdots\pi$ weak hydrogen bond was of a dispersive nature and evaluated the stabilization energy using different optimization protocols at the CCSD(T) level at 4.3 kcal·mol^{-1} (ref 12) or 2.45 kcal·mol^{-1} (ref 13). Furthermore, a study employing a faster DFT approach (the M05−2X functional with the 6-311++G** basis set) calculated the stabilization energy of the diborane···benzene complex as 3.43 kcal·mol^{-1} (ref 14). This span in the energy values made us revisit this model system. The CCSD(T) method is known to provide accurate stabilization energies, but it is necessary to combine it with an extended basis set or, preferentially, to extrapolate these calculations to the complete basis set (CBS) limit.[15,16]

The CCSD(T) procedure yields accurate total interaction energies but does not provide insight into the nature of stabilization. The symmetry-adapted perturbation theory (SAPT)[17] calculations, on the other hand, yield single-energy components, which are physically clearly defined and thus provide information on the interplay of the various terms. Moreover, the use of an extended basis set brings the SAPT interaction energies into a very close agreement with those from CCSD(T).

An analysis of the interaction energy components was carried out in both previous studies to provide insight into the relative importance of various energy components. Li et al.[12] used a simple decomposition scheme based on a comparison of the CCSD(T) and Hartree−Fock (HF) energies and minima, whereas Tian et al.[13] employed the HF-based symmetry-adapted perturbation theory (SAPT).[17] Both approaches showed a major contribution of dispersion energy (86%[12] or 170%[13] of the total interaction) and differed in the magnitude of other terms as well

† Part of the "Klaus Müller-Dethlefs Festschrift".

* To whom correspondence should be addressed. E-mail: pavel.hobza@uochb.cas.cz, lepsik@uochb.cas.cz.

‡ Institute of Organic Chemistry and Biochemistry and Center for Biomolecules and Complex Systems.

§ Institute of Inorganic Chemistry.

∥ Palacky University.

10.1021/jp104411x
Published on Web 09/10/2010

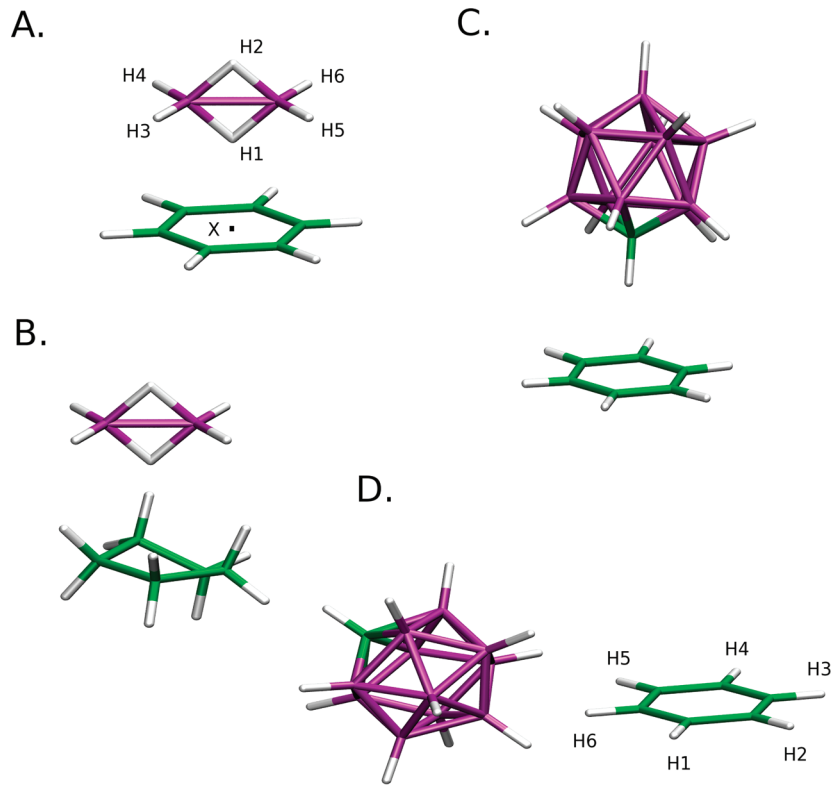

Figure 1. The optimized structures (minima) of the model complexes: (A) $C_6H_6\cdots B_2H_6$, (B) $C_5H_{10}\cdots B_2H_6$ (C) stacked $C_6H_6\cdots CB_{11}H_{12}^-$, and (D) planar $C_6H_6\cdots CB_{11}H_{12}^-$. $B_{12}H_{12}^{2-}$ interacts with benzene in a very similar geometry as in 1D (cf. Figure 2B).

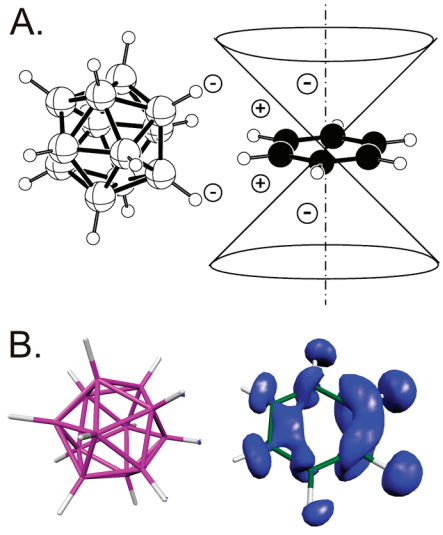

Figure 2. The $B_{12}H_{12}^{2-}\cdots$benzene interactions. (A) The electrostatic interactions between the monopole represented by the doubly negative charge of $B_{12}H_{12}^{2-}$ and the quadrupole of benzene. (B) The difference electron density in the $B_{12}H_{12}^{2-}\cdots$benzene complex describes the induction contribution to the interaction. The Figure was created using MOLEKEL, v. 4.3.[53]

(for example, the contribution of electrostatics was assessed at ~0 (ref 12) or 2.68 (ref 13) kcal·mol^{-1}). This span of the values available in the literature motivated us to determine a correct partitioning of the physically well-defined interaction-energy components using the novel density functional theory/symmetry-adapted perturbation theory (DFT-SAPT) method.[17,18]

The first aim of this work is an in-depth exploration of the diborane$\cdots$benzene interaction. The second is to investigate the effect of modifying either of the interacting partners. A similar task, which was however aimed at investigating the substituted diborane$\cdots$borazine complexes, has been carried out recently.[14] Here, we modified (i) benzene by heteroatom- and exosubstitutions or replaced it by cyclic aliphatic systems, and (ii) diborane, which was replaced by larger cage *closo*-borane and carba-*closo*-borane anions.

Cage carboranes have not only been found to form host−guest complexes stabilized by a C−H$\cdots\pi$ interaction[9,10] but also have been increasingly used as hydrophobic pharmacophores in molecular medicine.[19] As such, their ability to form noncovalent interactions with aromatic fragments of amino acids and nucleic acids has been studied here using benzene and its modifications as the model. The analysis of possible binding motifs and the DFT-SAPT interaction energy components broadens our understanding of the borane$\cdots$aromatic interaction.

Methods and Calculations

Systems Studied. Noncovalent complexes of boranes or carboranes with aromatic and cyclic aliphatic systems have been studied. The starting model system was the diborane$\cdots$benzene complex (Figure 1A). The benzene moiety was replaced by both heteroatom- and exosubstituted aromatic compounds as well as cyclic aliphatic ones. Most of the molecules represent amino-acid side chains (phenol for tyrosine, imidazole for histidine, pyrrolidine for proline) or selected nucleic acid bases (cytosine). Furthermore, we have explored the effect of aromaticity/planarity by utilizing pairs of aromatic/planar and cyclic aliphatic systems: benzene−cyclohexane, 1,3-cyclopentadiene−cyclopentane, pyrrole−pyrrolidine. The diborane$\cdots$cyclopentane complex is shown in Figure 1B.

In other complexes with benzene, diborane was replaced by two icosahedral cages: the monoanionic $CB_{11}H_{12}^-$ carborane (C_{5v} symmetry) (Figure 1C, D) and the dianionic $B_{12}H_{12}^{2-}$ borane (I_h symmetry). Note that the $B_{12}H_{12}^{2-}$ dianion exhibits zero dipole moment because of its symmetry element. The

dipole moment of the monocarbaborane coincides with the space diagonal of this deformed icosahedron.

Geometries. The initial structures of the investigated noncovalent complexes were built in a "stacked" motif[20,21] (i.e., borane above the face of the ring) similarly as the diborane···benzene complex in ref 12. In the monocarbaborane cage complex, the C−H bond was positioned so as to point toward or away from the centroid of the benzene ring.

Two important geometrical characteristics of the stacked structures are the distances between the centroid of the aromatic ring (X) and the hydrogen atom (H) pointing toward it or the non-hydrogen atom (Y) bound to it. We thus characterize the geometries of the complexes with the XH or XY distances (d_{XH}, d_{XY}).

The models of the anion···benzene interactions were investigated in a series of monoanions (F^-, Cl^-, and Br^-) and dianion SO_4^{2-}. All the complexes were built in a "planar" arrangement, the halide···benzene geometries were taken from ref 22.

Computational Details. Geometry optimizations of the complexes were carried out at the MP2(FC)/cc-pVTZ level of theory, since this level has been proven to provide reliable geometries.[23] Frozen core (FC) approximation was systematically used. Vibrational frequencies were calculated numerically at the above-mentioned level to confirm that the complexes represented true minima on the respective potential energy hypersurfaces.

The stabilization energies of the investigated complexes were determined at different levels of theory: MP2/aug-cc-pVD(T)Z, MP2/complete basis set (CBS),[16] MP2.5,[24] DFT-SAPT/aug-cc-pVDZ,[17,18] DFT-SAPT/CBS, and CCSD(T)/CBS.[15] The MP2 interaction energies were calculated with a medium-size aug-cc-pVDZ basis set, as the overestimation of stabilization energies caused by MP2 and underestimation owing to this basis set should approximately compensate for one another and give quite accurate results.[25] The MP2/aug-cc-pVDZ interaction energies were corrected for BSSE.[26]

Density functional theory (DFT)/symmetry-adapted perturbation theory (SAPT) (DFT-SAPT)[17,18] is a method for calculating the interaction energy in noncovalent complexes. This method combines the DFT approach[27,28] for intramolecular treatment with the SAPT approach[17] for the description of intermolecular interactions. The DFT part was treated using the PBE0AC exchange-correlation functional with density fitting and the aug-cc-pVDZ basis set.[18e] This combination of functional and basis set has been shown to provide a reasonably good description of electrostatics and induction, with the dispersion component being underestimated by approximately 10−20%.[18b] The use of a larger basis set for covering the dispersion term more appropriately is computationally too demanding for larger systems, so we performed this type of calculation with aug-cc-pVTZ only for the smallest model diborane···benzene complex. This more precise calculation enabled an extrapolation toward the CBS limit (DFT-SAPT/CBS) for all the systems to be carried out.

The total interaction energy in the DFT-SAPT[17,18] is given as the sum of the first- (E_1) and second-order (E_2) perturbation energy terms and a δHF energy terms. The former two terms represent: electrostatic (E_1^{Pol}), induction (E_2^{Ind}) and dispersion (E_2^{D}) together with the exchange-repulsion terms (E_1^{Ex}, $E_2^{Ex\text{-}Ind}$, $E_2^{Ex\text{-}D}$). The exchange-induction and exchange-dispersion terms are merged into the respective induction and dispersion terms. The δHF term represents higher than second-order terms covered by the Hartree−Fock approach (eq 1). The contributions of individual terms toward the interaction energy are calculated as a percentage of the term in question from the total DFT-SAPT/CBS stabilization energy.

$$E^{int} = E_1^{Pol} + E_1^{Ex} + E_2^{Ind} + E_2^{Ex\text{-}Ind} + E_2^{D} + E_2^{Ex\text{-}D} + \delta HF \quad (1)$$

The greatest improvement of the DFT-SAPT method over the original SAPT is the acceleration of the calculations by 1 order of magnitude.[17,18] The intramolecular treatment is conducted by the use of DFT and therefore suffers from inaccurate energies of the virtual orbitals. This drawback is corrected before the actual SAPT treatment by a gradient-controlled shift procedure, which uses the difference between the exact vertical ionization potential (IP) and the energy of the highest occupied molecular orbital (HOMO).[18e] In this work, the PBE0AC/TZVP and PBE0/aug-cc-pVDZ calculations were carried out to obtain the IP respective HOMO values.

The extrapolation to CBS in the DFT-SAPT approach (DFT-SAPT/CBS) was performed as follows. From the DFT-SAPT/aug-cc-pVDZ and DFT-SAPT/aug-cc-pVTZ results for the model diborane···benzene complex, the Helgaker[29] two-point extrapolation of the dispersion energy ($E_2^{D} + E_2^{Ex\text{-}D}$ terms) was made. Subsequently, this extrapolated dispersion energy ($E_2^{D/CBS}$) was combined with all the other terms from the DFT-SAPT/aug-cc-pVDZ calculation.

The benchmark calculations were conducted at the CCSD(T)/CBS level using the extrapolation scheme developed in our laboratory[15] (eq 2).

$$\Delta E_{CBS}^{CCSD(T)} = \Delta E_{CBS}^{MP2} + (\Delta E^{CCSD(T)} - \Delta E^{MP2})|_{6\text{-}31+G^*} \quad (2)$$

This scheme takes into account the fact that the interaction energies calculated by the MP2 as well as CCSD(T) methods exhibit the same basis-set dependence.[15] The MP2/CBS value was determined via the extrapolation by Kim et al.[16] This extrapolation scheme is based on the idea that both the basis set superposition error (BSSE)-corrected and -uncorrected interaction energies have the same value for an infinite basis set. The extrapolation in this work was done using energies obtained from MP2/aug-cc-pVDZ and MP2/aug-cc-pVTZ calculations.

The NBO analyses[30] were carried out at the MP2/cc-pVTZ level of theory. The ^{1}H NMR chemical shifts were calculated at the optimized geometry employing the gauge-including atomic orbitals (GIAO)[31] method at the B3LYP level of theory with a Huzinaga's TZP basis set.[32,33] Such an approach has proven useful in the structural chemistry of boranes and carboranes as reviewed in ref 34 and references therein. Electron densities were calculated at the B3LYP/6-31G* level. All of the calculations were carried out using the Turbomole v. 5.8,[35] Gaussian03,[36] and Molpro06[37] packages.

Results

1. Diborane···Benzene Complex. Recent quantum-chemical calculations of the diborane···benzene complex[12,13] have revealed a novel type of a weak hydrogen-bond interaction (denoted here as $B_2H\cdots\pi$). It is formed between the π-electron density of benzene and the bridging hydrogen (H1) of diborane (Figure 1A). The H1 atom bears a slightly positive charge, unlike the terminal hydrogen atoms H3−H6, which are slightly negatively charged.[3] The two subsystems were found in a

TABLE 1: Total Interaction Energy (kcal·mol^{-1}) of the Diborane···Benzene Complex Obtained with Different Types of Calculations

method	E_{int} (kcal·mol^{-1})
CCSD(T)/CBS	−4.0
DFT-SAPT/CBS	−3.6
DFT-SAPT	−2.8
MP2/CBS	−4.9
MP2.5	−4.3
CCSD(T)[a]	−4.3
CCSD(T)[b]	−2.5
MP2[b]	−3.3
DFT[c]	−3.4

[a] Reference 12. [b] Reference 13. [c] Reference 14.

"stacking" arrangement (Figure 1A) with a characteristic H1···X distance (where X is the centroid of the benzene ring), which varied depending on the method used: 2.53 Å for CCSD(T)//DFT;[12] 2.41 or 2.59 Å for BSSE-uncorrected or -corrected MP2, respectively;[13] or 2.33 Å for BSSE-uncorrected MP2/cc-pVTZ (this work). The interaction energy has been evaluated at −4.3 kcal·mol^{-1} using the CCSD(T)//DFT[12] approach, −3.27 and −2.45 kcal·mol^{-1} using MP2 and CCSD(T) methods, respectively,[13] or −3.43 kcal·mol^{-1} using DFT (M05−2X/6-311++G**).[14] This span in stabilization energies led us to an effort to determine the most accurate benchmark interaction energies[15] for this model.

The two previous studies have also asserted the major role of dispersion in stabilizing the diborane···benzene complex.[12,13] Using the difference between the Hartree−Fock (HF) and CCSD(T) values, Li et al. estimated the dispersion contribution (which is actually the correlation interaction energy) at 5.64 kcal·mol^{-1} (ref 12). By using a more robust method of the HF-based symmetry adapted perturbation theory (SAPT),[17] Tian et al. estimated the dispersion stabilization at 4.12 kcal·mol^{-1} (ref 13). The dispersion energy contribution calculated in this manner corresponds to the uncoupled dispersion energy, which is, however, overestimated.[17] In this study, we have used the novel DFT-SAPT approach[17,18] to determine the physically well-defined components of the interaction energy in the diborane···benzene complex.

1.1. Benchmark Value of Interaction Energy. A comparison of the values in the literature and those presented here of the interaction energy between diborane and benzene using various computational methods is shown in Table 1. The most accurate benchmark CCSD(T)/CBS value is −4.0 kcal·mol^{-1}. The DFT-SAPT approach underestimates the interaction by 1.2 kcal·mol^{-1} using the medium-sized aug-cc-pVDZ basis set. Using the extrapolation scheme to pass from the aug-cc-pVDZ basis set to the CBS limit, the dispersion term increases by 12%. This increment is added to the E_2^D term (designated as $E_2^{D/CBS}$) for all the other complexes.

The DFT-SAPT/CBS approach yields a stabilization of 3.6 kcal·mol^{-1}, which is in close agreement with the benchmark value. This result shows (in accord with our earlier findings; see e.g., ref.[38]) that the crucial role is played by the dispersion term (see also below).

Table 1 also lists the results when using the MP2, MP2.5, and CCSD(T) methods. As anticipated, the CBS extrapolation at the MP2 level overestimates the stabilization by 0.9 kcal·mol^{-1}. When passing to the recently introduced MP2.5 method,[24] the overestimation of MP2 is reduced and the agreement improves to a 0.3 kcal·mol^{-1} difference from the benchmark energy. This is a remarkable result given the feasibility of such a calculation in comparison with the CCSD(T)/CBS approach. Thus, the MP2.5 method can be recommended for future calculations of interaction energies in other borane/carborane complexes.

TABLE 2: Comparison of the DFT-SAPT and DFT-SAPT/CBS Interaction Energies (kcal·mol^{-1}) with the Benchmark CCSD(T)/CBS Data for the $C_6H_6\cdots B_2H_6$, $C_6H_6\cdots B_{12}H_{12}^{2-}$, and $C_6H_6\cdots CB_{11}H_{12}^-$ Complexes

systems	CCSD(T)/CBS	DFT-SAPT/CBS	DFT-SAPT
$C_6H_6\cdots B_2H_6$	−4.0	−3.6	−2.8
$C_6H_6\cdots B_{12}H_{12}^{2-}$	−11.0	−10.1	−9.2
$C_6H_6\cdots CB_{11}H_{12}^-$ [a]	−5.1	−5.3	−4.6

[a] Planar arrangement.

The last four rows in Table 1 list the values of the diborane···benzene interaction energies published recently. The CCSD(T)/6-31+G** single-point energies calculated at geometries obtained by a constrained DFT optimization result in a stabilization of 4.3 kcal·mol^{-1},[12] which is close to the benchmark value. In contrast, the CCSD(T) and MP2 single-point energies calculated at the BSSE-corrected MP2-optimized geometries[13] as well as the DFT (M05−2X/6-311++G**) calculation[14] underestimate the interaction.

In the preceding paragraphs, we have observed that the DFT-SAPT/CBS method is capable of providing reliable values of stabilization energies for the diborane···benzene complex. To check the scope of this finding, we have carried out a comparison of its performance for two larger complexes: $B_{12}H_{12}^{2-}$···benzene and planar $CB_{11}H_{12}^-$···benzene. Table 2 shows that the results of DFT-SAPT/CBS calculations reproduce the benchmark CCSD(T)/CBS values to within 10%. The DFT-SAPT/aug-cc-pVDZ method underestimates the benchmark data by 10−30%. Hence, we can see that the correction of dispersion for the CBS limit in the DFT-SAPT approach is crucial for obtaining reliable results for the stabilization energy.

1.2. Interaction Energy Components. We have seen that the DFT-SAPT/CBS calculation provided reliable stabilization energies for diborane and cage (car)borane complexes with benzene. The main strength of this approach is, however, the partitioning of the interaction energy into the physically well-defined components, electrostatic (E_1^{Pol}), induction (E_2^{Ind}), dispersion (E_2^D/CBS), exchange-repulsion (E_1^{Ex}), exchange-induction ($E_2^{Ex\text{-}Ind}$), exchange-dispersion ($E_2^{Ex\text{-}D}$), and the δHF terms.

The diborane···benzene complex is stabilized mainly by dispersion with a large contribution of 7.6 kcal·mol^{-1}. The second important stabilizing term is electrostatic, which yields 4.5 kcal·mol^{-1}. Another major term is exchange-repulsion, which opposes the interaction by 10.2 kcal·mol^{-1}. The last two terms are small and stabilizing; induction contributes 0.5 kcal·mol^{-1}, and δHF is 1.2 kcal·mol^{-1}. These rather small values of the induction and δHF energy terms indicate, among other things, that the charge transfer between the subsystems should be small. This supposition was independently confirmed by a natural bond orbital (NBO) analysis, which showed a small charge transfer of 0.016 *e* from the electron-rich benzene to the electron-poor diborane.

Having explored the diborane···benzene interaction, we can now modify either of the interacting partners to study the effects of such changes on the strength and nature of the interaction. We start by modifying the benzene molecule followed by the replacement of the diborane moiety. The optimized structures (at the MP2/aug-cc-pVTZ level) of the complexes are depicted in Figure 1B−D. All the energy calculations will be presented

TABLE 3: Comparison of the DFT-SAPT/CBS Interaction Energies (kcal·mol^{-1}) for the $B_2H_6\cdots C_6H_6$, $B_2H_6\cdots B_3N_3H_6$, $B_2H_6\cdots C_4N_2H_4$, $B_2H_6\cdots C_6H_5OH$, $B_2H_6\cdots C_4N_2H_3ONH_2$, and $B_2H_6\cdots C_3N_2H_4$ Complexes

systems	E_1^{Pol}	E_1^{Ex}	E_2^{Ind}	$E_2^{D/CBS}$	δHF	DFT-SAPT/CBS
$B_2H_6\cdots C_6H_6$	−4.5	10.2	−0.5	−7.6	−1.2	−3.6
$B_2H_6\cdots B_3N_3H_6$	−2.3	5.6	−0.3	−5.3	−0.4	−2.7
$B_2H_6\cdots C_4N_2H_4$	−1.9	6.0	−0.3	−5.7	−0.6	−2.5
$B_2H_6\cdots C_6H_5OH$	−4.8	11.3	−0.6	−8.3	−1.4	−3.7
$B_2H_6\cdots C_4N_2H_3ONH_2$	−3.3	9.6	−0.7	−7.7	−0.9	−2.9
$B_2H_6\cdots C_3N_2H_4$	−4.9	10.6	−0.7	−7.2	−1.4	−3.6

TABLE 4: Comparison of the DFT-SAPT/CBS Interaction Energies (kcal·mol^{-1}) for the $B_2H_6\cdots C_6H_6$, $B_2H_6\cdots C_6H_{12}$, $B_2H_6\cdots C_5H_6$, $B_2H_6\cdots C_5H_{10}$, $B_2H_6\cdots C_4NH_5$, and $B_2H_6\cdots C_4NH_9$ Complexes

systems	E_1^{Pol}	E_1^{Ex}	E_2^{Ind}	$E_2^{D/CBS}$	δHF	DFT-SAPT/CBS
$B_2H_6\cdots C_6H_6$[a]	−4.5	10.2	−0.5	−7.6	−1.2	−3.6
$B_2H_6\cdots C_6H_{12}$[b]	−1.0	3.6	−0.2	−4.0	−0.3	−1.9
$B_2H_6\cdots C_5H_6$[a]	−4.5	9.6	−0.6	−7.1	−1.4	−3.9
$B_2H_6\cdots C_5H_{10}$[b]	−1.4	4.7	−0.2	−5.0	−0.3	−2.3
$B_2H_6\cdots C_4NH_5$[a]	−5.6	11.1	−0.8	−7.6	−1.7	−4.5
$B_2H_6\cdots C_4NH_9$[b]	−6.0	10.1	−0.8	−6.2	−1.0	−3.9

[a] Aromatic/planar. [b] Cyclic aliphatic.

at the DFT-SAPT/CBS level, which was shown to be in close agreement with the benchmark CCSD(T)/CBS results.

2. Complexes of Diborane with Aromatic Systems. Our attention now turns to a study of the effect of replacing benzene with other aromatic interaction partners of diborane. We chose several systems with either a heteroatom and/or exocyclic substitution that at the same time cover the basic building blocks of biomolecules (see Methods). The diborane···borazine complex, which has recently been investigated computationally,[14] is included for comparison.

Table 3 lists the DFT-SAPT/CBS interaction energies for the benzene, borazine, pyrimidine, phenole, cytosine, and pyrrole complexes with diborane. The total values of the stabilization energies range from 2.5 to 3.7 kcal·mol^{-1}. It should be noted that the d_{XH} distances range from 2.31 Å for phenol and pyrrole to 2.46 Å for pyrimidine (the d_{XH} and d_{XY} distances for all the complexes are shown in Table S1 in the Supporting Information). The diborane complexes with benzene, phenole, and pyrrole (which have smaller intersystem separation) exhibit stronger binding (−3.6 to −3.7 kcal·mol^{-1}), whereas borazine, pyrimidine, and cytosine interact less strongly (−2.5 to −2.9 kcal·mol^{-1}). Like in the case of benzene, the main stabilization energy comes from the dispersion term followed by electrostatics. The drop in these two terms is mostly responsible for the differences in the total stabilization. The major term opposing the interaction comes from the E_1^{Ex} term. Given the slight variations in the size of the systems, the effect of a heteroatom or exocyclic substitution of the aromatic system interacting with diborane is rather small.

3. Complexes of Diborane with Cyclic Aliphatic Systems. To investigate the effect of aromaticity/planarity of the subsystems treated in the previous section on the interaction with diborane, we have systematically examined their cyclic aliphatic counterparts, yielding the following pairs: benzene—cyclohexane, 1,3-cyclopentadiene—cyclopentane, and pyrrole—pyrrolidine. The DFT-SAPT/CBS interaction energy components for these complexes are shown in Table 4.

Overall, the leading stabilizing term is dispersion followed by electrostatics, whereas the major term opposing binding is E_1^{Ex}. A comparison of the binding of the aromatic compounds on the one hand and the aliphatic ones on the other reveals that the stabilization energies as well as all of their energy components of the former group are systematically larger than the latter (Table 4). The main difference between these two groups (with the exception of the last, nitrogen-containing molecular pair) is the large decrease in the E_1^{Pol} term for the aliphatic compounds. Thus, the interaction with the aromatic compounds is stabilized by both electrostatics and dispersion, whereas the interaction with the aliphatic molecules is governed mainly by dispersion.

The energy differences are also connected with a different type of binding. Although the aromatic compounds interact with diborane in a stacking arrangement via their π-electron density involving a weak hydrogen bond ($B_2H\cdots\pi$ interaction)(Figure 1A), their aliphatic counterparts bind to diborane via a weak van der Waals interaction (Figure 1B). The former interaction type is characterized by the position of the B−H1−B bridge over the center of the aromatic ring with the X−H1 distances ranging from 2.31 Å for phenol and pyrrole to 2.46 Å for pyrimidine (cf., 2.59 Å for benzene optimized at the BSSE-corrected MP2 level[13]). The latter van der Waals interaction is characterized by maximizing the number of H···H contacts between the subsystems where the H···H distances are equal or slightly larger than the sum of their atomic van der Waals radii (2.4 Å for hydrogens plus a cutoff of 0.3 Å).[39] Indeed, in the complexes studied here, the H···H distances range from 2.37 to 2.60 Å. Overall, the above-mentioned type of van der Waals interaction contacts is characterized by a large dispersion contribution to the total stability.[21,40,41]

In the case of pyrrolidine, we additionally observe a short distance of 2.46 Å between the bridging hydrogen (H1) of diborane and the nitrogen atom of pyrrolidine. The geometry suggests an electrostatic interaction between the slightly positively charged H1 atom[3] with the nitrogen lone-pair. The actual increase of the E_1^{Pol} term (in its absolute value) in comparison with pyrrole (Table 4) supports this idea.

In summary, we find that the aromatic compounds investigated in this study interact up to twice as strongly with diborane than their aliphatic counterparts. From the geometries and DFT-SAPT results, it is evident that there are two types of interactions of diborane stabilized by a different interplay of energy terms: (i) "stacking" interaction with aromatic compounds via a weak $B_2H\cdots\pi$ hydrogen bond, characterized by stabilizing dispersion, and electrostatic terms; and (ii) van der Waals complexes with aliphatic compounds, where dispersion is the major stabilizing term.

4. Complexes of Cage Borane and Carborane Anions with Benzene. ***4.1. Structures of the Complexes.*** To further investigate the borane···aromatic type of interaction, we have exchanged diborane for the larger carba-*closo*-borane $CB_{11}H_{12}^-$ and *closo*-dodecaborane $B_{12}H_{12}^{2-}$ cages. It should be stressed here that both these cages are anionic, which influences their binding motifs. The geometries of their optimized complexes with benzene are shown in Figure 1C, D and are also supplied as Supporting Information. The $CB_{11}H_{12}^-\cdots$benzene complex exhibits two minima at the MP2/cc-pVTZ level: (i) a stacking arrangement with a C−H···π hydrogen bond (the XH distance is 2.26 Å) (Figure 1C) and (ii) a planar binding motif with five B−H···H−C dihydrogen bonds spanning an interval of 2.50−2.61 Å (Figure 1D). (The latter structure was obtained thanks to a referee's advice to search for other than the stacked minimum. We thus started a new geometry optimization from the modified $B_{12}H_{12}^{2-}$ planar complex in which the CH group

TABLE 5: Comparison of the DFT-SAPT/CBS Interaction Energies (kcal·mol^{-1}) for the $C_6H_6\cdots B_2H_6$, $C_6H_6\cdots CB_{11}H_{12}^-$ (In Both, Stacked and Planar Binding Motifs) and $C_6H_6\cdots B_{12}H_{12}^{2-}$ Complexes

systems	E_1^{Pol}	E_1^{Ex}	E_2^{Ind}	$E_2^{D/CBS}$	δHF	DFT-SAPT/CBS
$C_6H_6\cdots B_2H_6$[a]	−4.5	10.2	−0.5	−7.6	−1.2	−3.6
$C_6H_6\cdots CB_{11}H_{12}^-$ [a]	−3.2	10.5	−0.9	−9.7	−0.6	−3.9
$C_6H_6\cdots CB_{11}H_{12}^-$ [b]	−3.3	6.4	−1.9	−6.0	−0.6	−5.3
$C_6H_6\cdots B_{12}H_{12}^{2-}$ [b]	−6.5	11.9	−6.2	−7.9	−1.4	−10.1

[a] Stacked motif. [b] Planar motif.

was introduced at the part of the cage which pointed away from benzene.) The dianionic borane $B_{12}H_{12}^{2-}$ has shifted during the optimization process from a starting stacked to a planar structure with five C−H···H−B dihydrogen bonds (analogous to the planar geometry of the carborane···benzene complex) ranging from 2.28 to 2.45 Å.

4.2. Interaction Energy and its Components. Table 5 shows the components of the total stabilization energy of the benzene complexes with the cage carborane $CB_{11}H_{12}^-$ (in both, the stacked and planar geometries), the borane $B_{12}H_{12}^{2-}$ and diborane for comparison.

Larger stabilization energies are expected for the benzene complexes with *closo*-(car)boranes as compared to the diborane owing to the size of the cages. The main source of stabilization in all the complexes is dispersion energy, followed by electrostatics. These terms have been acknowledged to stabilize C−H···π hydrogen bonding,[42,43] dihydrogen bonding,[2,3,8,44,45] and anion···arene interactions (reviewed in ref 46) The exchange repulsion term opposes binding, the least in the planar $CB_{11}H_{12}^-\cdots$benzene complex, due to its largest intersystem separation (center-of-mass···center-of-mass distance of 6.2 Å as compared to 6.1 and 4.8 Å for the $B_{12}H_{12}^{2-}$ and the stacked $CB_{11}H_{12}^-$ complexes, respectively. The induction term contributes a little to the total stabilization except for the $B_{12}H_{12}^{2-}$ complex in which it is responsible for a significant portion of the stabilization (61%). The role of induction in noncovalent complexes, especially of anion···benzene type, will be discussed in detail below. In all, carborane and borane cages adopt either stacking or planar binding modes upon interaction with benzene, and the complexes are stabilized by dispersion, electrostatics, and in one case also induction energy terms.

Discussion

Diborane···Benzene Interactions. For the model diborane···benzene complex in vacuum, we have calculated the benchmark CCSD(T)/CBS value of stabilization energy of 4.0 kcal·mol^{-1}. One of the previous studies was in close agreement (4.3 kcal·mol^{-1}), [12] whereas the other substantially underestimated the stabilization energy (2.45 kcal·mol^{-1}).[13] In another recent study, a faster DFT method (M05−2X/6-311++G**) yielded an interaction energy of 3.43 kcal·mol^{-1},[14] in fair agreement with the CCSD(T)/CBS value. The DFT-SAPT/CBS approach (this work) slightly underestimated the benchmark value (a stabilization energy of 3.6 kcal·mol^{-1}). With such close agreement, we are confident about the interaction-energy components obtained using this method. The previous finding that the major stabilizing force is dispersion has thus been confirmed.[12−14] Quantitatively, the relative importance of this term was underestimated in the first study, where it accounted only for 86% of the total stabilization energy.[12] In the last two works[13,14] as well as in our current study, the E_2D term was roughly twice as large as the total stabilization energy. Besides dispersion, the other stabilizing term according to the DFT-SAPT/CBS approach was electrostatic. Again, its relative importance was neglected in the former work (∼0 kcal·mol^{-1}),[12] whereas in the later studies (this work and in refs 13 and 14) its contribution has been calculated to be approximately 120% of the total stabilization. In summary, the presented DFT-SAPT/CBS calculations on the model diborane···benzene complex agree quantitatively with the highly accurate CCSD(T)/CBS benchmark interaction energies. The energy components show a major stabilization caused by dispersion, followed by electrostatics.

Cage Carborane···Benzene Stacking Interactions. A less stable minimum of the $CB_{11}H_{12}^-\cdots$benzene complex exhibits a stacking binding motif with a C−H···π hydrogen bond (Figure 1C) reminiscent of typical C−H···π interactions between aliphatic and aromatic hydrocarbons (see e.g., refs 42, 43, and 47). Although the cage is on the whole an anion, the charge is delocalized on its surface with a partial positive charge on the carbon-attached hydrogen of the carborane,[3] positioned so that it can interact with the π-electron density. The distance characterizing the complex geometry (d_{XY} = 3.3 Å) falls within the span of 3.2 Å for chloroform to 3.8 Å for methane for the hydrocarbon···benzene interaction.[43] Similarly, the total stabilization energy of 3.9 kcal·mol^{-1} for $CB_{11}H_{12}^-$ is in the range of 1.45 kcal·mol^{-1} for methane to 5.64 kcal·mol^{-1} for chloroform.

The comparison of the DFT-SAPT/CBS interaction energy components for hydrocarbons and the cage carborane showed some differences. The major driving force for complex formation is dispersion in all cases. For hydrocarbons, it accounts for 140−160% of the total stabilization,[43] whereas for $CB_{11}H_{12}^-$ it is 249%. The other stabilizing term is electrostatic, which gives 17−43% for hydrocarbons,[43] whereas it is as large as 82% for $CB_{11}H_{12}^-$. This observation underlies a stronger directionality of the C−H···π hydrogen bond of cage carboranes. In summary, we have computationally described a dispersion-driven stacking interaction of a C−H···π type with a different balance of the energy components, namely, with a larger stabilizing contribution due to the electrostatic term.

Cage Carborane/Borane···Benzene Planar Interactions. The more stable minimum of the $CB_{11}H_{12}^-\cdots$benzene complex as well as the only minimum found for the $B_{12}H_{12}^{2-}$ complex displays a "planar" binding motif with five B−H···H−C dihydrogen bonds. Such structures are analogous to small anion (e.g., halides, nitrate, perchlorate)···benzene planar complexes that have been thoroughly studied previously.[22,46,48] The partially negatively charged boron-bound hydrogens of the carborane/borane cages[3] (Figure 1D) present interaction partners for the C−H groups of benzene, similarly as the halides or oxygens of the nitrate, perchlorate or sulfate anions do. We note that the cage carborane offers those hydrogens for the interaction that are the most distant from the cage C−H group, that is, the most negatively charged (Figure 1D).[3] The calculated H···H distances in the carborane/borane···benzene complexes of 2.3−2.6 Å compare well with the X(O)···H distances in small anion complexes of 2.1−3.1 Å in which the larger atomic radius of X(O) must be taken into account.[22,46,48]

In terms of the DFT/SAPT interaction energy components, the dispersion and electrostatic terms constitute the main attraction terms in the planar carborane···benzene complex, whereas in the $B_{12}H_{12}^{2-}$ complex induction is just as important (c.f., Table 5). The dispersion term is the leading attractive component, which makes up 79−114% of the total stabilization in the carborane/borane···benzene complexes. This is due to

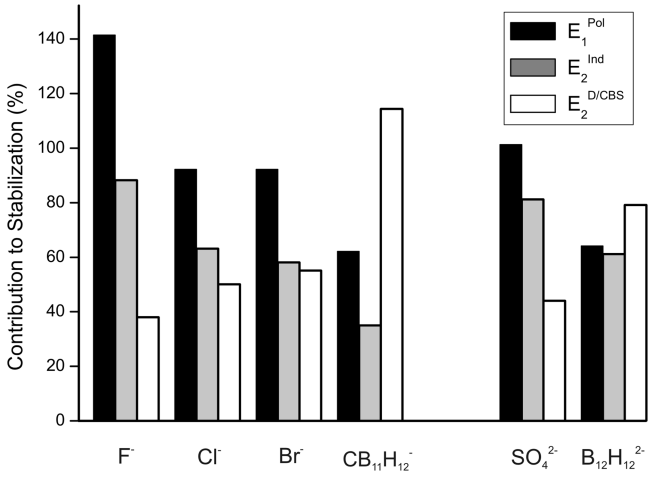

Figure 3. The percentages of the individual attractive components in the total stabilization energy in the anion···benzene interaction.

the high polarizability of both interaction partners and their close proximity. The attractive electrostatic term (62−64% of the total stabilization) is due to the interactions between the negative charge of the cages and the quadrupole of benzene (Figure 2A) and also due to five B−H···H−C dihydrogen bonds (Figure 1D). The strength of these interactions is enhanced in the $B_{12}H_{12}^{2-}$ complex by the electron density redistribution due to induction.

The induction interaction in the $B_{12}H_{12}^{2-}$···benzene complex (61% of the total stabilization) is exerted by the permanent monopole of $B_{12}H_{12}^{2-}$ on the polarizable benzene ring in the apt complex geometry. The electron density redistribution is apparent from the calculated ^{1}H NMR chemical shifts (the H5 and H6 atoms are deshielded the most, by 3 ppm) and also from the visualization of difference electron-density maps (Figure 2B).

Induction in Planar Anion···Benzene Complexes. Induction is not as universal source of stabilization in noncovalent complexes as electrostatics or dispersion, which drive, for example, the formation of hydrogen bonds or π-interactions, respectively.[21,40,41] The reliable computational description of induction requires the use of correlated ab initio methods, flexible basis sets, and methods to capture the polarizable nature of the interacting partners.[49] Two examples of an interaction type where induction has gradually been acknowledged to play an important role are cation-π[50−52] and anion···arene[46] binding motifs.

The contributions of the three major attractive terms (dispersion, electrostatics and induction) toward the stabilization of planar anion···benzene complexes are plotted for the $CB_{11}H_{12}^-$ and $B_{12}H_{12}^{2-}$ cages and compared with halides and sulfate (Figure 3). It can be seen that the percentages of the E_1^{Pol} and E_2^{Ind} terms decrease with the increasing size of the anions due to increasing intersystem separation and decreasing surface charge density, whereas the contribution of the $E_2^{D/CBS}$ term increases due to increasing polarizability. In the absolute values (Table S2 in the Supporting Information); however, the dispersion contribution decreases since this effect is overwhelmed by the increasing interatomic distances.

The δHF term is rather small (Table S2), consistent with the lack of charge transfer (e.g., 0.004e is transferred from $B_{12}H_{12}^{2-}$ to the benzene) in these types of complexes, acknowledged earlier.[46] The two exceptions are SO_4^{2-} and F^-···benzene complexes with short intersystem distances (S═O(X)···H−C of 1.93 and 1.64 Å, respectively).

Altogether, the $B_{12}H_{12}^{2-}$···benzene planar complex is stabilized by three major energy components, universal dispersion and electrostatics and moreover induction, the contributions of which are uniquely balanced ($E_2^{D/CBS}$ = 79%; E_1^{Pol} = 64%; E_2^{Ind} = 61%).

Conclusions

Our findings are summarized below:

(1) We have determined the benchmark interaction energy at the CCSD(T)/CBS level in the diborane···benzene complex to be −4.0 kcal·mol^{-1}.

(2) The DFT-SAPT/CBS approach yielded a stabilization energy for the diborane···benzene complex of 3.6 kcal·mol^{-1}, which is in close agreement with the benchmark energy. We can thus be confident about the further partitioning of the energy terms. The major stabilization in the diborane···benzene complex comes from dispersion (7.6 kcal·mol^{-1}), followed by electrostatics (4.5 kcal·mol^{-1}). Exchange repulsion opposes binding by 10.2 kcal·mol^{-1}. The induction and δHF terms are slightly favorable for the binding, but their small value indicates negligible roles of polarization and charge transfer.

(3) Diborane interactions with aromatic systems are virtually unaffected by either the heteroatom or exosubstitutions of the benzene ring.

(4) Replacing aromatic systems with cyclic aliphatic ones results in a change of the binding motif and a roughly 50% drop in the stabilization energy. Specifically, the stacking B_2H···π interaction is replaced by van der Waals contacts of the interacting hydrogen atoms. The source of stabilization comes in the former case from both dispersion and electrostatic terms, whereas the latter interactions are governed by dispersion only.

(5) Larger icosahedral cage carborane, monoanionic $CB_{11}H_{12}^-$, interacts with benzene employing two binding motifs: (i) The less stable minimum displays a stacking arrangement with a C−H···π hydrogen bond. The interaction is slightly stronger (DFT-SAPT/CBS value of −3.9 kcal·mol^{-1}) than for the diborane. Like the B_2H···π bonding of diborane, the leading stabilizing terms are dispersion, followed by electrostatics. (ii) The more stable minimum has a planar arrangement, reminiscent of small anion···benzene complexes, with five bifurcated dihydrogen bonds of the B−H···H−C type. Its interaction energy amounts to −5.3 kcal·mol^{-1} and is composed as well of attractive dispersion and electrostatic terms. Unlike the stacked arrangement, its exchange repulsion is smaller by 4.1 kcal·mol^{-1} due to a larger intersystem separation (by 1.4 Å).

(6) The dianionic $B_{12}H_{12}^{2-}$ molecule interacts with benzene only in the planar arrangement (and is repelled from the stacking one) with five bifurcated dihydrogen bonds of the B−H···H−C type. The interaction energy amounts to −10.1 kcal·mol^{-1}, which is 2−3 times stronger than for the diborane···benzene complex. The $B_{12}H_{12}^{2-}$···benzene complex is stabilized by two universal attractive forces, dispersion (79%) and electrostatics (64%) and in addition by induction (61%), which occurs less frequently in noncovalent complexes. The balance of these three attractive components in stabilizing the $B_{12}H_{12}^{2-}$···benzene complex is unique.

Acknowledgment. We thank the referee for the inspiring advice to compare the carborane and borane···benzene interactions with planar anion···arene complexes. We also thank Drs. Pavel Jungwirth, Michael L. McKee, and Zdeněk Havlas for fruitful discussions; and Dr. Tibor András Rokob for help with the MOLEKEL program. This work was a part of Research Project No. Z40550506 of the Institute of Organic Chemistry and Biochemistry, Academy of Sciences of the Czech Rep-

ublic, and was supported by Grants No. LC512, MSM6198959216, and 1M0508 from the Ministry of Education, Youth and Sports of the Czech Republic; and Grant No. IAAX00320901 from the Grant Agency of the Academy of Sciences of the Czech Republic. The support of Praemium Academiae, Academy of Sciences of the Czech Republic, awarded to P. H. in 2007, is also acknowledged. The work was also supported by Korea Science and Engineering Foundation (World Class Univ. Program: R32-2008-000-10180-0).

Supporting Information Available: Distances between the interacting systems, DFT-SAPT/CBS interaction energy components for planar complexes and optimized geometries of the cage carborane and borane···benzene complexes. This material is available free of charge via the Internet at http://pubs.acs.org.

References and Notes

(1) Crabtree, R. H.; Siegbahn, P. E. M.; Eisenstein, O.; Rheingold, A. L. *Acc. Chem. Res.* **1996**, *29*, 348–354.
(2) Custelcean, R.; Jackson, J. E. *Chem. Rev.* **2001**, *101*, 1963–1980.
(3) Fanfrlík, J.; Lepšík, M.; Horinek, D.; Havlas, Z.; Hobza, P. *ChemPhysChem* **2006**, *7*, 1100–1105.
(4) Richardson, T. B.; deGala, S.; Crabtree, R. H.; Siegbahn, P. E. M. *J. Am. Chem. Soc.* **1995**, *117*, 12875–12876.
(5) Klooster, W. T.; Koetzle, T. F.; Siegbahn, P. E. M.; Richardson, T. B.; Crabtree, R. H. *J. Am. Chem. Soc.* **1999**, *121*, 6337–6343.
(6) Planas, J. G.; Vinas, C.; Teixidor, F.; Comas-Vives, A.; Ujaque, G.; Lledos, A.; Light, M. E.; Hursthouse, M. B. *J. Am. Chem. Soc.* **2005**, *127*, 15976–15982.
(7) Glukhov, I. V.; Lyssenko, K. A.; Korlyukov, A. A.; Antipin, M. Y. *Russ. Chem. Bull.* **2005**, *54*, 547–559.
(8) Belkova, N. V.; Shubina, E. S.; Epstein, L. M. *Acc. Chem. Res.* **2005**, *38*, 624–631.
(9) Blanch, R. J.; Williams, M.; Fallon, G. D.; Gardiner, M. G.; Kaddour, R.; Raston, C. L. *Angew. Chem., Int. Ed.* **1997**, *36*, 504–506.
(10) Raston, C. L.; Cave, G. W. V. *Chem.—Eur. J.* **2004**, *10*, 279–282.
(11) Hamilton, E. J. M.; Kultyshev, R. G.; Du, B.; Meyers, E. A.; Liu, S. M.; Hadad, C. M.; Shore, S. G. *Chem.—Eur. J.* **2006**, *12*, 2571–2578.
(12) Li, H. Z.; Min, D. H.; Shore, S. G.; Lipscomb, W. N.; Yang, W. *Inorg. Chem.* **2007**, *46*, 3956–3959.
(13) Tian, S. X.; Li, H. B.; Bai, Y. B.; Yang, J. L. *J. Phys. Chem. A* **2008**, *112*, 8121–8128.
(14) Ravinder, P.; Subramanian, V. *J. Phys. Chem. A* **2010**, *114*, 5565–5572.
(15) Jurečka, P.; Hobza, P. *Chem. Phys. Lett.* **2002**, *365*, 89–94.
(16) Lee, E. C.; Kim, D.; Jurečka, P.; Tarakeshwar, P.; Hobza, P.; Kim, K. S. *J. Phys. Chem. A* **2007**, *111*, 3446–3457.
(17) Jeziorski, B.; Moszynski, R.; Szalewicz, K. *Chem. Rev.* **1994**, *94*, 1887–1930.
(18) (a) Jansen, G.; Hesselmann, A. *J. Phys. Chem. A* **2001**, *105*, 11156–11157. (b) Hesselmann, A.; Jansen, G.; Schutz, M. *J. Chem. Phys.* **2005**, 122. (c) Hesselmann, A.; Jansen, G. *Chem. Phys. Lett.* **2002**, *357*, 464–470. (d) Hesselmann, A.; Jansen, G.; Schutz, M. *J. Am. Chem. Soc.* **2006**, *128*, 11730–11731. (e) Hesselmann, A.; Jansen, G. *Chem. Phys. Lett.* **2003**, *367*, 778–784. (f) Hesselmann, A.; Jansen, G. *Chem. Phys. Lett.* **2002**, *362*, 319–325. (g) Williams, H. L.; Chabalowski, C. F. *J. Phys. Chem. A* **2001**, *105*, 646–659. (h) Misquitta, A. J.; Szalewicz, K. *Chem. Phys. Lett.* **2002**, *357*, 301–306. (i) Podeszwa, R.; Bukowski, R.; Szalewicz, K. *J. Phys. Chem. A* **2006**, *110*, 10345–10354. (j) Rybak, S.; Szalewicz, K.; Jeziorski, B.; Corongiu, G. *Chem. Phys. Lett.* **1992**, *199*, 567–573.
(19) Lesnikowski, J. Z. *Collect. Czech. Chem. Commun.* **2007**, *72*, 1646–1658.
(20) Jurečka, P.; Šponer, J.; Černý, J.; Hobza, P. *Phys. Chem. Chem. Phys.* **2006**, *8*, 1985–1993.
(21) Hobza, P.; Müller-Dethlefs, K. In *Non-Covalent Interactions*; The Royal Society of Chemistry: Cambridge, UK, 2010.
(22) Coletti, C.; Re, N. *J. Phys. Chem. A* **2009**, *113*, 1578–1585.
(23) Dabkowska, I.; Jurečka, P.; Hobza, P. *J. Chem. Phys.* **2005**, 122.
(24) Pitoňák, M.; Neogrady, P.; Černý, J.; Grimme, S.; Hobza, P. *ChemPhysChem* **2009**, *10*, 282–289.
(25) Kolář, M.; Hobza, P. *J. Phys. Chem. A* **2007**, *111*, 5851–5854.
(26) Boys, S. F.; Bernardi, F. *Mol. Phys.* **1970**, *19*, 553.
(27) Hohenberg, P.; Kohn, W. *Phys. Rev. B* **1964**, *136*, B864.
(28) Kohn, W.; Sham, L. J. *Phys. Rev.* **1965**, *1*, 1697.
(29) Halkier, A.; Helgaker, T.; Jorgensen, P.; Klopper, W.; Koch, H.; Olsen, J.; Wilson, A. K. *Chem. Phys. Lett.* **1998**, *286*, 243–252.
(30) Reed, A. E.; Curtiss, L. A.; Weinhold, F. *Chem. Rev.* **1988**, *88*, 899–926.
(31) Cheeseman, J. R.; Trucks, G. W.; Keith, T. A.; Frisch, M. J. *J. Chem. Phys.* **1996**, *104*, 5497–5509.
(32) Huzinaga, S. *J. Chem. Phys.* **1965**, *42*, 1293.
(33) Dunning, T. H. *J. Chem. Phys.* **1970**, *53*, 2823.
(34) Hnyk, D.; Rankin, D. W. H. *Dalton Trans.* **2009**, 585–599.
(35) Ahlrichs, R.; Bär, M.; Häser, M.; Horn, H.; Kölmel, C. *Chem. Phys. Lett.* **1989**, *162*, 165–169.
(36) Frisch, M. J.; Trucks, G. W.; Schlegel, H. B.; Scuseria, G. E.; Robb, M. A.; Cheeseman, J. R.; Montgomery, Jr., J. A.; Vreven, T.; Kudin, K. N. ; Burant, J. C.; Millam, J. M.; Iyengar, S. S.; Tomasi, J.; Barone, V.; Mennucci, B.; Cossi, M.; Scalmani, G.; Rega, N.; Petersson, G. A.; Nakatsuji, H.; Hada, M.; Ehara, M.; Toyota, K.; Fukuda, R.; Hasegawa, J.; Ishida, M.; Nakajima, T.; Honda, Y.; Kitao, O.; Nakai, H.; Klene, M.; Li, X.; Knox, J. E.; Hratchian, H. P.; Cross, J. B.; Bakken, V.; Adamo, C.; Jaramillo, J.; Gomperts, R.; Stratmann, R. E.; Yazyev, O.; Austin, A. J.; Cammi, R.; Pomelli, C.; Ochterski, J. W.; Ayala, P. Y.; Morokuma, K.; Voth, G. A.; Salvador, P.; Dannenberg, J. J.; Zakrzewski, V. G.; Dapprich, S.; Daniels, A. D.; Strain, M. C.; Farkas, O.; Malick, D. K.; Rabuck, A. D.; Raghavachari, K.; Foresman, J. B.; Ortiz, J. V.; Cui, Q.; Baboul, A. G.; Clifford, S.; Cioslowski, J.; Stefanov, B. B.; Liu, G.; Liashenko, A.; Piskorz, P.; Komaromi, I.; Martin, R. L.; Fox, D. J.; Keith, T.; Al-Laham, M. A.; Peng, C. Y.; Nanayakkara, A.; Challacombe, M.; Gill, P. M. W.; Johnson, B.; Chen, W.; Wong, M. W.; Gonzalez, C.; Pople, J. A. *Gaussian 03, revision C.02*; Gaussian, Inc.: Pittsburgh, PA, 2003.
(37) Werner, H.-J. Knowles, P. J. Lindh, R. Manby, F. R. Schütz, M. Celani, P. Korona, T. Mitrushenkov, A. Rauhut, G. Adler, T. B. Amos, R. D. Bernhardsson, A. Berning, A. Cooper, D. L. Deegan, M. J. O. Dobbyn, A. J. Eckert, F. Goll, E. Hampel, C. Hetzer, G. Hrenar, T. Knizia, G. Köppl, C. Liu, Y. Lloyd, A. W. Mata, R. A. May, A. J. McNicholas, S. J. Meyer, W. Mura, M. E. Nicklaβ, A. Palmieri, P. Pflüger, K. Pitzer, R. Reiher, M. Schumann, U. Stoll, H. Stone, A. J. Tarroni, R. Thorsteinsson, T. Wang, M. Wolf. A. *MOLPRO 2006*; University College Cardiff: Cardiff, 2006.
(38) Sedlak, R.; Jurečka, P.; Hobza, P. *J. Chem. Phys.* **2007**, 127.
(39) Desiraju, G. R. *Acc. Chem. Res.* **2002**, *35*, 565–573.
(40) Müller-Dethlefs, K.; Hobza, P. *Chem. Rev.* **2000**, *100*, 143–167.
(41) Hobza, P.; Zahradník, R.; Müller-Dethlefs, K. *Collect. Czech. Chem. Commun.* **2006**, *71*, 443–531.
(42) Tsuzuki, S.; Honda, K.; Uchimaru, T.; Mikami, M.; Tanabe, K. *J. Am. Chem. Soc.* **2000**, *122*, 11450–11458.
(43) Tsuzuki, S.; Fujii, A. *Phys. Chem. Chem. Phys.* **2008**, *10*, 2584–2594.
(44) Zierkiewicz, W.; Hobza, P. *Phys. Chem. Chem. Phys.* **2004**, *6*, 5288–5296.
(45) Cybulski, H.; Tyminska, E.; Sadlej, J. *ChemPhysChem* **2006**, *7*, 629–639.
(46) Hay, B. P.; Bryantsev, V. S. *Chem. Commun.* **2008**, *21*, 2417–2428.
(47) Ringer, A. L.; Figgs, M. S.; Sinnokrot, M. O.; Sherrill, C. D. *J. Phys. Chem. A* **2006**, *110*, 10822–10828.
(48) Bryantsev, V. S.; Hay, B. P. *J. Am. Chem. Soc.* **2005**, *127*, 8282–8283.
(49) Chalasinski, G.; Szczesniak, M. M. *Chem. Rev.* **1994**, *94*, 1723–1765.
(50) Cubero, E.; Luque, F. J.; Orozco, M. *Proc. Natl. Acad. Sci. U. S. A.* **1998**, *95*, 5976–5980.
(51) Tsuzuki, S.; Yoshida, M.; Uchimaru, T.; Mikami, M. *J. Phys. Chem. A* **2001**, *105*, 769–773.
(52) Singh, N. J.; Min, S. K.; Kim, D. Y.; Kim, K. S. *J. Chem. Theory Comput.* **2009**, *5*, 515–529.
(53) Flükiger, P.; Lüthi, H. P.; Portmann, S.; Weber, J. *MOLEKEL 4.3*; Swiss National Supercomputing Centre CSCS: Manno, Switzerland, 2000.

JP104411X